論文 / 著書情報
Article / Book Information

題目(和文)	
Title(English)	Control Design of the Pneumatic Servo System Considering the Effect of Connected Pipelines
著者(和文)	LiJun
Author(English)	Jun Li
出典(和文)	学位:博士(工学), 学位授与機関:東京工業大学, 報告番号:甲第9318号, 授与年月日:2013年9月25日, 学位の種別:課程博士, 審査員:川嶋 健嗣,香川 利春,横田 眞一,吉田 和弘,吉岡 勇人
Citation(English)	Degree:Doctor (Engineering), Conferring organization: Tokyo Institute of Technology, Report number:甲第9318号, Conferred date:2013/9/25, Degree Type:Course doctor, Examiner:,,,,
学位種別(和文)	博士論文
Type(English)	Doctoral Thesis

Control Design of the Pneumatic Servo System Considering the Effect of Connected Pipelines

Supervisor:

Professor Kenji Kawashima

Professor Toshiharu Kagawa

Department of Mechano-Micro Engineering
Tokyo Institute of Technology

Jun Li

August, 2013

Contents

Nomenclature

a:	acceleration of the pneumatic servo table	[m/s^2]
A:	pressured area	[m^2]
$A_{1,2,3}$:	gains of 3rd order linear model	
b:	critical pressure ratio	[-]
B:	viscous damping coefficient	[N·s /m]
$B_{1,\ldots,5}$:	gains of 5th order linear model	
c:	sonic speed	[m/s]
$C_{1,\ldots,7}$:	gains of 7th order linear model	
C_v:	specific heat of a gas at a constant volume	[J/(kg·K)]
D:	diameter of pipelines	[m]
d_f:	flow force	[N]
f:	frequency	[Hz]
F_M:	force of VCM	[N]
G:	mass flow	[kg/s]
$G(s)$:	transfer function	
h:	heat transfer coefficient	[W/(m^2·K)]
i:	current	[A]
K_a:	acceleration gain of servo table	[V·s^2/m]
K_{ap}:	proportional gain of the servo valve	[N/V]
K_{ai}:	integral gain of the servo valve	[N/(V·s)]
K_f:	flow coefficient	[-]
K_{Fc}:	gain of VCM	[N/A]
K_i:	gain of current amplifier	[A/V]
K_n:	gain of the pneumatic actuator	[1/ (m s)]
K_p:	proportional gain of servo table	[V/m]
K_{pd}:	differential gain	[N·s /mm]
K_{pp}:	proportional gain	[N/mm]
K_{sv}:	proportional gain of servo valve	[(kg/s)/V]

K_v:	velocity gain of servo table	[V·s/m]
l:	full stroke of pneumatic actuator	[m]
L:	length of pipelines	[m]
m:	mass of the slider	[kg]
m_a:	mass of air	[kg]
Ms:	mass of the spool	[kg]
P:	pressure	[Pa]
P(s):	open loop transfer function	
P_r:	Prandtl number	[-]
Q:	volume flow	[m^3/s (ANR)]
R:	gas constant	[J/(kg·K)]
R_e:	Reynolds number	[-]
s:	Laplace operator	[s^{-1}]
S:	heat transmission area	[m^2]
Se:	effective Cross-sectional area	[m^2]
t:	time	[s]
Δt:	sampling time	[s]
u:	velocity of air	[m/s]
V:	volume of cylinder chamber	[m^3]
vol:	control voltage	[V]
w:	operator	[-]
x:	position	[m]
x_d:	position of the slider	[m]
$x_{ref:}$	reference position	[m]
x_{sp}:	spool position of servo valve	[m]
Δx :	length of every grid	[m]
α:	coefficient of 3rd order control	[-]
β:	coefficient of 3rd order control	[-]
δ:	coefficient of chalk flow	[-]

θ:	atmospheric temperature	[K]
κ:	specific heat ratio	[-]
ρ:	density	[kg/m^3]
τ_1:	normalized Laplace operator	[-]
μ:	dynamic viscosity of air	[m^2/s]
λ:	coefficient of pipe friction	[-]
ω:	natural frequency	[Hz]
ζ:	damping ratio	[-]

Subscript

1_IN:	results of Pipeline1 when pressure signals measured by sensors at the control ports of the servo valve
1_OUT:	results of Pipeline1 pressure signals measured by sensors at the cylinder chambers
1_DM:	results of Pipeline1 pressure signals estimated by distributed model in real time
2_IN:	results of Pipeline2 when pressure signals measured by sensors at the control ports of the servo valve
2_OUT:	results of Pipeline2 pressure signals measured by sensors at the cylinder chambers
2_DM:	results of Pipeline2 pressure signals estimated by distributed model in real time
a:	atmospheric
ANR :	standard reference atmosphere
c:	charging side
d:	discharge side
k:	charging or discharging side
L:	left chamber
max:	maximum

n:	pneumatic actuator
pc:	the charging port of cylinder chambers
R:	right chamber
re:	resolution
ref:	reference
s:	supply
t:	pipeline
v:	servo valve
0:	equilibrium pressure
1; ⋯; *NX; NX+1* ; i:	mesh index of pipeline
3^{rd}:	transfer function of the 3^{rd} order linear model
5^{th}:	transfer function of the 5^{th} order linear model
7^{th}:	transfer function of the 7^{th} order linear model
~:	estimated value

Chapter 1 Introduction

1.1 Background

1.1.1 Precision and ultra-precision positioning devices

In recent years, with the development of precision machines, the demand of positioning technique has become high-speed and ultra-precision [1]. The ultra-precision positioning device is applicable to instruments in many fields which require high precision positioning in *X* and *Y* directions [2]. It is called precision positioning when the positioning accuracy is 0.1μm to 1μm, while the accuracy is 0.01μm it will be treated as ultra-precision positioning [3]. The issue of achieving sub-micrometer accuracy over a range of a few hundred millimeters has been mainly targeted in the field of ultra-precision machine tools and semiconductor manufacturing equipment such as lithographers and steppers [4].

Precision positioning system consists of actuator, guide elements, power transmission sector, and position sensor together with control algorithm and computer.

·Actuator

As Fig.1.1 (a) shows catalogues of actuators used in precision positioning device [3], the most widely used actuators are rotary servo motors and linear motors. Pneumatic cylinders, hydraulic cylinders and piezoelectric elements are also used as the precision positioning actuators [3]. According to Fig.1.1 (a) [3], the widely used precision positioning actuators are almost electrical driven. The rotary servo motor combined with ball screw has a high proportion of use because of low cost and specific control algorithm. However it is difficult to realize high-speed with such kind of combination, since the axis of ball screw is easily broken at a high-speed and the system will be sensitive to parameter variations such as changes in payload [5].

In recent years, the research on precision positioning device including high-speed and

ultra-precision response actuators and linear motors is popular [5]. Compared with ball screws, with linear motors the system can realize a long stroke, because there is no speed limit for linear motors. Moreover, because linear motors are non-contact driven, there is no frictions which enable them work longer. Based on these characteristics, the linear motor is suitable to high-speed and ultra-precision positioning device. However, it is expensive and temperature of coil is high which needs cooling system to protect thermal expansion [6].

Compared with solid-state actuators, piezoelectric actuators are more suitable to be used small position-variable control [7]. Research on using voice coil motors and piezoelectric actuators combined with other mechanism in precision positioning device with a long stroke is working on [8]. Since hydraulic cylinders can provide a high torque, they are often used on airplanes and ships. High electricity cost and heat generation limit the use of hydraulic cylinders [9, 10].

When pneumatic cylinders are used, the nonlinearity compression of air makes it difficult to control. However air power is compressible at a high power ratio and air is a clean, renewable energy source. Advantages of low heat generation and non-magnetic nature make it universal in precision positioning control. Table 1.1 shows the advantages and disadvantages of several actuators.

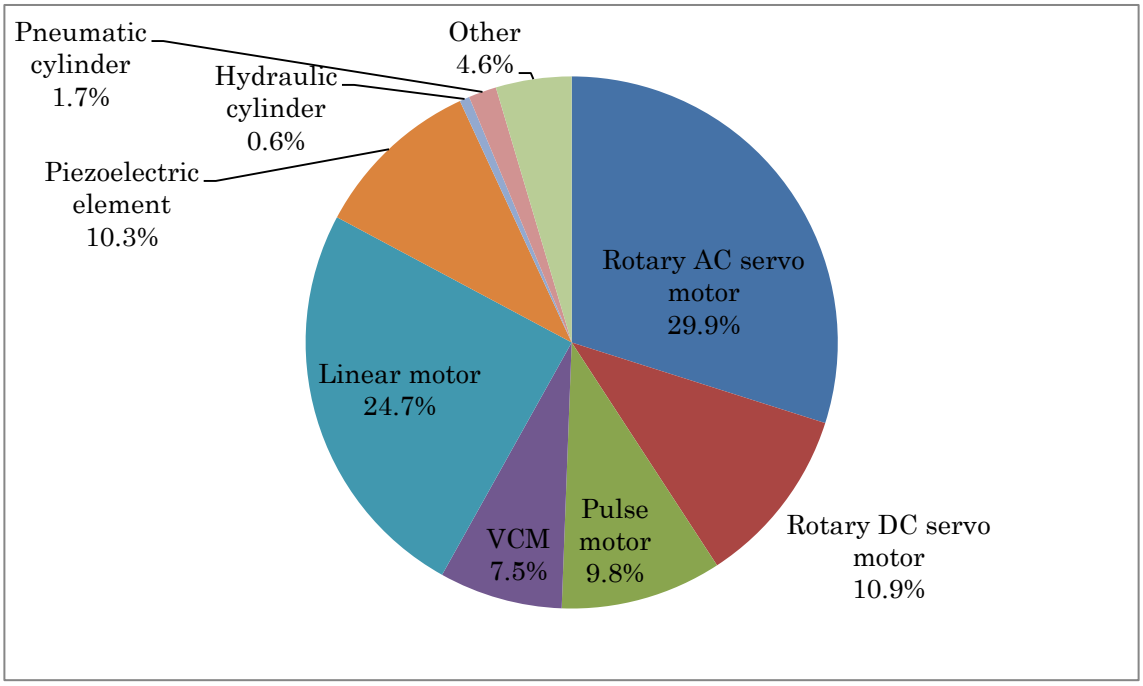

(a) Actuator

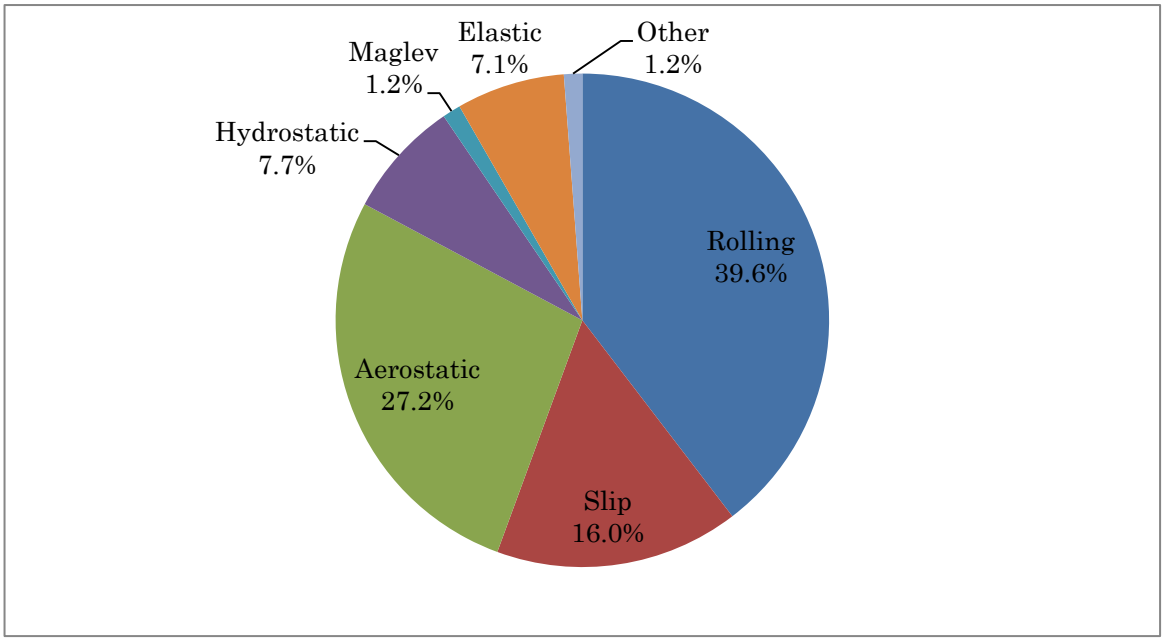

(b) Guide elements

Fig.1.1 Distribution of primary element

Table 1.1 Comparison of actuator for precision positioning

	Advantage	Disadvantage
Ball screw	specific control algorithm easy to be used	friction and noise hard to realize high-speed
Linear motor	ultra-precision positioning maintenance-free	heat-generation external disturbance electromagnetic noise
Piezoelectric element	ultra-precision positioning in light weight	short stroke heat-generation
Hydraulic cylinder	high torque	heat-generation
Pneumatic cylinder	low heat generation non-magnetic and clean	nonlinearity hard to realize ultra-precision control

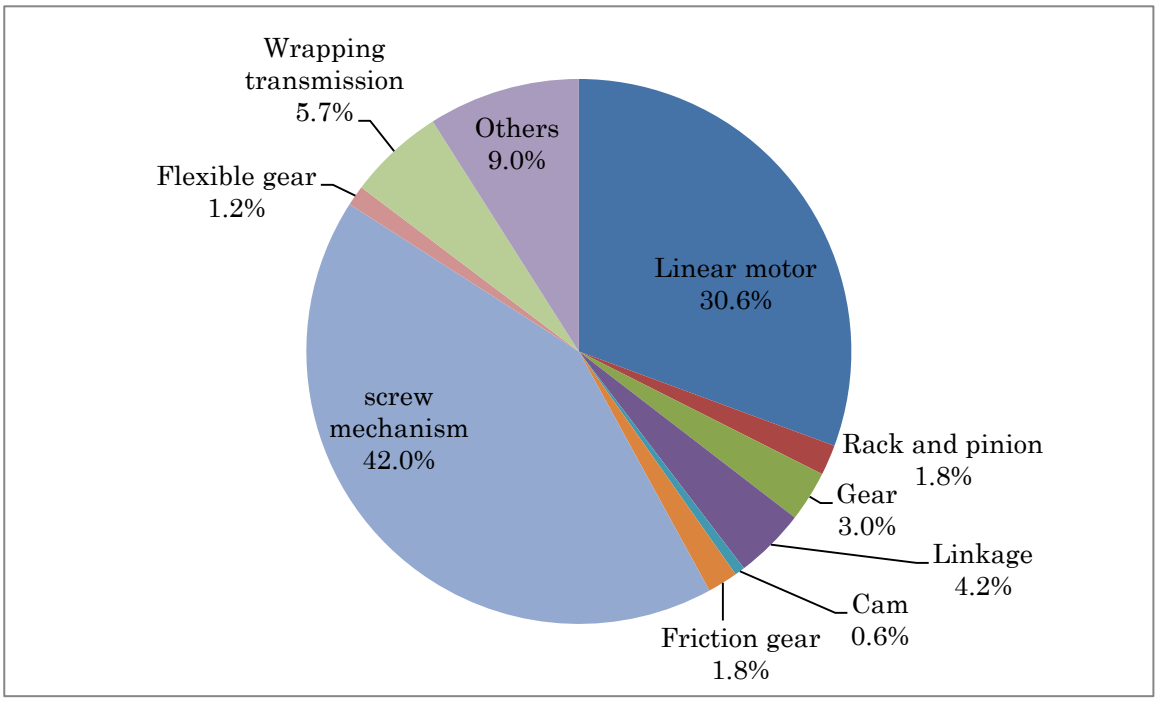

Fig.1.2 Driving force transmission mechanism

·Guide elements

Frictional characteristic, rigidity and loading capacity of guide elements will have significant impact on the precision positioning accuracy. Common used guide elements are shown in Fig.1.1 (b) [3]. According to investigations, the advantage of no friction which enable high-speed and ultra-precision makes air bearing universal.

Scatter gram of driving force transmission mechanism is shown in Fig.1.2 [3]. Along with the increasing use of linear motors, systems without direct-driving mechanism become widely used.

Feedback sensor is the most important element in precision positioning control system. Based on experience, it is better to select the sensor, the resolution of which is 5 times higher than the required resolution. And the frequency responsibility is 10 times higher than the required one of the system [11].

1.1.2 The pneumatic actuator

Modern force-reflecting tele-operation, haptic interfaces, and other applications in robotics require high performance force actuators, with high force output per unit weight. It is also important to have linear, fast and accurate response, as well as low friction and mechanical impedance [12]. Air power is compressible at a high power ratio and air is a clean, renewable energy source. Thanks to their advantages of low heat generation and non-magnetic nature, pneumatic cylinders can offer a better alternative to electrical or hydraulic actuators for certain types of applications. Pneumatic servo systems are used in pneumatic robot systems, spherical glass molding machines, and vibration isolation systems [13].

Pneumatic actuators provide the previously enumerated qualities at low cost. They are also suitable for clean environments and safer and easier to work with. However, position and force control of these actuators in applications that require high bandwidth

is somehow difficult, because of compressibility of air and highly nonlinear flow through pneumatic system components [14]. In addition, due to design and space considerations, in many applications the command valve is positioned at relatively large distance from the pneumatic cylinder. Thus, the effects of time delay and attenuation due to the connected tubes becomes significant [12]. Above all, friction forces occur in a nonlinear and uncertain manner in the seals for avoiding air leakage and may cause unfavorable stick-slip oscillation at extremely low operation speed [15]. Subsequently, more complete mathematical models for the thermodynamic and flow equations in the charging-discharging processes were developed (Shearer, [16]). As a result more complex position controllers, based on the linearization around the mid stroke position, were developed (Burrows, [17]; Liu and Bobrow [13]). These simplified models provided only modest performance improvements. During the last decade, nonlinear control techniques were implemented using digital computers. Bobrow and Jabbari [18] and McDonell and Bobrow [19] used adaptive control for force actuation and trajectory tracking, applied to an air powered robot. Improved results were presented for low frequencies (approx. 1 Hz). Sliding mode position controllers were also tested (Arun et al. [20], Tang and Walker [21]), again with improved results at low frequencies. As a general characteristic the mathematical models used in these controllers assumed no piston seals friction, linear flow through the valve, and neglected the valve dynamics. Ben-Dov and Salcudean [22] developed a forced-controlled pneumatic actuator that provided a force with amplitude of 2 N at 16 Hz. Their model included the valve dynamics and the nonlinear characteristics of the compressible flow through the valve. A comparison between linear and nonlinear controllers applied to a rotary pneumatic actuator is presented by Richard and Scavarda [23]. The mathematical model accounted for the leakage between actuator's chambers and the nonlinear variation of the valve effective area with the applied voltage. Their model depends heavily on curve fitting using experimental values, making it difficult to apply to even slightly different systems. Effects of nonlinear flow through the valve, air compressibility in cylinder chambers, leakage between chambers, end of stroke inactive volume, and time delay and

attenuation in the pneumatic lines were carefully considered to develop high performance nonlinear pneumatic force controller [12]. In many recent researches, fuzzy and slider controller is used to compensate the nonlinear of the pneumatic system [24, 25].

1.1.3 The pneumatic servo table system with air bearing

The pneumatic servo table system designed by our group is mainly composed by a pneumatic actuator, high-performance pneumatic servo valves, a linear scale and pipelines. The pneumatic actuator includes a slider which is 1DOF moving part and a fixed guide. The slider is mounted externally pressurized air bearing which acts through holes in the surface of the guide. Use of this air bearing can avoid contact between the slider and the guide and also allows smooth acceleration and movement without stick-slip effect. Since it can avoid the friction between the slider and the guide which has influence on the control ability of the pneumatic system, it is possible to realize high-speed and ultra-precision positioning control. The high-performance pneumatic servo valve has high dynamics up to 300Hz and the natural frequency and damping ratio of which can be set optionally [26]. High dynamics of servo valve can improve the control ability of the system. However, the dynamics of pipelines have bad influence on the system's control ability [27]. When the length of pipeline becomes longer, the system's stability will decrease. Since the friction which will limit the performance of the linear controller [15] can be neglected by utilized air bearing and the flow in the system is low, a linear model of the system was designed.

1.1.4 The pneumatic servo system with long connected pipelines

Due to design and space considerations, in many applications the servo valve is positioned at relatively large distance from the pneumatic cylinder. The phenomena introduced by long pipelines may have crucial incidence in some industrial applications

[28]. The long pipelines connected the servo valve with the cylinder chambers have two kinds of influence on the pneumatic system. The one is that the pressure loss along the pipelines will induce a decrease in the steady-state air flow through the servo valve. The other one is that the flow profile at the outlet will be delayed with respect to the one at the inlet by the time increment necessary for the flow to travel through the entire length of the pipelines [12]. The effects of time delay and attenuation will cause bad effect on the position control of the system [29]. Usually to avoid the influence of long connected pipelines, sensors are utilized to measure the state in the cylinder chambers. However, sensors are sensitive and cannot adapt to high temperature or intensive radiation environment and they also generate electromagnetics which limit the advantages of pneumatic actuators, like non- electromagnetics [30, 31].

The pipeline model was proposed in many control method [32]-[36]. Pipelines used in most of these researches have short lengths. The pipelines used in [36] are shorter than 2m. Since the flow is laminar and pressure losses through the connected pipelines and the amplitude of the pressures are small, the pipeline model is approximated as a 2^{nd} order lag model. Even though the method of characteristics shows excellent agreement with experimental results in small amplitude wave [37]-[40], it cannot be applied to a flow computation when the bulk velocity is not negligibly small.

To compensate the influence of long connected pipelines, the system is applied which is mainly composed by a pressure regulator, a five-port servo valve, four pressure sensors, long connected pipelines, a metal pneumatic cylinder, an encoder and an AD/DA converter. The five-port servo valve is used to control the mass flow at the inlets of pipelines. Pressure values at the inlets of the pipelines and cylinder chambers are obtained by the AD converter and pressure sensors. In this experiment, to confirm the influence of pressure sensors' locations on the position accuracy and the effectiveness of the distributed model of pipelines, four pressure sensors are utilized. In every case, two pipelines with the same length and diameter are used to connect the two cylinder chambers with the control ports of the servo valve. The supply pressure is 700kPa (absolute) and the full stroke of the cylinder is 300mm. The AD / DA converter

is selected, the sampling time of which is 1 ms.

1.2 Objective of this study

Due to design and space considerations, in many applications long pipelines are needed to connect the servo valve with the pneumatic cylinder and the pneumatic actuator is non-electromagnetic. To reduce the total magnetic leak of the pneumatic actuator, pressure sensors are released from the cylinder chamber side. For this reason, the design method is developed to reduce the bad influence of connected pipelines on the position control of the system when pressure sensors are kept from the cylinder chambers.

The purposes of this thesis are:

1.2.1 The pneumatic servo table system with air bearing

Firstly, to develop the suitable linear model of each main element used in the system, including the linear model of pneumatic actuator, connected pipeline and high-performance pneumatic servo valve.

Secondly, to design a linear model for whole pneumatic servo table system with air bearing, different orders models have been compared to find a suitable and easy to realized linear model.

Finally to design a feed forward to decrease the trajectory errors of the pneumatic servo table system with air bearing, with a 5^{th} order feed forward the maximum trajectory error is decreased to sub-micrometer.

1.2.2 The pneumatic servo system with long connected pipelines

Firstly, to develop the distributed model of connected pipelines which can estimate the pressure in the cylinder chambers precisely by the measured values at the control ports of the servo valve in the real time, with which pressure sensors can be released

from the cylinder chamber to reduce total magnetic leak around cylinder side.

Secondly, to use the estimated pressure values as control signal in the real control system which can compensate the influence of long connected pipelines without using pressure sensors around the cylinder chamber side.

Finally, since the distributed model is complex, the index to judge the necessity of the distributed pipeline model in the pneumatic servo system is designed.

1.3 Summary

The outline of the thesis is shown in Fig.1.3. This thesis is summarized as follows:

Chapter 2 “Precise position control of the pneumatic servo table considering the dynamics of pipelines”

This chapter introduces the pneumatic servo table system and main components, like the pneumatic actuator, connected pipelines and high-performance pneumatic servo valves and the mathematical models of the main elements used in the system. Based on the linear model of the main elements, the different orders linear models of the whole system are represented. Comparison of simulation and experimental results are shown in this chapter to find out the suitable and easy to be realized linear model of the whole pneumatic servo table system. At last, the 3^{rd} and 5^{th} order feed forward have been designed to minimize the trajectory errors. Experimental results with these two kinds of feed forward have been represented. Experimental results with a 5^{th} order feed forward show that the maximum trajectory error is decrease to sub-micrometer.

Chapter 3 “Distributed model of connected pipelines”

This chapter discusses the control design of a pneumatic system using long connected pipelines to release pressure sensors at cylinder chambers. The distributed model estimates the pressure losses and time delay through long connected pipelines in real time. To confirm the effectiveness of the proposed control method, a simulation model

of the whole system is designed. The pipelines with different parameters are used. Compared simulation and experimental results, it has been found that the simulation model represents the real system well. Based on the estimated and measured pressure values in cylinder chambers, it is found that with this distributed model, the pressure in the cylinder chambers is estimated precisely by the measured values at the control ports of the servo valve in the real time. The experimental results demonstrate that the position accuracy is almost the same as that of using the measured pressure signals in the cylinder chambers. With this distributed model in the control system, the influence of long connected pipelines can be ignored and the cylinder sider is free of pressure sensors.

Chapter 4 “Index to judge the necessity of the distributed pipeline model”

The index to judge the necessity of the distributed pipeline model in the pneumatic servo system is proposed in this chapter. The distributed model estimates the pressure loss and time delay through long connected pipelines precisely in real time. However, this distributed model is complex and in some situations, the effect of connected pipelines can be ignored. The index is designed based on judgment of the pressure loss along pipelines for practical use. The pressure loss along pipelines is influenced by pipeline diameter, pipeline length, supply pressure, moving speed of the slider and pressurized area of cylinder chamber. The index is designed from the maximum pressure loss along pipelines divided by the resolution of the pressure sensors (±10kPa).

Chapter 5 “Conclusions and future work”

This chapter summarizes the results of this study and proposes the future works of this research.

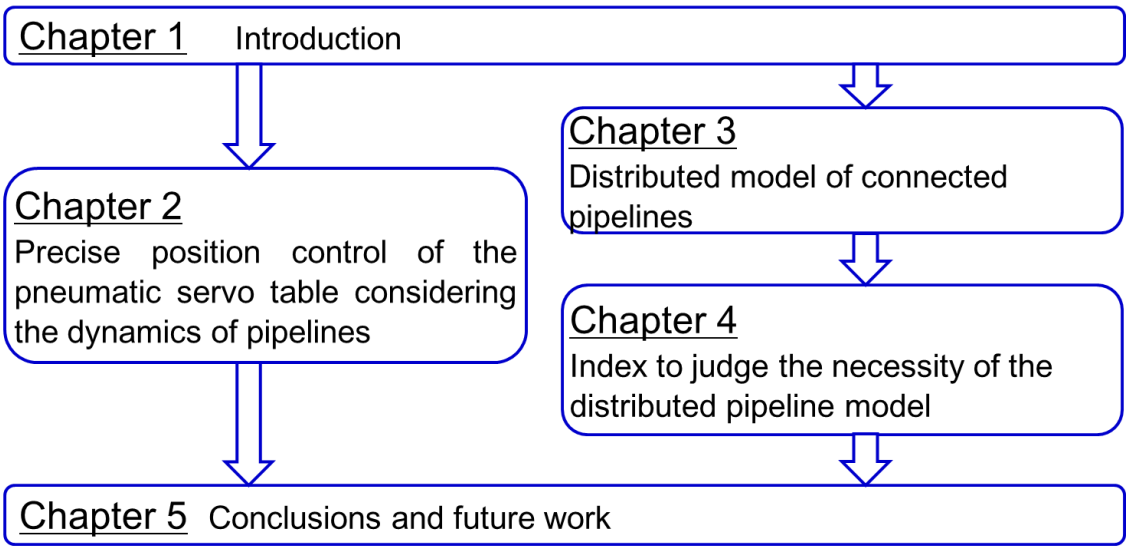

Fig.1.3 Thesis outline

Chapter 2 Precise position control of the pneumatic servo table considering the dynamics of pipelines

2.1 The pneumatic servo table system with air bearing

Fig.2.1 is the photo of the pneumatic servo table system which is pneumatically driven. The experimental setup including a schematic view of the pneumatic servo table system is shown in Fig.2.2. In these figures, it is clear that the pneumatic servo table is mainly composed by high-performance pneumatic servo valves, pipelines, a linear scale, the slider and the guides. The part made up by the slider and the guide is called the pneumatic actuator.

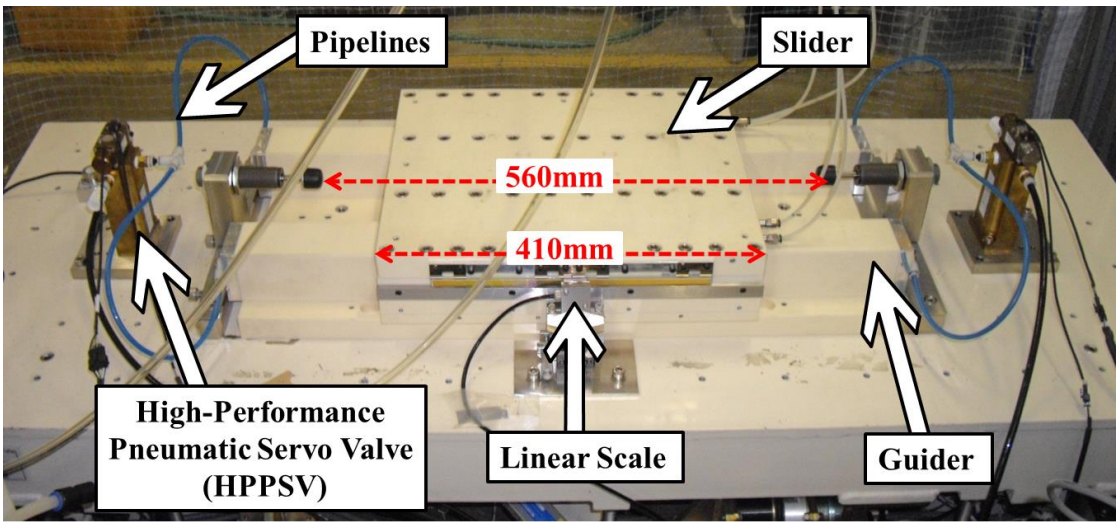

Fig. 2.1 The photo of the pneumatic servo table system

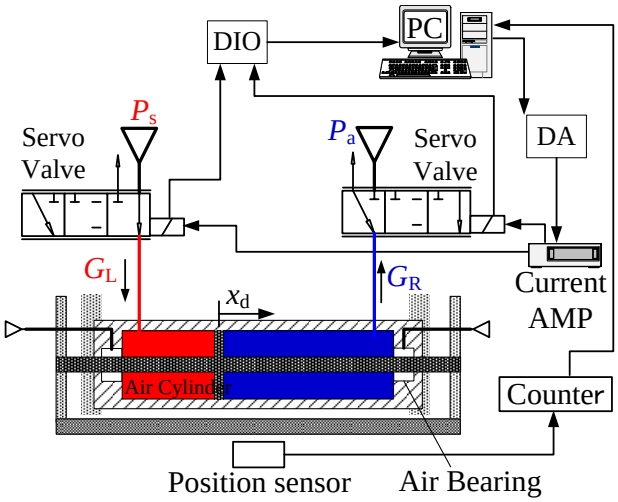

Fig. 2.2 Schematic of the pneumatic servo table system

2.1.1 Pneumatic actuator

The pneumatic actuator including a 1 degree-of-freedom moving slider and a fixed guide is made of ceramics. The slider is mounted externally pressurized air bearing which acts through holes in the surface of the guide. Use of this air bearing can avoid contact between the slider and the guide and also allows smooth acceleration and movement without stick-slip effect. Since it can avoid the friction between the slider and the guide which has influence on the control ability of the pneumatic system, there is no heat generation and non-magnetics. The slider is driven by the pressure difference between both pressurized chambers.

Parameters of pneumatic servo table system are shown in Table 2.1. The inner area of the piston, the mass of the slider and the average pressure in the chamber are $1.2\times10^{-3}\mathrm{m}^2$, 26 kg and 1.18×10^5 Pa, respectively. The resolution of the linear scale is 62.5pm, used to measure the displacement of the slider. The displacement data are taken into a PC through a digital input (DI) module. The PC acts as a controller and sends the control signals to the servo valves which will be introduced in the next section.

Table 2.1 Parameters of pneumatic servo table system

Symbol	Value
l	±70 [mm]
m	26 [kg]
A	1.2×10^{-3} [m^2]
V_0	1.92×10^{-4} [m^3]
Δt	200 [μs]

2.1.2 High-performance servo valve

To improve the controllability of the servo table system, a high-performance servo valve (HPPSV) is utilized. Figs.2.3 and 2.4 shows the photo and schematic structure of this servo valve. This servo valve is direct driving type three-port spool valve. The driving system consists of a voice coil motor (VCM). The VCM has lightweight moving parts, high dynamic characteristics and good linearity between the coil current and the thrust. A digital controller and a control algorithm are applied, which allow the natural frequency and the damping ratio of the HPPSV to be set optionally. Moreover by using an air bearing, the spool is held under non-contact condition, which realizes the high-speed response of the HPPSV. The dynamic characteristic is up to 300Hz. The full stroke of the spool is ±0.75mm and accuracy of the spool position is 0.1% to the full stroke. The maximum sonic conductance is 9.0×10^{-9} m^4s/kg. The spool mass, spool diameter and effective area are 10.0g, 6.0mm and $5.0mm^2$, respectively. The gap between the spool and the sleeve is maintained about 5μm. The dimension of the servo valve is 200 mm × 140 mm × 90 mm. In order to detect the spool position, a position sensor with the resolution of 0.125μm is used. This sensor outputs a 15-bit digital signal and measurements are fed to a PC via a digital input (DI) module. In order to control the spool position, a digital controller including a calculation delay compensator and a disturbance observer is designed and applied to the servo valve [26].

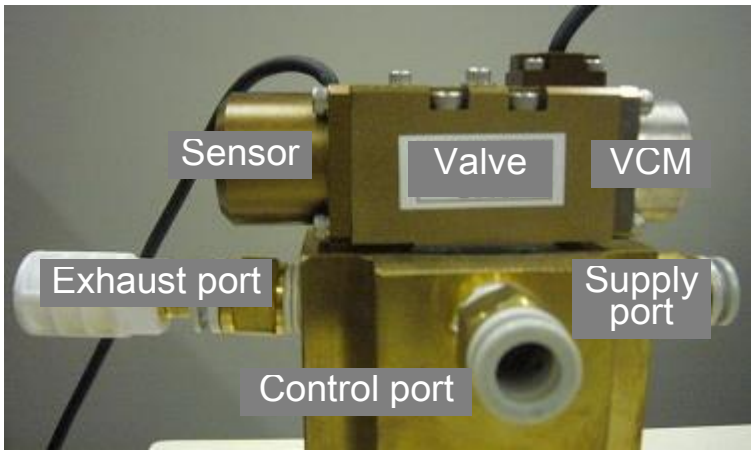

Fig. 2.3 Photo of high-performance pneumatic servo valve

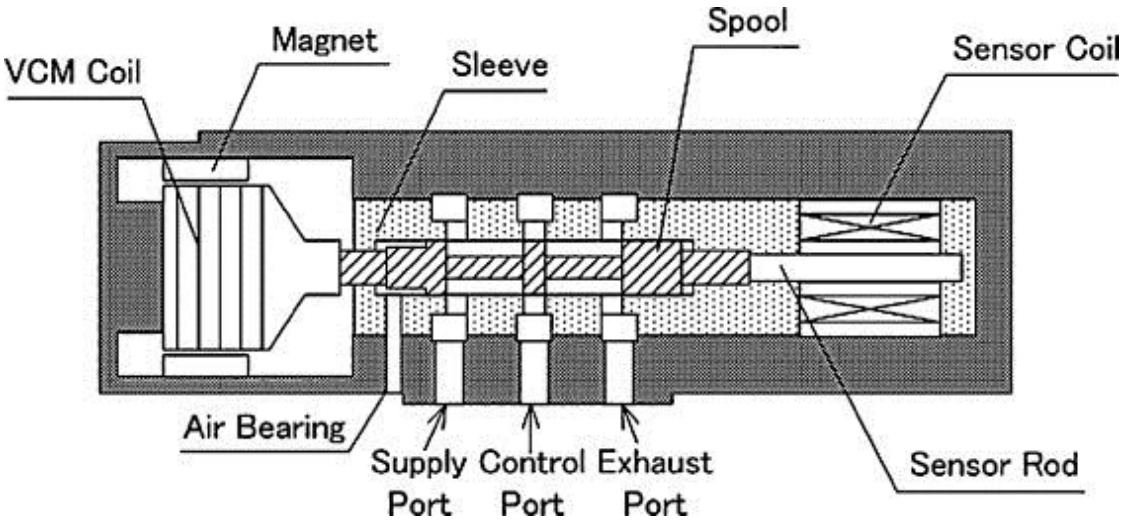

Fig. 2.4 Schematic diagram of high-performance pneumatic servo valve

2.1.3 Pipelines

As shown in Fig. 2.2, the pipelines are used to connect the pneumatic actuator with the HPPSV. In this paper, the parameters of pipelines were chosen as shown in Table 2.2.

Table 2.2 Pipelines' parameter

D [mm]	4.0, 8.0
L [m]	0.5, 1.0, 2.0

2.2 Element Model

In the pneumatic servo system, the controllability will be influenced by the friction of the piston and the dynamics of the composed elements. It is known that pipelines also play an important role in the pneumatic system. Another key element is the pneumatic servo valve. Its structure and parameters are important to achieve good performance [41-44]. Since air bearing is used, the friction of the piston is less than 2N which can be neglected. When a suitable linear model of the pneumatic servo table system is designed to reduce the trajectory errors, the dynamics of main elements should be taken into consideration. The design of suitable linear model for each main element used in system is proposed in the following sections.

2.2.1 Linear model of pneumatic actuator

A linearized model of the pneumatic actuator has been derived. Because of the air bearing, the friction can be negligible. The equation of motion is given as:

$$m\ddot{x}_d = A(P_L - P_R) \tag{2.1}$$

From the simulation results of nonlinear model, the state change of pressurized chambers is assumed as an isothermal condition. The total differentiation of the state equation of ideal gas linearized around the equilibrium point is given as:

$$PV = m_a R\theta \tag{2.2}$$

$$\frac{dP_L}{dt} = \frac{R\theta}{V_0} G_L - \frac{AP_0}{V_0}\dot{x}_d \tag{2.3}$$

$$\frac{dP_R}{dt} = \frac{R\theta}{V_0} G_R + \frac{AP_0}{V_0}\dot{x}_d \tag{2.4}$$

Here, R is gas constant, θ is atmospheric temperature, initial volume of chamber V_0 is 1.92×10^{-4} m^3, P_0 is equilibrium pressure, G_L and G_R is the mass flow rate of left and right chambers, respectively. The characteristic between the valve of effective area and

input can be assumed as linear. The moving direction of slider from left to right is defined as positive direction. The mass flow is caused by the change of choked and non-choked flow which is determined by pressure ratio between up- and down-stream pressures [45]. The critical pressure ratio used in this system is equal to 0.4. When the table moves from the left side to the right side like the Fig.2.2 shown, the pressure ratio of the left chamber is equal to P_0/P_s and the pressure ratio of the right chamber is equal to P_a/P_0. Here P_0 and P_s are equal to 0.11MPa and 0.25MPa, respectively. P_a is the atmospheric pressure. For the pressure ratio of the left chamber is 0.4 which is almost equal to the critical pressure ratio, the flow of the left chamber is approximated as sonic flow. Since the pressure ratio of the right chamber is 0.9 which is larger than the critical pressure ratio, the mass flow is calculated by Eq. (2.6) [46].

$$G_c = \frac{K_f}{\sqrt{R\theta}} P_s S_{ec} \tag{2.5}$$

$$G_d = \delta \frac{K_f}{\sqrt{R\theta}} P_s S_{ed} \tag{2.6}$$

$$K_f = \sqrt{\kappa \left(\frac{2}{\kappa+1}\right)^{\frac{\kappa+1}{\kappa-1}}} \tag{2.7}$$

$$\delta = \sqrt{1 - \left(\frac{P_a/P_0 - b}{1-b}\right)^2 \frac{P_0}{P_s}} \tag{2.8}$$

$$S_{ek} = K_{sv} vol_k \tag{2.9}$$

The open loop block diagram of pneumatic actuator is shown in Fig.2.5 and the simplification is shown in Fig.2.6. From the Eq. (2.5) to (2.9), the open loop transfer function of the pneumatic actuator is given as:

$$P_n(s) = \frac{K_{sv} K_n {\omega_n}^2}{s(s^2 + {\omega_n}^2)} \tag{2.10}$$

$$K_n = \frac{(1+\delta) K_f P_s \sqrt{R\theta}}{2AP_0} \tag{2.11}$$

$$\omega_n = \sqrt{\frac{2A^2 P_0}{mV_0}} \tag{2.12}$$

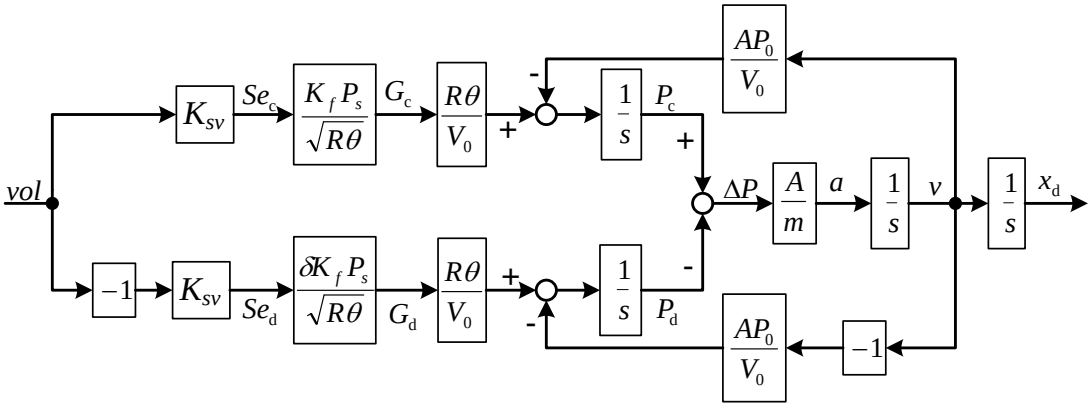

Fig. 2.5 Open loop block diagram of pneumatic actuator

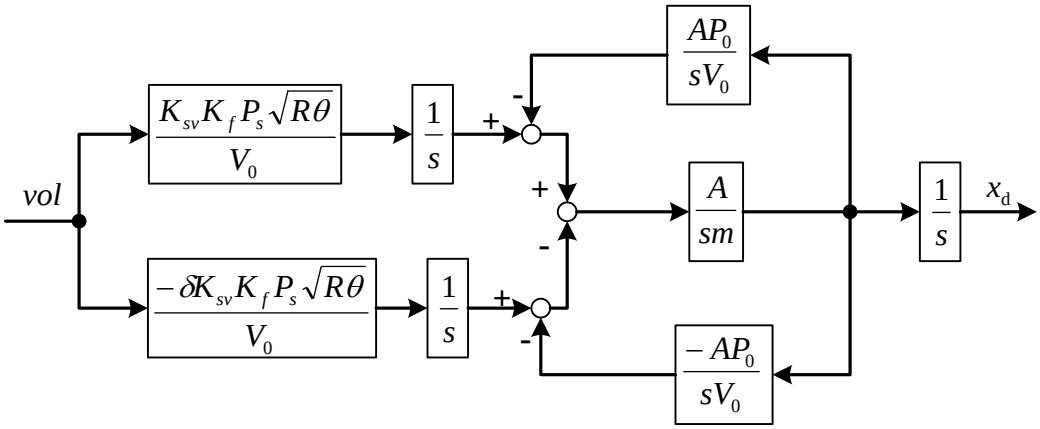

(a)

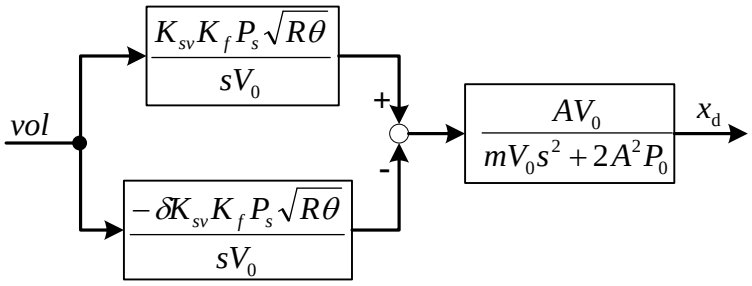

(b)

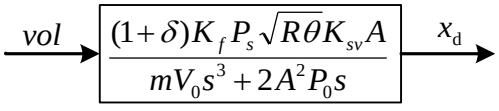

(c)

Fig. 2.6 Simplification of open loop block diagram

2.2.2 HPPSV model

A linearized model of this servo valve is derived to construct an optimized controller. The friction force is negligible because of the air bearing. The dynamic characteristics of the current control loop are sufficiently higher than those of the motion of the spool. The thrust of the VCM is assumed to be proportional to the current input. Airflow through the servo valve generates the flow force acting on the spool. Thus, the governing equations of the servo valve are the equation of motion on the spool, the equation of the VCM, and the equation of the current amplifier as shown in the following equations [26]:

Equation of motion is shown as Eq. (2.13). The flow force in this equation is determined by the pressure and plays as a disturbance.

$$F_M = M_s \ddot{x}_{sp}(t) + d_f(t) \tag{2.13}$$

Equation of the VCM:

$$F_M = K_{Fc} i(t) \tag{2.14}$$

Equation of current amplifier:

$$i = K_i vol(t) \tag{2.15}$$

From these governing equations, the open loop transfer function of the servo valve is as follows:

$$P_v(s) = \frac{K_{Fc} K_i}{M_s} \frac{1}{s^2} \tag{2.16}$$

In Eq. (2.16), the input signal of the transfer function is the control voltage *vol(t)*, and the output signal is the spool position $x_{sp}(t)$. The parameters used in the equations are listed in Table 2.3. In order to control the spool position, a digital controller including a

calculation delay compensator and a disturbance observer is designed and applied to the servo valve [26]. The open loop transfer function is modeled as a second order delay system. Using the state feedback, the closed loop transfer function is given as follows:

$$G_v(s) = \frac{X_{sp}(s)}{VOL(s)} = \frac{{\omega_v}^2}{s^2 + 2\zeta_v\omega_v s + {\omega_v}^2} \tag{2.17}$$

By using this control, the natural frequency (ω_v) and damping ratio (ζ_v) of HPPSV can be set optionally. Fig. 2.7 shows the results of the frequency response test of the spool position with 10% of the full stroke when the natural frequency is set 50 × 2π, 100 × 2π and 300 × 2π rad/s, respectively. As can be seen in the figure, the bandwidth of the HPPSV is up to 300 Hz [47]. Here the damping ratio is fixed at 0.7. From the flow characteristics of HPPSV, the spool positioning is linearly related to the effective cross-sectional area as shown in Fig.2.8.

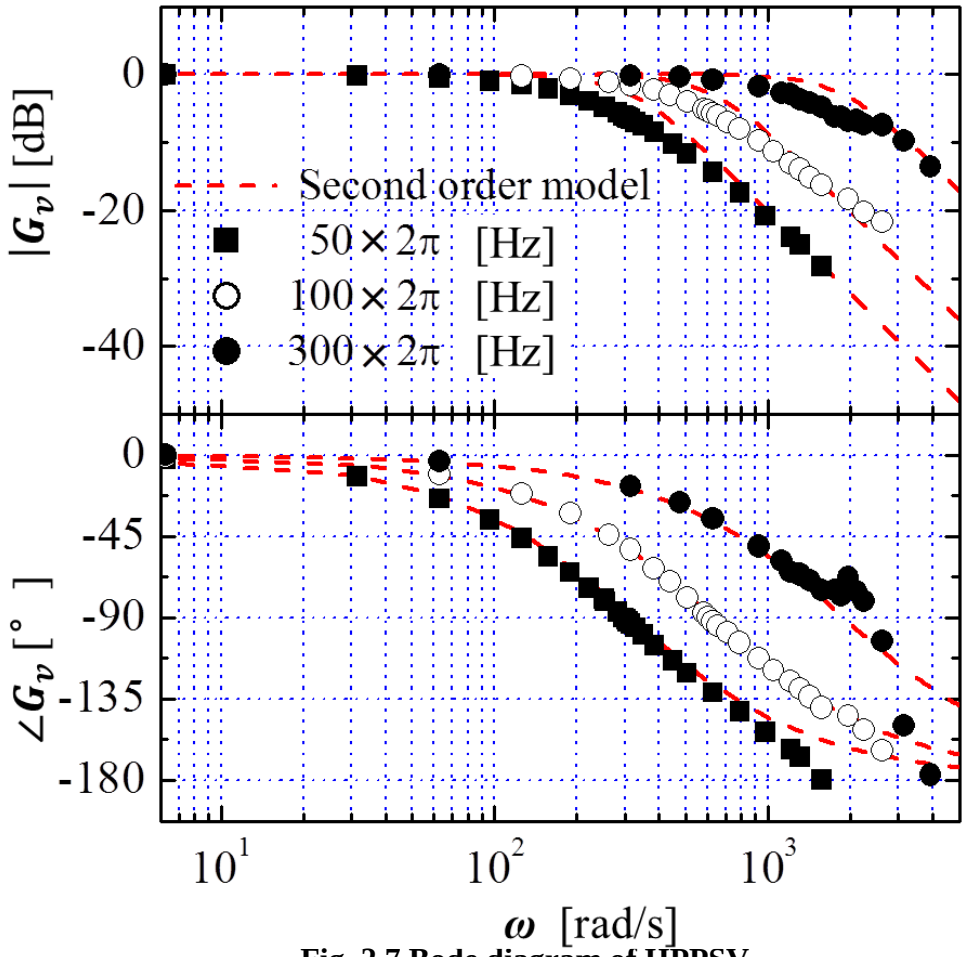

Fig. 2.7 Bode diagram of HPPSV

Table 2.3 Parameters of HPPSV

Symbol	Value
M_s	0.061 [kg]
K_{Fc}	13.62 [N/A]
K_i	1.0 [A/V]
Δt	0.1 [ms]

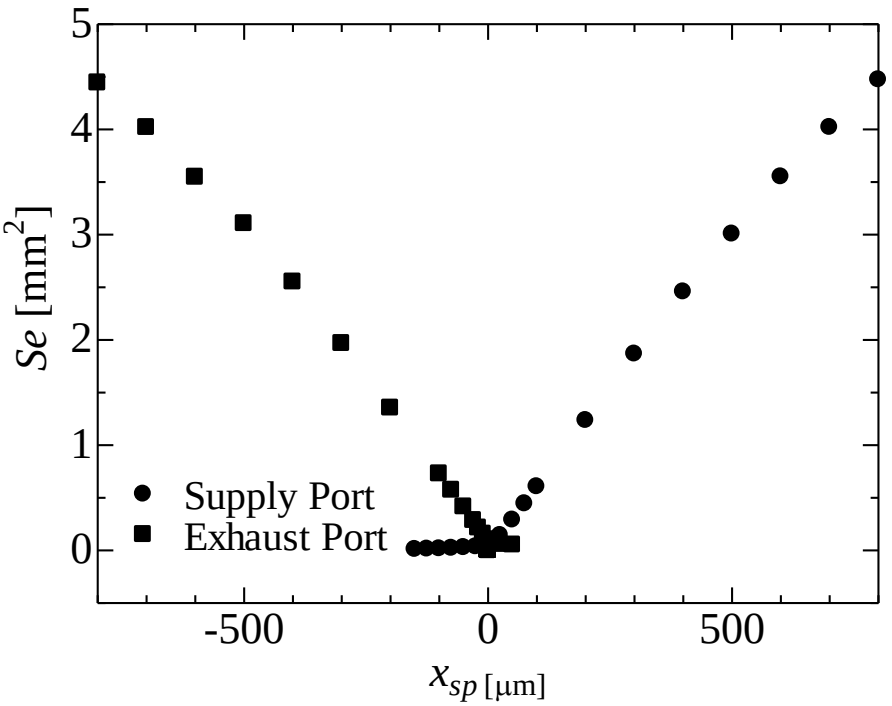

Fig.2.8 Flow characteristics of servo valve

2.2.3 Pipeline model

Fig.2.9 shows an experimental apparatus for modeling pipeline using the HPPSV. Sampling time is 2ms, supply pressure (P_s) 0.25MPa (abs) and downstream pressure (P_a) 0.1MPa (abs). The experimental condition is shown in Table 2.4. The spool position value (x_{sp}) and isothermal chamber pressure [48] (P_c) are measured. The HPPSV's spool positioning is linearly related to the effective cross-sectional area as shown in Fig.2.8. The upstream mass flow can be calculated by the HPPSV's spool positioning. While the downstream mass flow can be calculated by the pressure change in the isothermal chamber with the state equation. The maximum pipeline mass flow is 2.5×10^{-5} m^3/s and the average 1.0×10^{-5} m^3/s and the Reynolds number 387.75. The flow is laminar. As shown in Fig.2.10, the up- and downstream pipeline pressures differ only slightly, so the pipeline transfer function is given by mass flow alone. Connected pipeline features are shown in Fig.2.11. According to this figure, the pipeline model is approximated as a 2nd order lag model [48], as shown in the formula below. Transfer function input and output are the up- and downstream mass flow.

$$G_t(s) = \frac{G_{OUT}(s)}{G_{IN}(s)} = \frac{{\omega_t}^2}{s^2 + 2\zeta_t\omega_t s + {\omega_t}^2} \tag{2.18}$$

The natural frequency (ω_t) and damping ratio (ζ_t) of pipelines is obtained by the characteristic of the connected pipeline, e.g., as shown in Fig.2.11 a pipeline 1.0m in length and 5.0mm in diameter, from the approximate curve, the natural frequency (ω_t) and the damping ratio (ζ_t) of pipelines is known as 80Hz and 0.005. The Bode diagrams with different parameters obtained from experimental results are shown in Figs.2.12 and 2.13. Based on Bode diagrams, the natural frequency (ω_t) and damping ratio (ζ_t) of pipelines with different parameters obtained from experimental results are shown in Tables 2.5 and 2.6[48].

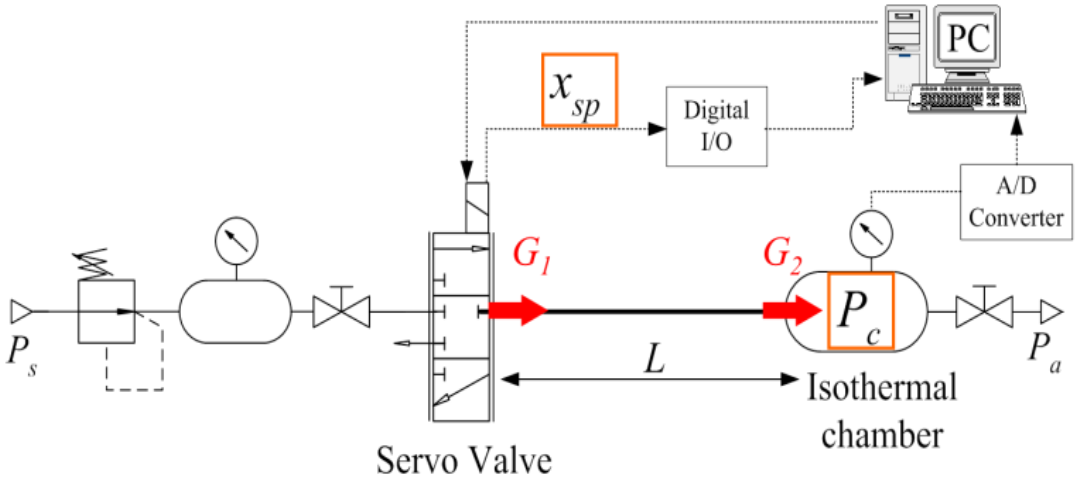

Fig. 2.9 Experimental apparatus

Table 2.4 Experimental conditions

Symbol	Value	
P_s	300	[kPa](abs)
P_a	101.32	[kPa] (abs)
Δt	2	[ms]
L	0.5, 1.0, 2.0	[m]
D	4.0, 6.5, 8.0	[mm]

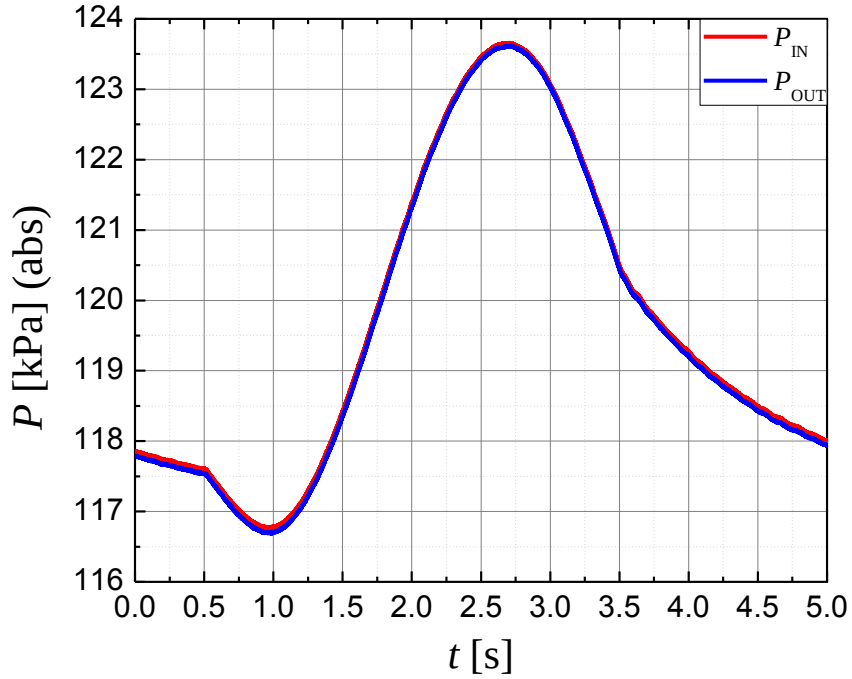

Fig.2.10 Pipeline up- and downstream pressure (*L* = 1.0m, *D* = 8.0mm)

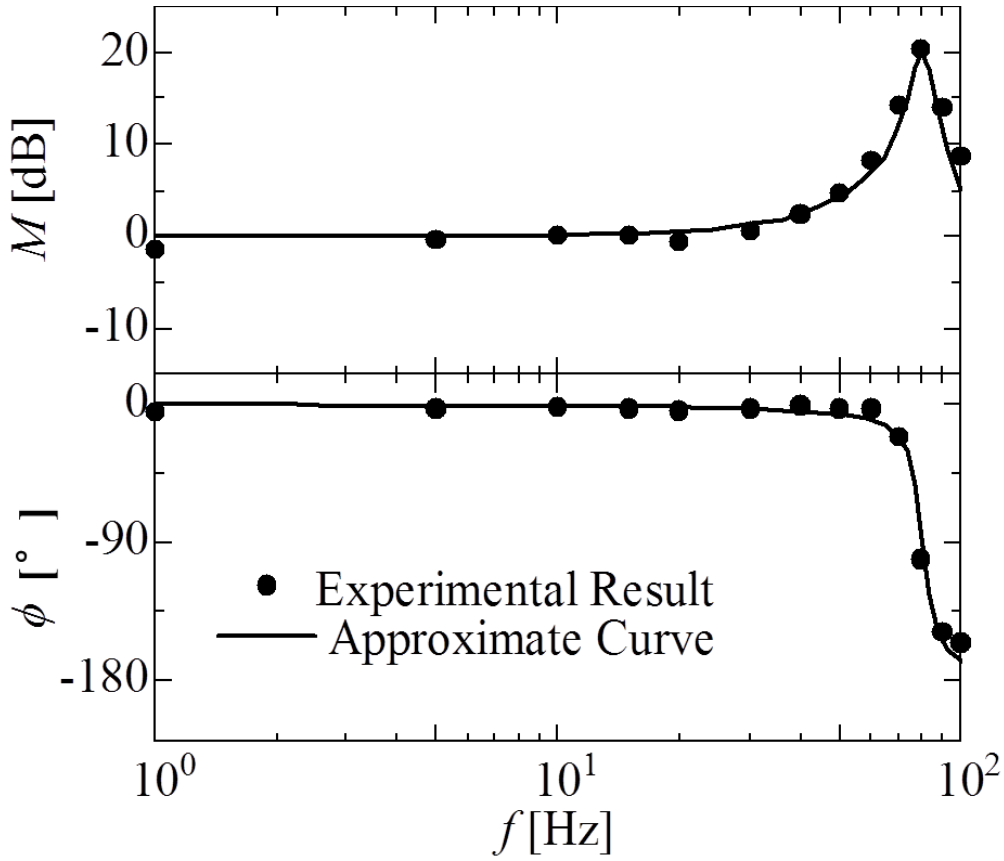

Fig.2.11 Connected pipelines characteristic (*L* = 1.0m, *D* = 5.0mm)

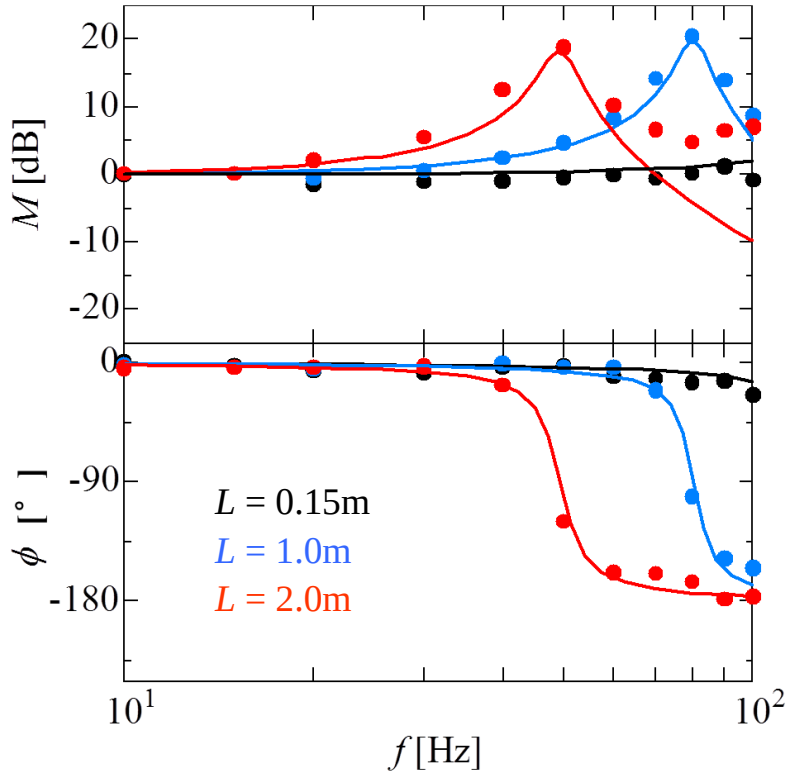

Fig.2.12 Bode diagram (*D* = 5.0mm)

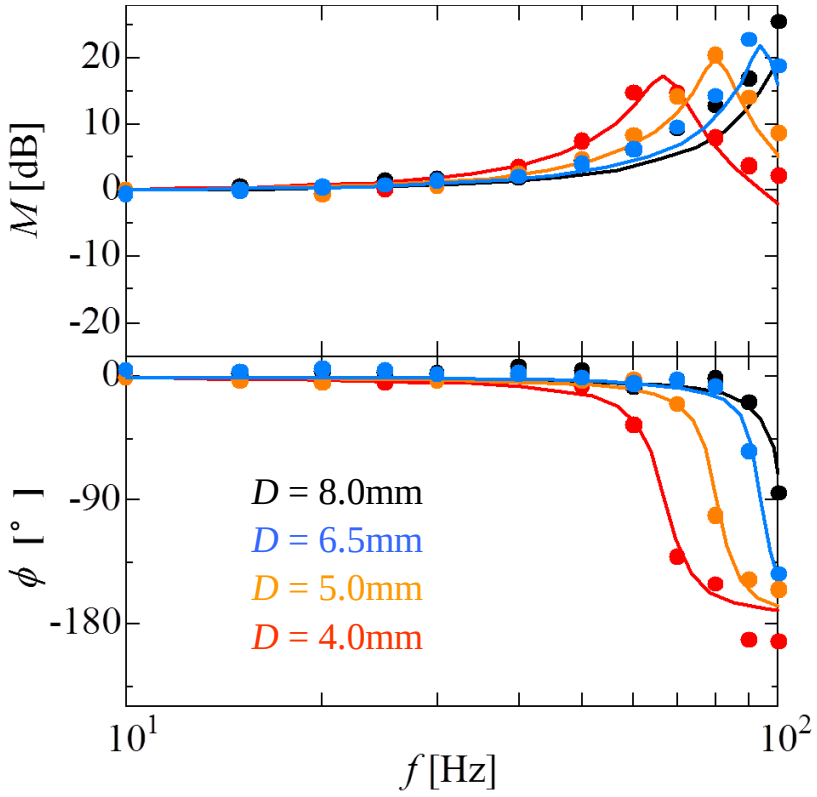

Fig.2.13 Bode diagram (*L* = 1.0m)

Table 2.5 Pipeline parameters (*D* = 4.0mm)

L [m]	ω_t [rad/s]	ζ_t
0.5	110×2π	0.068
1.0	67×2π	0.068
2.0	41×2π	0.07

Table 2.6 Pipeline parameters (*D* = 8.0mm)

L [m]	ω_t [rad/s]	ζ_t
0.5	146×2π	0.06
1.0	102×2π	0.048
2.0	60×2π	0.050

2.3 Control method

In order to reduce trajectory errors, a linear model which is as similar to the real system as possible should first be obtained. In the following section, the linear model with different orders of the system is illustrated. And the comparison of the linear model is also presented. The closed loop block diagram of pneumatic servo table system is shown in Fig.2.14. In this control model, a PPD^2 controller involving position, velocity and acceleration feedback is used and Kalman filter is used. K_a, K_v and K_p are the gains of acceleration, velocity and position. l_1, l_2 and l_3 are equal to 530.5, 140739.9 and 1.85×10^7 respectively.

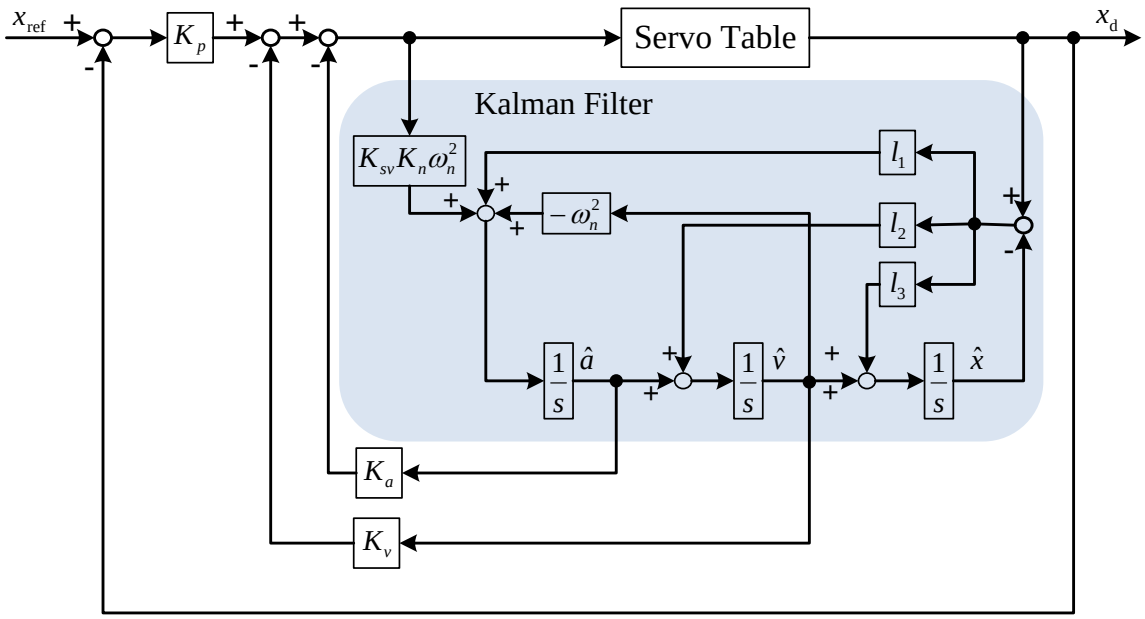

Fig.2.14 Closed loop block diagram of servo table system

2.3.1 3rd order linear model

At first, we considered only the pneumatic actuator when designing the control model because the servo valve response is much faster than that of the pneumatic actuator. The servo table system is approximated as a 3rd order linear model. Fig.2.15 shows the block diagram.

The closed loop transfer function of the pneumatic actuator is given as:

$$G_3(s) = \frac{A_3}{s^3 + A_1 s^2 + A_2 s + A_3} \tag{2.19}$$

$$A_1 = K_a K_n K_{sv} {\omega_n}^2 \tag{2.20}$$

$$A_2 = (K_v K_n K_{sv} + 1){\omega_n}^2 \tag{2.21}$$

$$A_3 = K_p K_n K_{sv} {\omega_n}^2 \tag{2.22}$$

To determine gains by the α-β method [49], the transfer function is normalized using normalized Laplace operator τ_1 and dimensionless parameters α and β:

$$\tau_1 = \sqrt[3]{A_3 t} \tag{2.23}$$

$$G_{3n}(s_1) = \frac{1}{{s_1}^3 + \alpha {s_1}^2 + \beta s_1 + 1} \tag{2.24}$$

Here,

$$\alpha = A_1 / \sqrt[3]{A_3}, \quad \beta = A_2 / \sqrt[3]{{A_3}^2} \tag{2.25}$$

When α=2.0 and β=2.0 [49], K_v and K_a can be calculated.

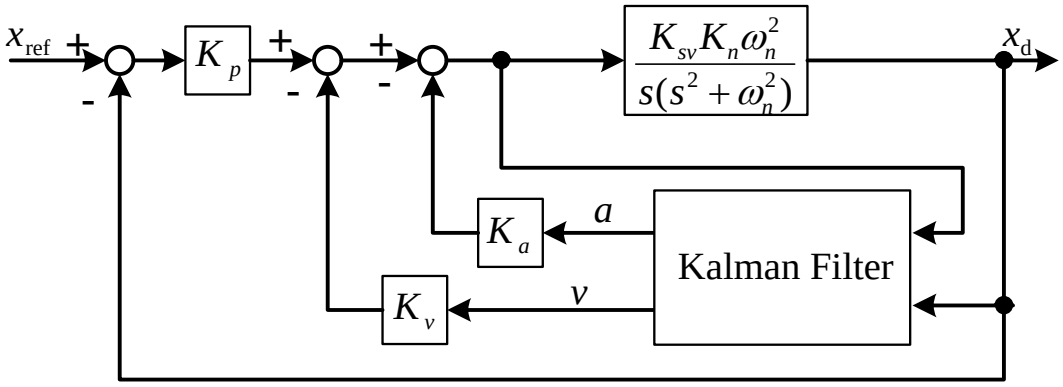

Fig.2.15 Block diagram of servo table system（3rd order linear model）

2.3.2 7th order linear model

When two elements – the pipeline and the servo valve-- are considered, the linear model becomes 7th order. The block diagram of the system is shown in Fig.2.16 and the simplification of the block diagram is shown in Fig.2.17.The system's closed loop transfer function is given as:

$$G_7(s) = \frac{w^7}{s^7 + C_1 w s^6 + C_2 w^2 s^5 + C_3 w^3 s^4 + C_4 w^4 s^3 + C_5 w^5 s^2 + C_6 w^6 s + w^7} \quad (2.26)$$

$$C_1 w = 2(\zeta_t \omega_t + \zeta_v \omega_v) \quad (2.27)$$

$$C_2 w^2 = {\omega_t}^2 + {\omega_n}^2 + {\omega_v}^2 + 4\zeta_t \zeta_v \omega_t \omega_v \quad (2.28)$$

$$C_3 w^3 = 2\{(\zeta_t \omega_t + \zeta_v \omega_v){\omega_n}^2 + \omega_t \omega_v (\zeta_t \omega_v + \zeta_v \omega_t)\} \quad (2.29)$$

$$C_4 w^4 = (\omega_t \omega_v)^2 + {\omega_n}^2({\omega_t}^2 + {\omega_v}^2 + 4\zeta_t \zeta_v \omega_t \omega_v) \quad (2.30)$$

$$C_5 w^5 = 2\omega_t \omega_v {\omega_n}^2(\zeta_t \omega_v + \zeta_v \omega_t + K_a K_n K_{sv}(\omega_t \omega_v \omega_n)^2 \quad (2.31)$$

$$C_6 w^6 = (\omega_t \omega_v \omega_n)^2(1 + K_v K_n K_{sv}) \quad (2.32)$$

$$w^7 = (\omega_t \omega_v \omega_n)^2 K_p K_n K_{sv} \tag{2.33}$$

When pipelines with different parameters are selected, the corresponding natural frequency (ω_t) and damping ratio (ζ_t) are found from Tables 2.5 and 2.6. Servo valve dynamics are set optionally.

The ITAE index is used to determine control gain [50]. The numerical coefficients in the characteristic equation are arranged in the form. Take the 5th order transfer function as an example. The coefficient of s^5 is equal to 1. The coefficient of s^4 is small and the coefficients become larger until the coefficient of s^2, the value of which is largest. The coefficient of s^1 is larger than the coefficient of s^0. Since the four equations are determined by 3 unknown parameters, this 7th order linear model cannot be as well as required by the ITAE index. We designed control gain as follows:

The value of K_p and w is set, then the value from C_1 to C_4 obtained. The range of the other two coefficients is known based on the regular pattern above. The optimum value is obtained by plotted the step response with different value of C_5 and C_6. For pipelines 0.5m long and 4.0mm in diameter, K_p is set as 1.0 and C_5 and C_6 are selected as 45 and 11.

The value of K_p is selected, then K_v and K_a are calculated based on pipeline and servo valve parameters as follows:

$$K_{a=} \frac{C_5 w^{5/7} - 2\omega_t \omega_v {\omega_n}^2 (\zeta_t \omega_v + \zeta_v \omega_t)}{K_n K_{sv} (\omega_t \omega_v \omega_n)^2} \tag{2.34}$$

$$K_{v=} \frac{C_6 w^{6/7} - (\omega_t \omega_v \omega_n)^2}{K_n K_{sv} (\omega_t \omega_v \omega_n)^2} \tag{2.35}$$

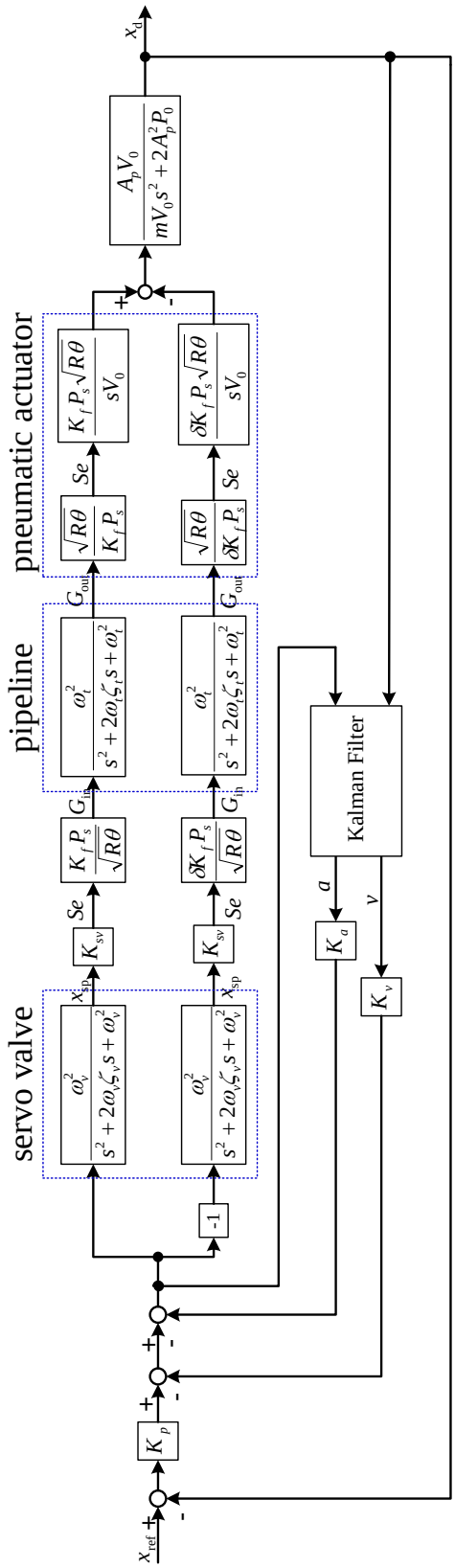

Fig.2.16 Block diagram of servo table system（7^{th} order linear model）

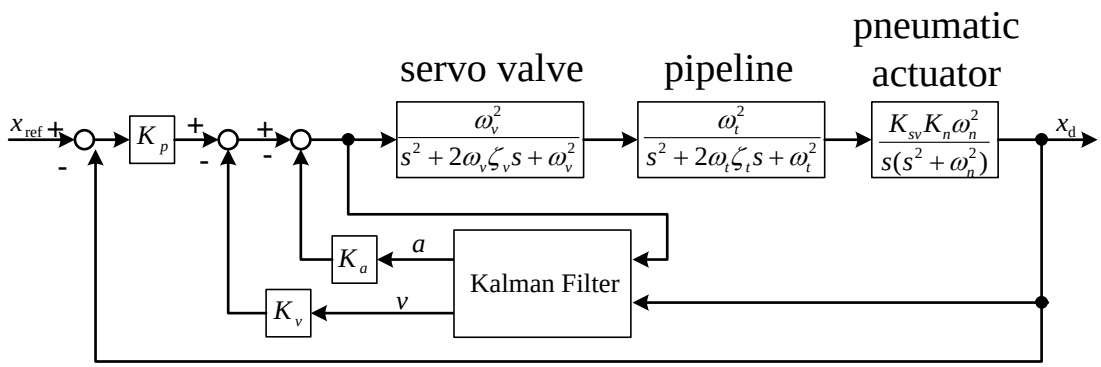

Fig.2.17 Simplification of block diagram（7th order linear model）

2.3.3 5th order linear model

Although the 7th order linear model is more similar with the real system than 3rd order model, it also becomes complicated, especially a feed forward is needed in the control method. Since in the real system, the input signal must be derived seven times to realize a 7th order feed forward. The curve will become complicated and hard to be realized in the real system. A reduction in the model's order is necessary.

Fig.2.18 shows the pole loci of the 7th order linear model. It is clear that two poles are much farther from the imaginary axis than the other five poles. In this case the influence of those two poles can be neglected. Therefore, the model of the system can be simplified to a 5th order model.

In this 5th order linear model, the servo valve and pipeline are treated as one element and approximated as a 2nd lag model. The block diagram is shown in Fig.2.19. The closed loop transfer function of the whole system can be expressed as:

$$G_5(s)=\frac{w^5}{s^5+B_1ws^4+B_2w^2s^2+B_3w^3s^2+B_4w^4s+w^5} \tag{2.36}$$

$$B_1w=2\omega_o\zeta_o \tag{2.37}$$

$$B_2 w^2 = {\omega_o}^2 + {\omega_n}^2 \tag{2.38}$$

$$B_3 w^3 = 2{\omega_n}^2 \zeta_o \omega_o + K_a K_n K_{sv} (\omega_n \omega_o)^2 \tag{2.39}$$

$$B_4 w^4 = (\omega_n \omega_o)^2 (1 + K_v K_n K_{sv}) \tag{2.40}$$

$$w^5 = (\omega_n \omega_o)^2 K_p K_n K_{sv} \tag{2.41}$$

Here the ITAE index [50] is also used to calculate the gains. K_p is selected, K_v and K_a can be calculated based on the value of operator *w*.

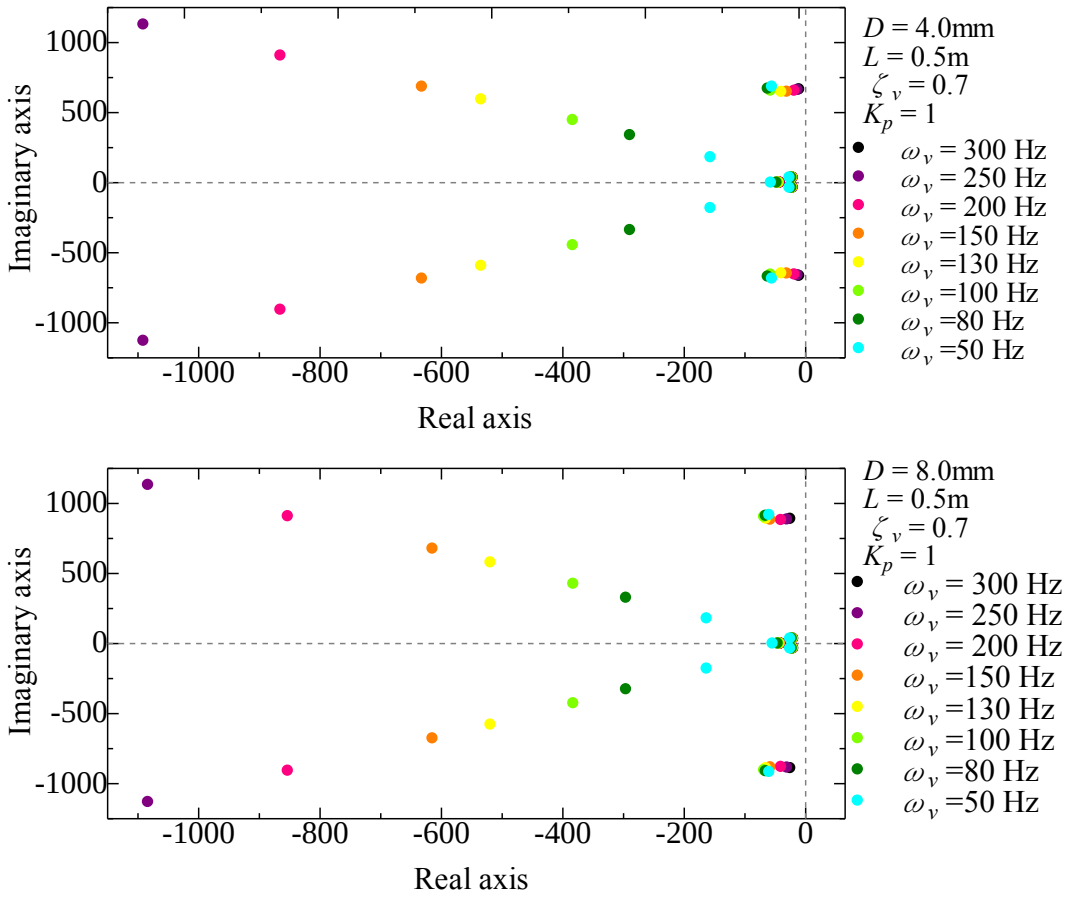

Fig.2.18 Pole loci of servo table system (L = 0.5m, ζ_v = 0.7)

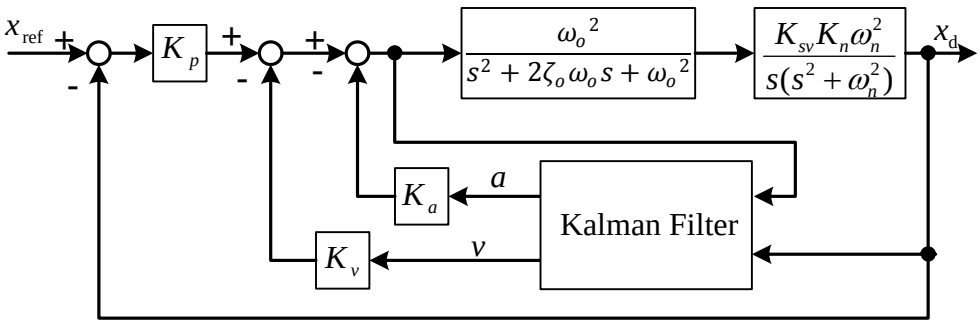

Fig.2.19 Block diagram of servo table system（5th order linear model）

2.4 Comparison of linear model experimentally

The comparison of experimental and simulation results will be represented to find a model matching up well with the real system. Table 2.7 shows the experimental and simulation conditions. The trajectory is shown in Fig.2.20.

Table 2.7 Experimental and simulation conditions

Symbol		Value	
x_d		100	[mm]
ω_v		100	[Hz]
ζ_v		0.70	[-]
ω_t		110	[Hz]
ζ_t		0.068	[-]
L		0.5	[m]
D		4.0	[mm]
P_s		251.3	[kPa] (abs)
3rd order	K_p	1.0	[V/m]
	K_v	5.49×10^{-2}	[V·s/m]
	K_a	1.57×10^{-3}	[V·s^2/m]
5th order	K_p	1.0	[V/m]
	K_v	6.48×10^{-2}	[V·s/m]
	K_a	1.50×10^{-3}	[V·s^2/m]
7th order	K_p	1.1	[V/m]
	K_v	4.96×10^{-2}	[V·s/m]
	K_a	1.10×10^{-3}	[V·s^2/m]

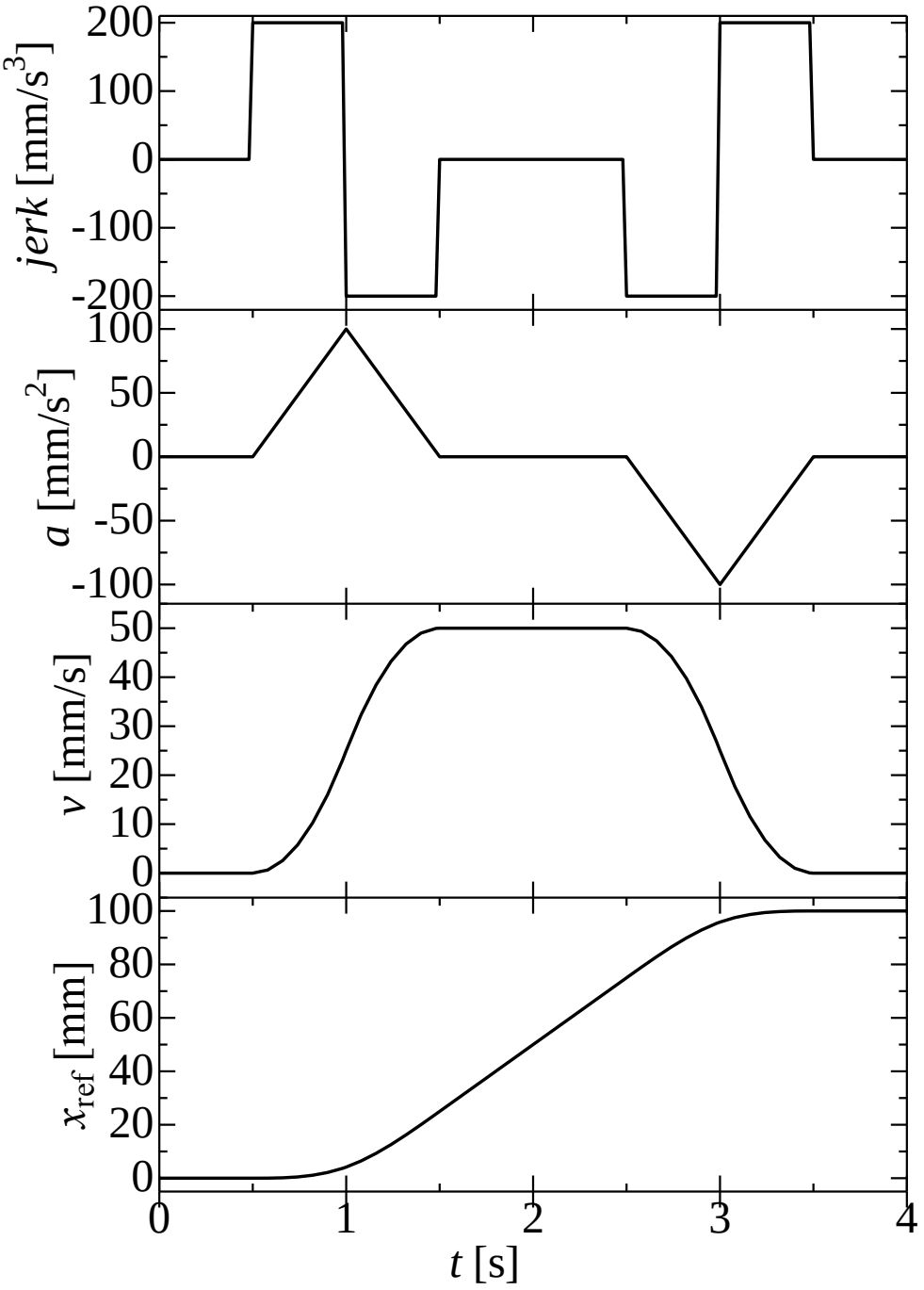

Fig.2.20 Input curve (3rd order)

2.4.1 3rd order linear model

Fig.2.21 compares experimental and simulation results. The gain of acceleration (K_a) is 1.57×10^{-3} V·s^2/m, of velocity (K_v) 5.49×10^{-2} V·s/m and of positioning (K_p) 1.0 V/m. The upper and lower figures show the positioning and the trajectory errors, respectively. Note that the large discrepancy between experimental and simulation results, e.g., the difference is 540μm in maximum.

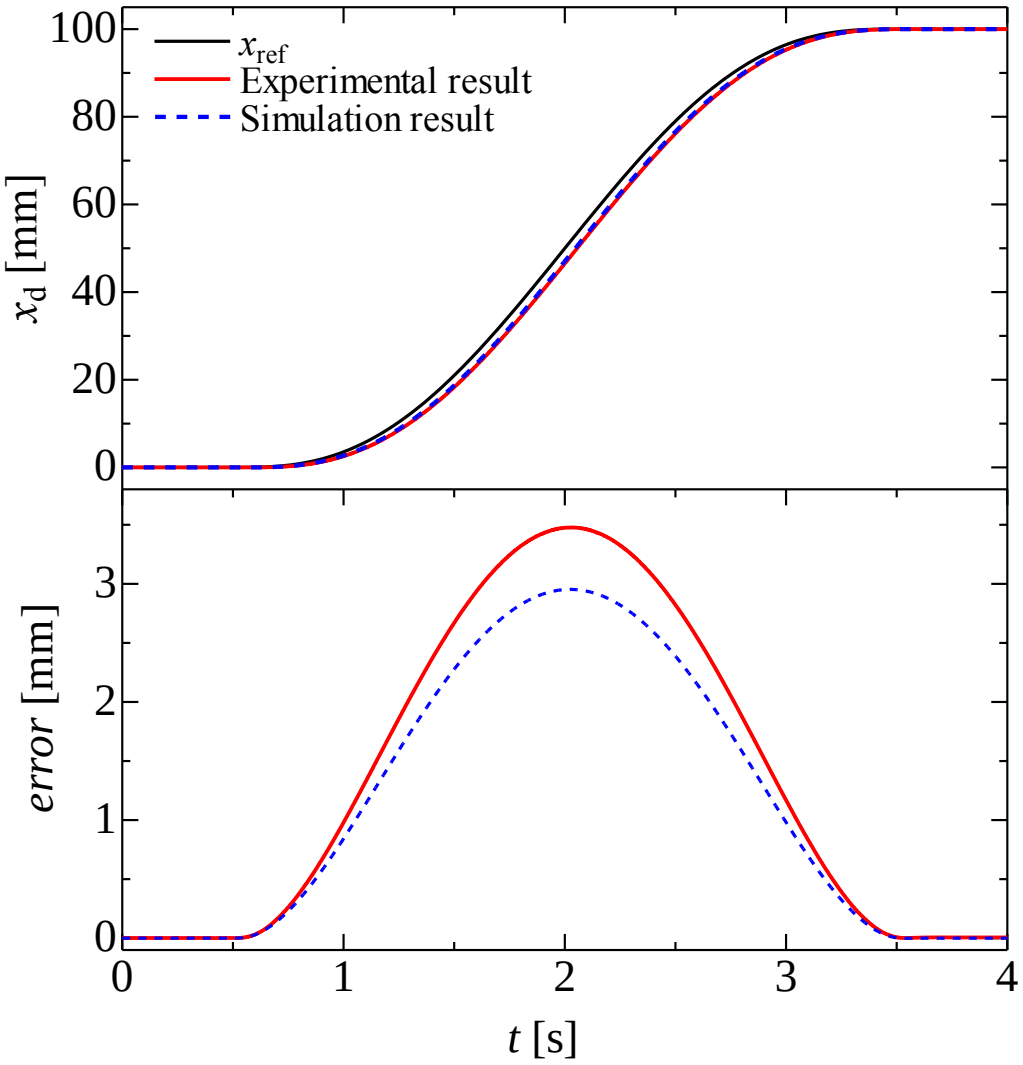

Fig.2.21 Experimental and simulation results (3rd order)

(D = 4.0mm, L = 0.5mm, ω_v=100Hz, ζ_v = 0.7)

2.4.2 7th order linear model

Experiments have been done using the gains determined by the ITAE index. The gain of acceleration (K_a) is 1.50×10^{-3} V·s^2/m, of velocity (K_v) 6.48×10^{-2} V·s/m and of positioning (K_p) 1.0 V/m. Results are shown in Fig.2.22. The upper and lower figures show the positioning and the trajectory errors, respectively. No difference between experimental and simulation results is obvious in the lower part. In Fig.2.23, an enlargement of Fig.2.22's lower part, the difference is 14μm -- much smaller than in the case of a 3rd order model.

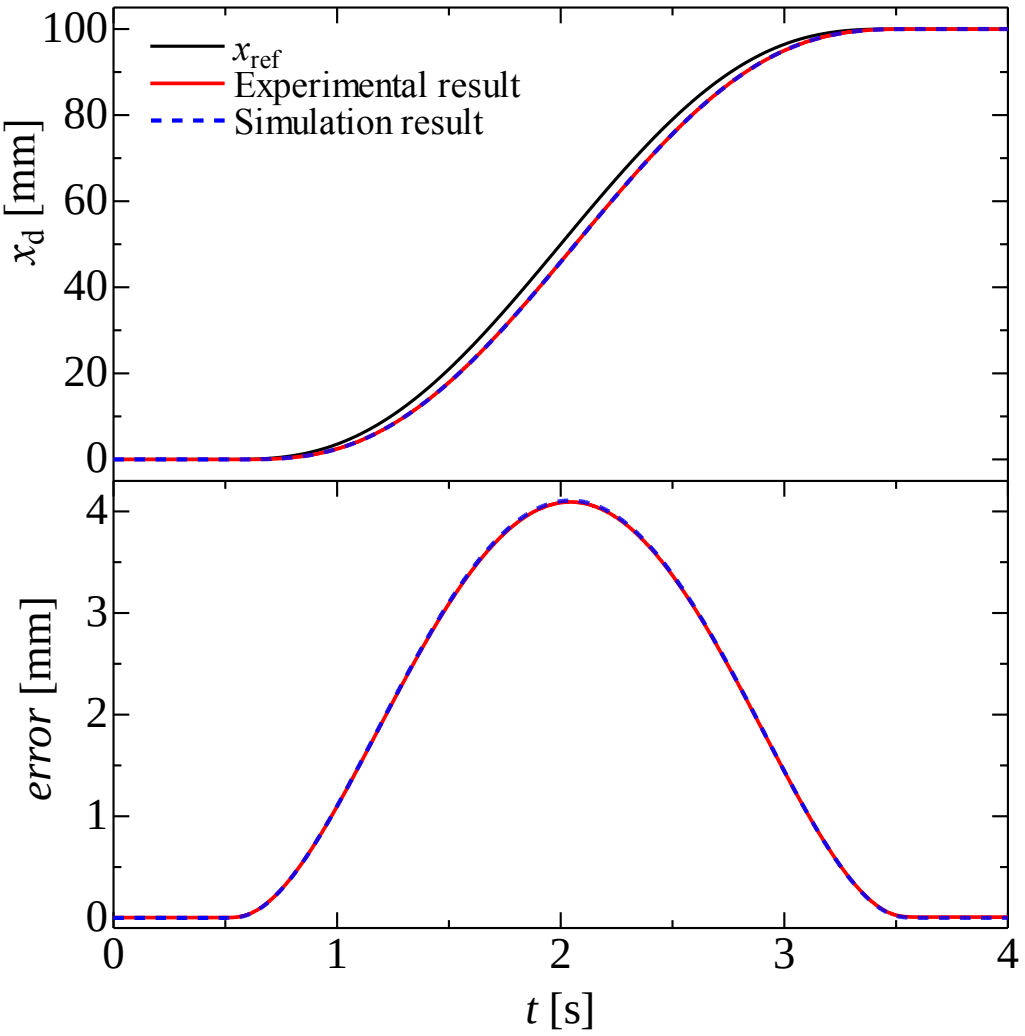

Fig.2.22 Experimental and simulation results (7th order)

(D = 4.0mm, L = 0.5mm, ω_v=100Hz, ζ_v = 0.7)

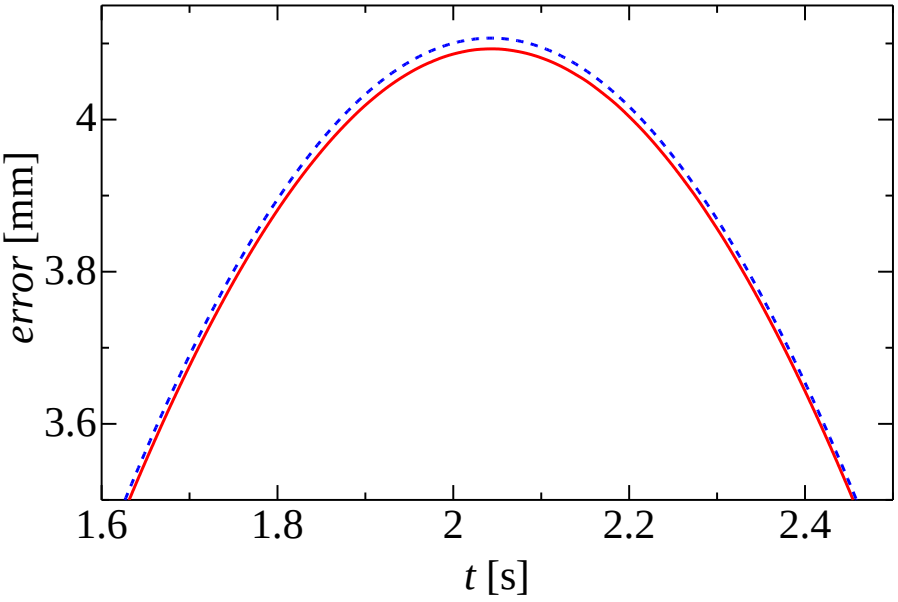

Fig.2.23 Enlargement of Fig.2.22's lower part

2.4.3 5th order linear model

Experimental and simulation results are compared in Fig.2.24. The gain of acceleration (K_a) is 1.10×10^{-3} V·s^2/m, of velocity (K_v) 4.96×10^{-2} V·s/m and of positioning (K_p) 1.1 V/m. The upper and lower figures show the positioning and the trajectory errors, respectively. No difference between experimental and simulation results is obvious in the lower part. In Fig.2.25, enlargement of Fig.2.24's lower part, the difference is 22μm. Based on this result, the pneumatic servo table system is approximated as a 5th order linear model. The same tendency can also be seen with a pipeline diameter of 8mm.

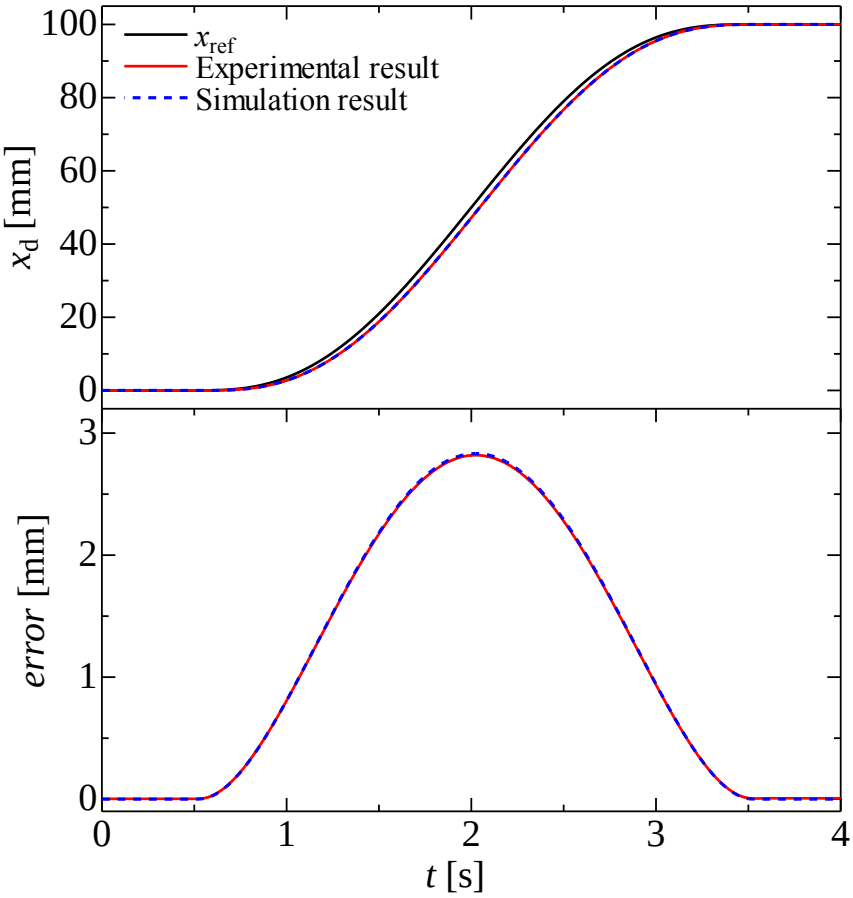

Fig.2.24 Experimental and simulation results (5th order)

(D = 4.0mm, L = 0.5m, ω_v=100Hz, ζ_v = 0.7)

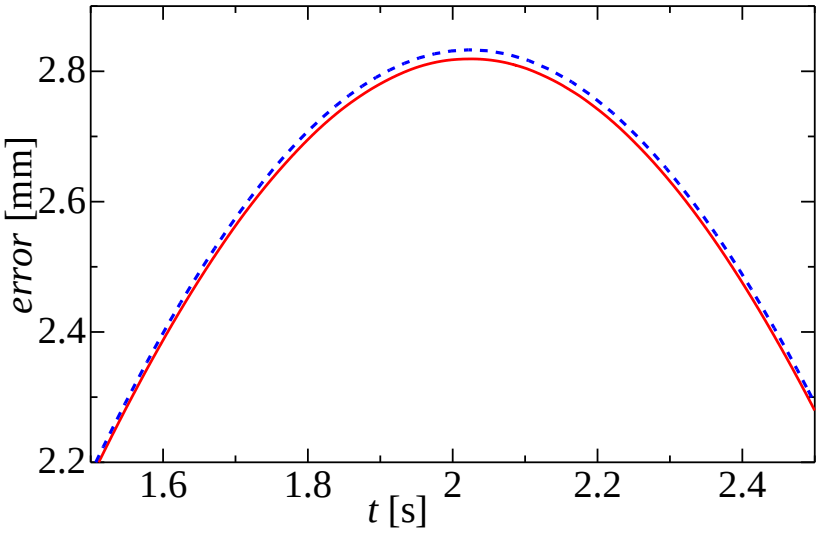

Fig.2.25 Enlargement of Fig. 2.24's lower part

2.5 Trajectory control method

2.5.1 Feed forward

Based on the suitable linear model obtained above, a feed forward compensator can be designed. The block diagram of the pneumatic servo table with feed forward compensator is shown in Fig.2.26. Since the transfer function of the servo table and the controller are decided, the part in the blue box can be expressed in one formula. Here it is defined as *G(s)*.

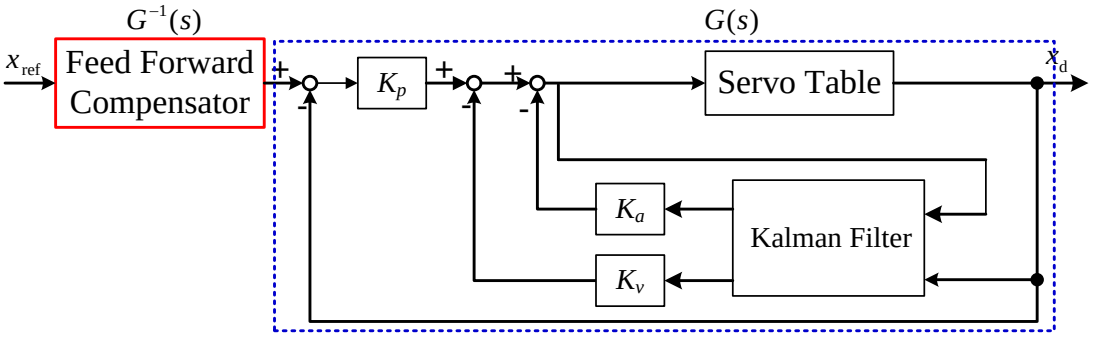

Fig.2.26 Block diagram of servo table system（with feed forward）

2.5.2 3rd order feed forward

Although there is a discrepancy between the simulation and experimental results when the model of the whole system is approximated as a 3rd order linear model, the model's order is low and the corresponding feed forward can easily be realized in the real system. For this reason, a 3rd order feed forward is also designed. The expression is shown in Eq. (2.42).

$$G_3^{-1}(s) = \frac{s^3 + A_1 s^2 + A_2 s + A_3}{A_3} \tag{2.42}$$

2.5.3 5th order feed forward

The experimental and simulation results can match up well with a 5th order linear model. Based on this result, a 5th order feed forward has been designed. The expression is shown in Eq. (2.43).

$$G_5^{-1}(s) = \frac{s^5 + B_1 w s^4 + B_2 w^2 s^2 + B_3 w^3 s^2 + B_4 w^4 s + w^5}{w^5} \tag{2.43}$$

2.6 Experimental results

The experimental results with 3rd and 5th order feed forwards are represented. Table 2.8 shows the experimental conditions.

Table 2.8 Experimental conditions

Symbol			Value	
x_d			100, 70, 50, 20	[mm]
ω_v			100	[Hz]
ζ_v			0.70	[-]
P_s			251.3	[kPa] (abs)
L			0.5, 1.0	[mm]
D			4.0, 8.0	[m]
D = 4.0mm, L = 0.5m	ω_t		102	[Hz]
	ζ_t		0.048	[-]
	3rd order feed forward	K_p	1.2	[V/m]
		K_v	6.21×10^{-2}	[V·s/m]
		K_a	1.67×10^{-3}	[V·s^2/m]
	5th order feed forward	K_p	1.2	[V/m]
		K_v	5.40×10^{-2}	[V·s/m]
		K_a	1.30×10^{-3}	[V·s^2/m]
D = 8.0mm, L = 1.0m	ω_t		110	[Hz]
	ζ_t		0.068	[-]
	3rd order feed forward	K_p	1.5	[V/m]
		K_v	7.23×10^{-2}	[V·s/m]
		K_a	1.79×10^{-3}	[V·s^2/m]
	5th order feed forward	K_p	1.5	[V/m]
		K_v	1.80×10^{-3}	[V·s/m]
		K_a	6.00×10^{-2}	[V·s^2/m]

2.6.1 With 3rd order feed forward

The input curve is shown in Fig.2.20 which can be derived three times, when the feed forward is 3rd order. In addition, the natural frequency (ω_v) of the servo valve chosen is 100Hz and damping ratio (ζ_v) chosen is 0.70. The supply pressure is 0.25MPa. The experimental conditions are shown in Table 2.8. In this section, experimental results with two kinds of pipelines are presented to explain the trajectory method.

Experiments with different pipelines have been done. The experimental results using pipeline with 4mm in diameter and 0.5m in length are shown in Fig.2.27. The gain of acceleration (K_a) is 1.67×10^{-3} V·s^2/m, of velocity (K_v) 6.21×10^{-2} V·s/m and of positioning (K_p) 1.2 V/m. Compared with Fig.2.28, which is an enlargement of Fig.2.27's lower part, it is clear that the trajectory errors with the 3rd order feed forward becomes much smaller than that without the feed forward. The maximum value is reduced from 3.27×10^{3}μm to 22.67μm. Fig.2.29 shows experimental results with 8mm in diameter and 1.0m in length pipeline. The gain of acceleration (K_a) is 1.79×10^{-3} V·s^2/m, of velocity (K_v) 7.23×10^{-2} V·s/m and of positioning (K_p) 1.5 V/m. Compared with Fig.2.30, which is an enlargement of Fig.2.29's lower part, it is clear that the maximum value of trajectory errors with the 3rd order feed forward is reduced from 3.036×10^{3}μm to 21.50μm. Based on the results, when the 3rd order feed forward is used in the control system, the trajectory errors are decreased significantly.

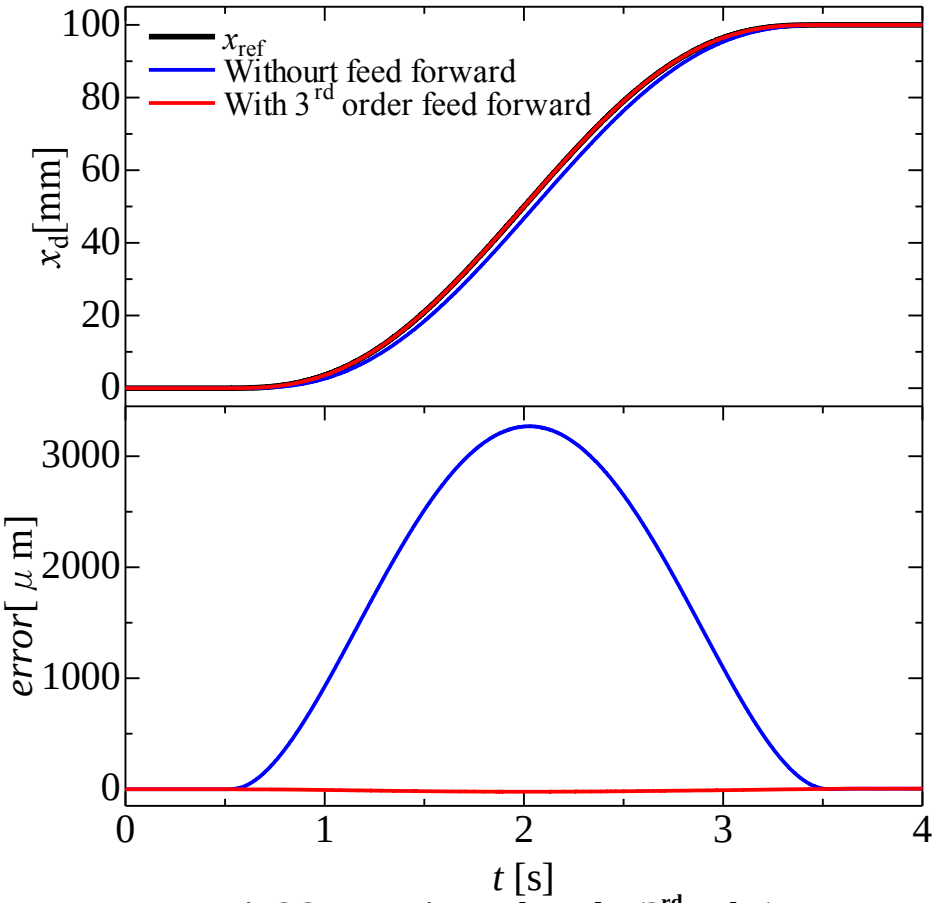

Fig.2.27 Experimental results (3rd order)

(*D* = 4.0mm, *L* = 0.5m, ω_v=100Hz, ζ_v = 0.7)

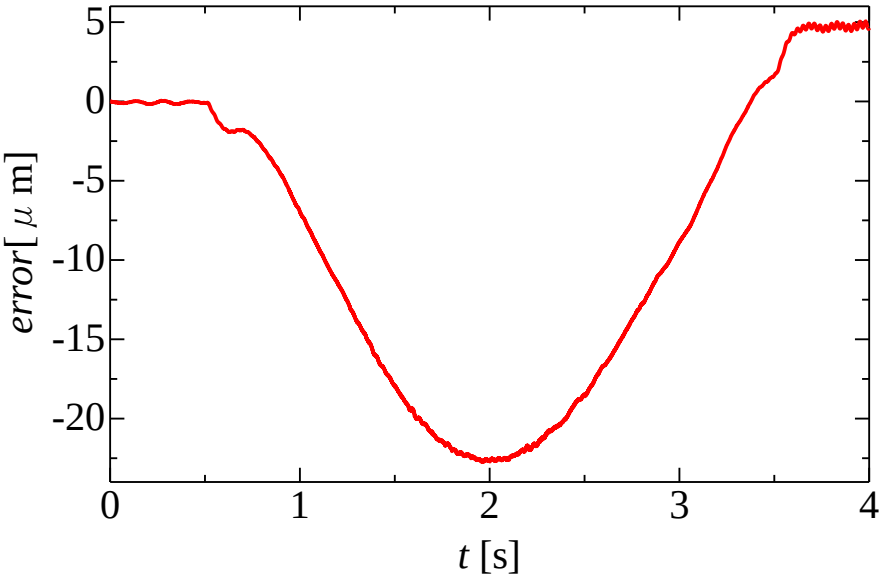

Fig.2.28 Enlargement of Fig.2.27's lower part

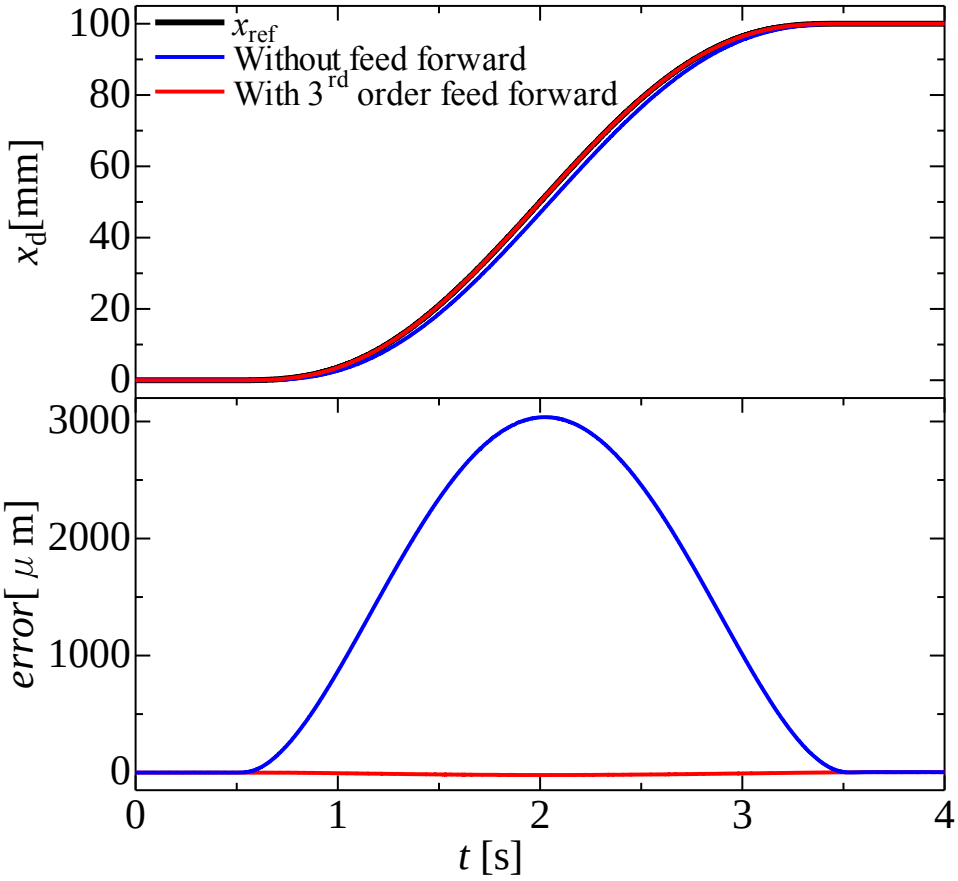

Fig.2.29 Experimental results (3rd order)

(D = 8.0mm, L = 1.0m, ω_v=100Hz, ζ_v = 0.7)

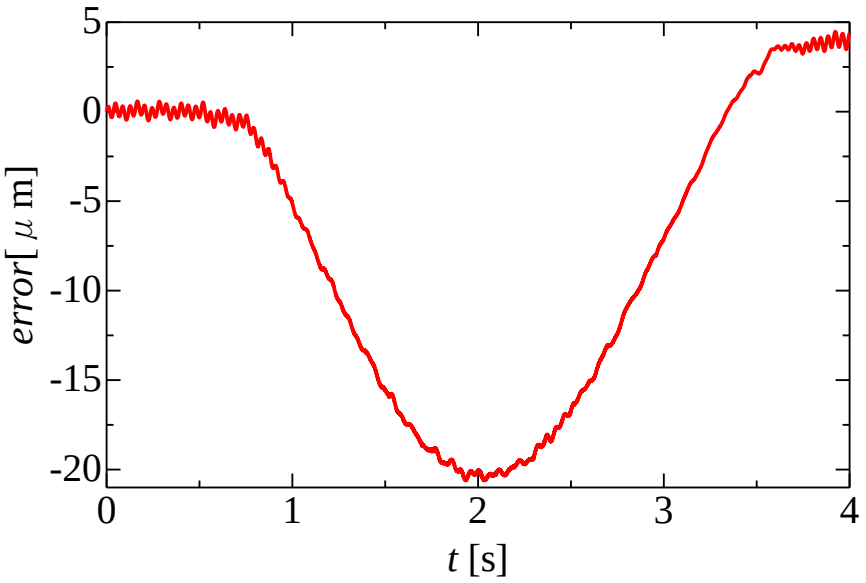

Fig.2.30 Enlargement of Fig.2.29's lower part

2.6.2 With 5th order feed forward

When there is a 5th order feed forward in the system, the input curve which can be derived five times is shown in Fig.2.31. In addition, the natural frequency (ω_v) of the servo valve chosen is 100Hz and damping ratio (ζ_v) chosen is 0.70, respectively. The supply pressure is 0.25MPa. The experimental conditions are shown in Table 2.8. In this section, experimental results with two kinds of pipelines are presented to explain the trajectory method.

Experiments with different pipelines have been done. The experimental results using pipeline with 4mm in diameter and 0.5m in length are shown in Fig.2.32. For the 5th order feed forward, the gain of acceleration (K_a) is 1.30×10^{-3} V·s^2/m, of velocity (K_v) 5.40×10^{-2} V·s/m and of positioning (K_p) 1.2 V/m. While for the 3rd feed forward, the gain of acceleration (K_a) is 1.67×10^{-3} V·s^2/m, of velocity (K_v) 6.21×10^{-2} V·s/m and of positioning (K_p) 1.2 V/m. The input curve used in these experiments is shown in Fig.2.31. In Fig.2.32, it is clear that the trajectory errors with the 5th order feed forward are smaller than that with the 3rd order feed forward. The maximum value is reduced by 21.07μm, from 22.67μm to 1.60μm. Fig.2.33 shows experimental results with 8mm in diameter and 1.0m in length pipeline. For the 5th order feed forward, the gain of acceleration (K_a) is 1.80×10^{-3} V·s^2/m, of velocity (K_v) 6.00×10^{-2} V·s/m and of positioning (K_p) 1.5 V/m. While for the 3rd order feed forward, the gain of acceleration (K_a) is 1.79×10^{-3} V·s^2/m, of velocity (K_v) 7.23×10^{-2} V·s/m and of positioning (K_p) 1.5 V/m. It is clear that the trajectory errors with the 5th order feed forward is smaller than that with the 3rd order feed forward. The maximum value is reduced by 21.20μm, from 21.50μm to 0.30μm. Compared with Fig.2.28 and 2.30 the 5th order feed forward can decrease the maximum trajectory error by about 20μm, compared with the 3rd order feed forward used. The steady state errors are caused by the leakage of the joints used in the system. Another reason is that there are two chambers in pneumatic servo table system to actuate the slider. The movement in both two chambers cannot be exactly same, which also will cause these steady state errors. Because of these reasons, no matter the control system is improved; the steady state errors cannot be avoided.

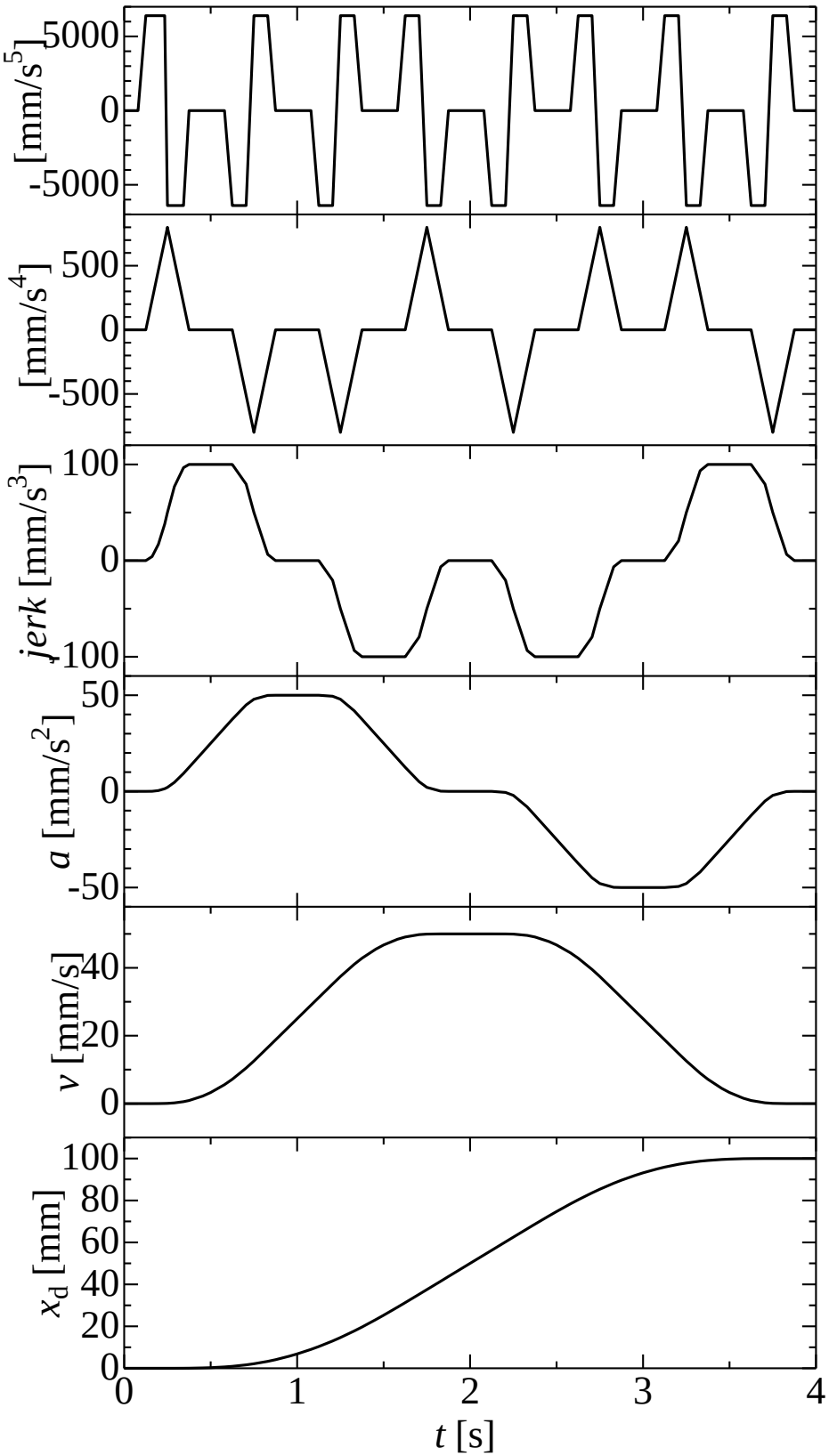

Fig.2.31 Input curve (5th order)

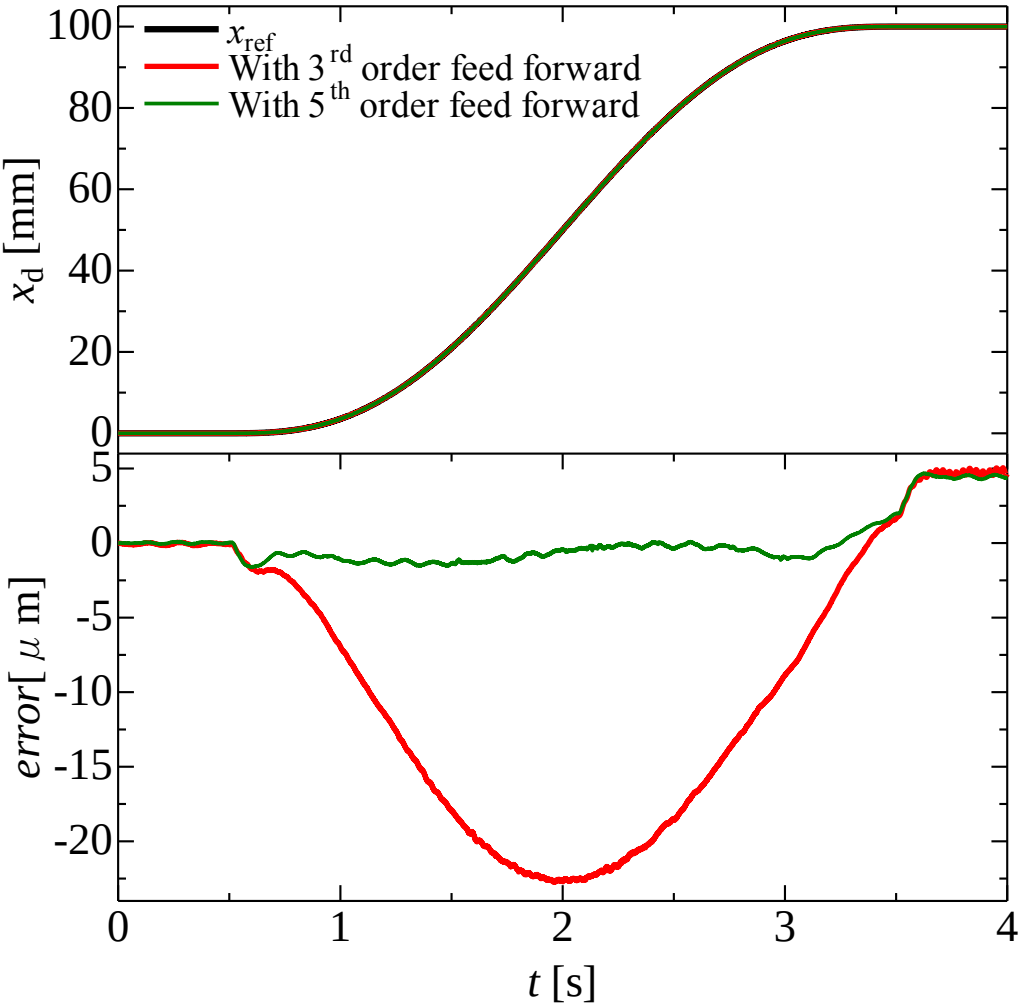

Fig.2.32 Experimental results (with 3rd and 5th order feed forward)

(D = 4.0mm, L = 0.5m, ω_v=100Hz, ζ_v = 0.7)

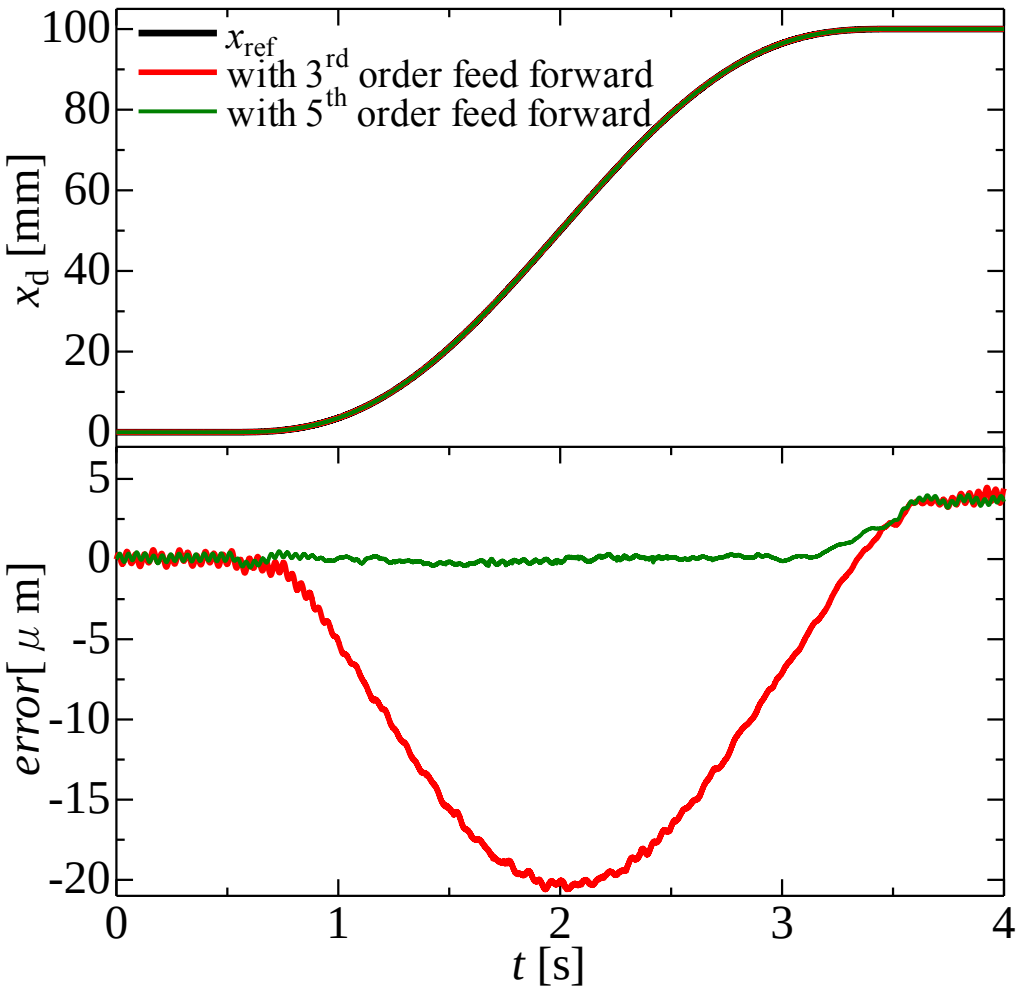

Fig.2.33 Experimental results (with 3rd and 5th order feed forward)

(D = 8.0mm, L = 1.0m, ω_v=100Hz, ζ_v = 0.7)

2.7 Conclusions

The integrated control method of the pneumatic servo table system, considering the dynamics of the pipeline and the servo valve is proposed in this chapter.

The pneumatic servo table system used in the study and main components, like pneumatic actuator, servo valve and pipelines are introduced. Mathematical models of the main components used in the system are designed. A linear model which takes into consideration the dynamics of pneumatic actuator, connected pipelines and servo valve is designed to simulate the system. At first, we considered only the pneumatic actuator when the control model was designed, since the servo valve response is much faster than that of the pneumatic actuator. The servo table system was approximated as a 3^{rd} order linear model. A PPD^2 controller involving position, velocity and acceleration feedback is used in the control system. Comparing experimental and simulation results, we found that there is a large discrepancy between simulation and experimental results. Based on this, we designed a 7^{th} order linear model whose simulation results matched experimental results well. Based on this result, it is found that the servo valve and connected pipelines greatly impacted on system accuracy. Minimizing errors requires feed forward, but the 7^{th} order linear model is complex. A low-dimensional model is necessary for practical use. The analysis showed that in the pole loci of the 7^{th} order model, two poles are much farther from the imaginary axis than are the other five poles. Therefore, the model can be reduced to one of the 5^{th} order. By comparing the simulation and experiment results, we confirmed that the 5^{th} order model could also match up well with the system.

The 5^{th} order control model's maximum trajectory error with feedback control is $3.036\times10^{3}\mu m$ when stoke is 100mm, which is still too large for precision positioning, however, and 5^{th} order feed forward is required to minimize it. We therefore plan to design an input curve which is derived five times to obtain 5^{th} order feed forward in the real system. Based on the linear model obtained before, 3^{rd} and 5^{th} order feed forward controllers have been designed. We have found from the experimental results that the

feed forward used in the system can significantly reduce trajectory errors. By comparing the experimental results using different orders of feed forwards, we have found that the 5^{th} order feed forward can decrease the maximum trajectory error into 0.3μm when stoke is 100mm.

Chapter 3 Distributed model of connected pipelines

3.1 Experimental apparatus

Fig.3.1 and Fig.3.2 shows schematic view and photo of the experimental apparatus. The system used in my research is mainly composed by a pressure regulator, a five-port servo valve, four pressure sensors, long connected pipelines, a metal pneumatic cylinder, an encoder, an AD/DA converter and payload. The five-port servo valve is used to control the mass flow at the inlets of pipelines. Pressure values at the inlets of the pipelines and cylinder chambers are obtained by the AD converter and pressure sensors. In this experiment, to confirm the influence of pressure sensors' locations on the position accuracy and the effectiveness of the distributed model of pipelines, four pressure sensors are utilized. In every case, two pipelines with the same length and diameter are used to connect the two cylinder chambers with the control ports of the servo valve. These two pipelines are numbered as 1 and 2. Here, the pressure values measured at the control ports of the servo valve are defined as P_{1_IN} and P_{2_IN}. While the pressure values measured in the cylinder chambers are defined as P_{1_OUT} and P_{2_OUT}. Nine cases with the diameters and lengths of connected pipelines are investigated. The linear guider is used to install the payload with the cylinder. The mass of it is weight 1.25kg.

The supply pressure is 700kPa (absolute) and the full stroke of the cylinder is 300mm. Sampling time of the AD / DA converter is 1 ms. The experimental conditions are shown in Table 3.1.

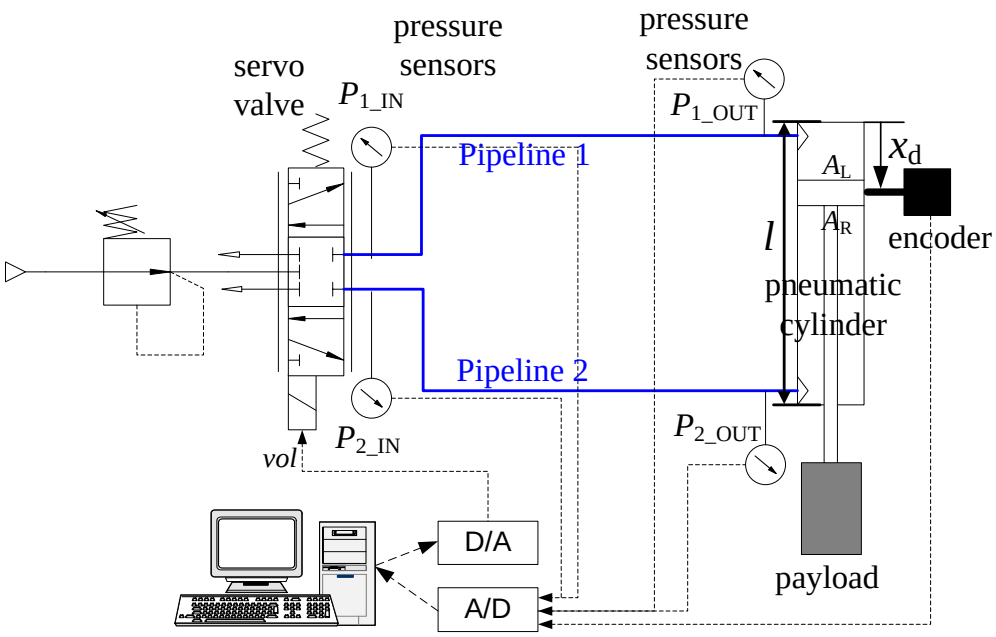

Fig.3.1 Experimental apparatus

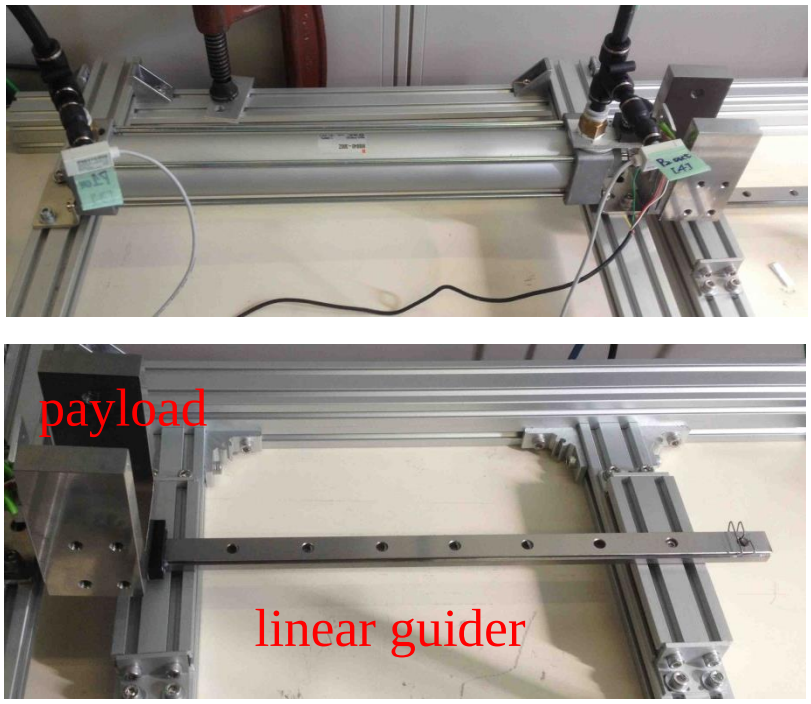

Fig.3.2 Photo of experimental apparatus

Table 3.1 Experimental conditions

Symbol		Value	
A_L	area	1257	[mm^2]
A_R	area	1056	[mm^2]
l	full stroke	300	[mm]
P_s	supply pressure	0.7	[MPa] (abs)
L	length	2.0	[m]
		5.0	[m]
		10.0	[m]
D	diameter	4.15	[mm]
		6.10	[mm]
		7.65	[mm]
m	payload	0	[kg]
		1.25	[kg]
x_d	displacement		[mm]

3.2 Distributed model of pipelines

The model is designed based on the distributed characteristics of pipelines. Theoretically, the flow in the pipeline is three dimensional. However, it requires a substantial amount of time to calculate the three dimensional model. Since the pressure distribution in the pipeline is mainly in the length direction and the pressure values must be estimated in real time to use in control, the pipeline is given as one dimensional distributed model [51]. This distributed model is based on four equations, as state equation of air (3.1), motion equation (3.2), continuity equation (3.3), and energy equation (3.4). Equation (3.4) is based on the first law of thermodynamics. By using the state equation of air (3.1), motion equation (3.2), continuity equation (3.3), the first law of thermodynamics can be represented in the form of Equation (3.4).

$$P = \rho R\theta \tag{3.1}$$

$$\frac{\partial u}{\partial t} + u\frac{\partial u}{\partial x} = -\frac{1}{\rho}\frac{\partial P}{\partial x} - H \tag{3.2}$$

$$\frac{\partial \rho}{\partial t} + \rho\frac{\partial u}{\partial x} + u\frac{\partial \rho}{\partial x} = 0 \tag{3.3}$$

$$\frac{\partial \theta}{\partial t} = \frac{4h(\theta_a - \theta)}{\rho C_v D} - u\frac{\partial \theta}{\partial x} - \frac{R\theta}{C_v}\frac{\partial u}{\partial x} + \frac{1}{C_v}\frac{\lambda|u|u^2}{2D} \tag{3.4}$$

Pressure loss due to friction along a pipe to the average velocity of the fluid flow is described with the Darcy-Weisbach equation as shown in Eq. (3.5). In this research, when the Reynolds number is less than 2300, a coefficient of laminar flow is given as Eq. (3.6). As a flow coefficient of turbulence, the Blasius friction factor is described in Eq. (3.7). The rate of convective heat transfer between the pipe wall and the air is given by Eq. (3.8). Heat transfer coefficient is described in the formulation given as Eq. (3.9). Thermal conductivity is approximated by Eq. (3.10).

$$H = \frac{\lambda}{2D}|u|u \tag{3.5}$$

$$\lambda = \frac{64}{R_e} \qquad R_e \le 2300 \qquad (3.6)$$

$$\lambda = 0.3164 {R_e}^{-0.25} \qquad R_e > 2300 \qquad (3.7)$$

$$T = \frac{4h(\theta - \theta_a)}{\rho C_v D} \qquad (3.8)$$

$$h = 0.046 {R_e}^{0.8} {P_r}^{0.4} k/D \qquad (3.9)$$

$$k = 7.95 \times 10^{-5}\theta + 2.0465 \times 10^{-3} \qquad (3.10)$$

A staggered grid system as shown in Fig.3.3 is used for a stable computation. The actual system and the computation model of the distributed model are shown in Fig.3.4.

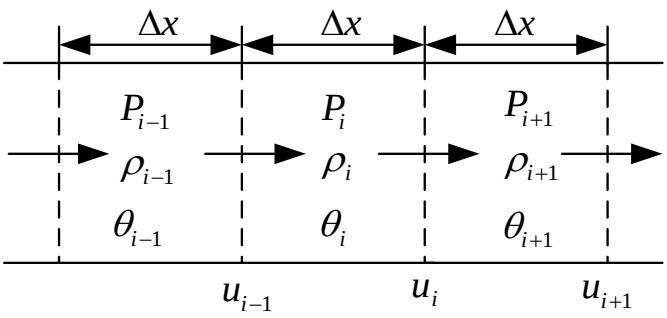

Fig.3.3 Staggered grid system

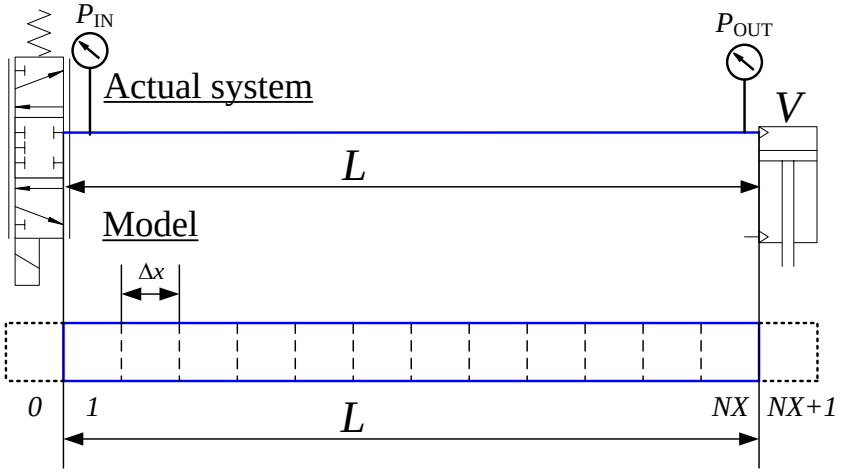

Fig.3.4 The distributed model of pipelines

3.3 Simulation model

Firstly, a simulation model with the distributed model of pipelines is developed to confirm the controllability of a pneumatic cylinder. The block diagram of the whole pneumatic system is shown in Fig.3.5. As shown in Fig.3.5, a five-port flow type servo valve is used. A PD control is applied to the position control as a main feedback loop. A force feedback is used as a minor loop to improve the position controllability. The force is obtained from the pressure difference between the pneumatic cylinder chambers. Here the pipelines connected the servo valve with the pneumatic cylinder must be considered. The simulation model of each element has been designed as shown in the following sections.

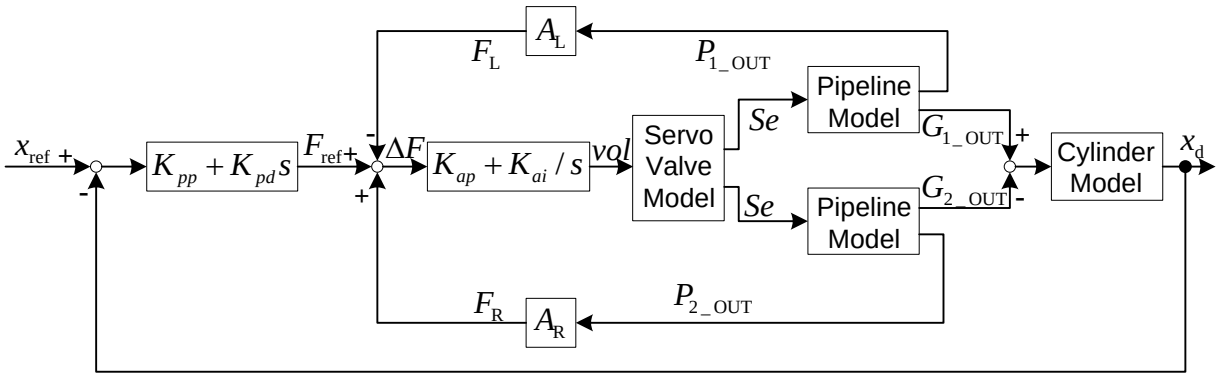

Fig.3.5 Simulation model of the system

3.3.1 Servo valve model

In the simulation, the volume flow at the inlets of pipelines is needed which is calculated by the effective area and the up and down stream pressure of the servo valve. The input signal of the servo valve model is the voltage. The *Se-Voltage* characteristic of the servo valve is needed which is obtained from experiment. Fig.3.6 shows the experimental apparatus of *Se* measurement which consists of a pressure regulator, a buffer tank, hand valves, a pressure gauge, the five-port servo valve and a flow meter.

The *Se-Voltage* characteristic of the servo valve is shown in the Fig.3.7. The dynamics of the servo valve is considered to be fast enough compared with that of the pipelines.

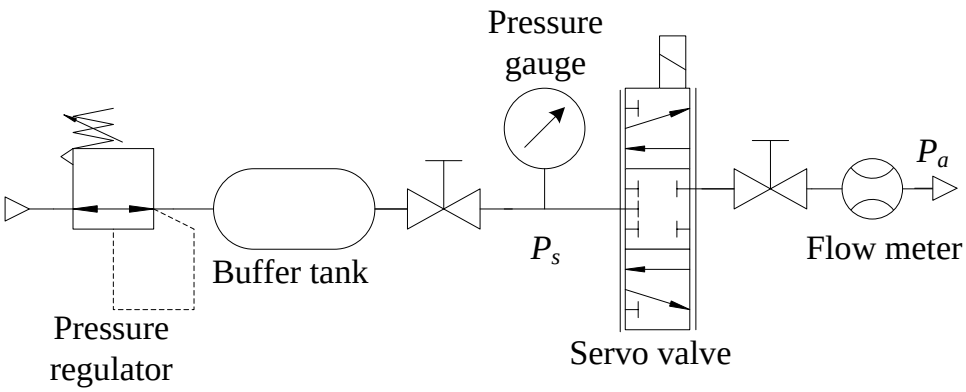

Fig.3.6 Experimental apparatus of *Se* measurement

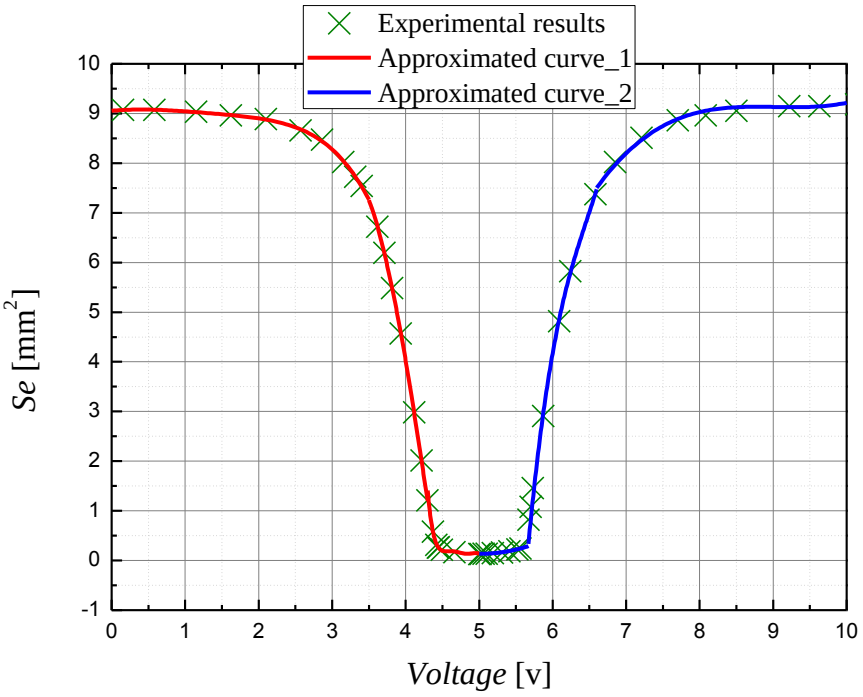

Fig.3.7 *Se* -*Voltage* characteristics of the servo valve

3.3.2 Pipeline model

The pipeline models used here is the distributed model. In order to calculate state variables of the first and last grids, two virtual grids are set here as $Grid_0$ and $Grid_{NX+1}$ as shown in Fig.3.4.The state variables of these two virtual grids are the inlet and outlet boundary conditions. The initial pressure value of $Grid_0$ is equal to the supply pressure, while the initial values of other grids of the pipeline are equal to the atmospheric pressure and the gradient of flow velocity is equal to 0. The input signal of the pipeline model is the effective area of servo valve which is used to calculate the volume flow. The output signals of the pipeline model is the pressure values in cylinder chambers and the mass flow charging into and discharging out of cylinder chambers.

3.3.2.1 Inlet boundary conditions

The inlet boundary of the pipelines model is the flow velocity of $Grid_0$, obtained from the volume flow rate passing through the servo valve. The critical pressure ratio b of the servo valve is measured in advance which is equal to 0.35. When the compressed air is charging into the pipeline, the volume flow is calculated by Eq. (3.11) and (3.12).

$$Q_{ANR} = K_f S e P_s \sqrt{\frac{293}{\theta_s}} \qquad \frac{P_1}{P_s} \le b \qquad (3.11)$$

$$Q_{ANR} = K_f S e P_s \sqrt{\frac{293}{\theta_s}} \sqrt{1 - \left(\frac{\frac{P_1}{P_s} - b}{1 - b}\right)^2} \qquad \frac{P_1}{P_s} > b \qquad (3.12)$$

While the compressed air is discharging out of the pipeline, the volume flow is calculated by Eq. (3.13) and (3.14).

$$Q_{ANR} = K_f S e P_1 \sqrt{\frac{293}{\theta_1}} \qquad \frac{P_a}{P_1} \le b \tag{3.13}$$

$$Q_{ANR} = K_f S e P_1 \sqrt{\frac{293}{\theta_1}} \sqrt{1 - \left(\frac{\frac{P_a}{P_1} - b}{1 - b}\right)^2} \qquad \frac{P_a}{P_1} > b \tag{3.14}$$

3.3.2.2 Outlet boundary conditions

The outlet boundary condition is calculated from the state equation and energy equation in cylinder chambers. The temperature change in the cylinder chamber is calculated by the energy equation. Then with temperature change, the pressure in the cylinder chamber can be estimated by the state equation. Time derivative of the state equation in the cylinder chambers are written as follows:

$$V_d \frac{dP_d}{dt} = A_d P_d \left|\dot{x}_d\right| + R\theta_d G_d + \frac{P_d V_d}{\theta_d} \frac{d\theta_d}{dt} \tag{3.15}$$

$$V_c \frac{dP_c}{dt} = -A_c P_c \left|\dot{x}_d\right| + R\theta_c G_c + \frac{P_c V_c}{\theta_c} \frac{d\theta_c}{dt} \tag{3.16}$$

The time derivative of energy equation in the cylinder chambers can be given as follows [52, 53]:

$$\frac{C_v P_d V_d}{R\theta_d} \frac{d\theta_d}{dt} = R\theta_d G_d + A_d P_d \left|\dot{x}_d\right| + Sh_d(\theta_a - \theta_d) \tag{3.17}$$

$$\frac{C_v P_c V_c}{R\theta_c} \frac{d\theta_c}{dt} = C_v G_c(\theta_{pc} - \theta_c) + R\theta_{pc} G_c - A_c P_c \left|\dot{x}_d\right| + Sh_c(\theta_a - \theta_c) \tag{3.18}$$

In Eq. (3.15) to (3.18), the time derivative of air's mass is represented as the mass flow calculated by the velocity of air and the volume change of cylinder chambers is calculated by the velocity of the slider. The velocity of the slider used in these equations is the absolute value.

The mass flow here is calculated by flow velocity at the outlet of pipelines. When

the air flows into the cylinder chamber, the mass flow is given as Eq. (3.19). When the air discharges from the cylinder chamber, the flow equation is shown as Eq. (3.20).

$$G = \frac{\pi D^2}{4}\rho_{NX}u_{NX} \tag{3.19}$$

$$G = \frac{\pi D^2}{4}\rho_{NX+1}u_{NX} \tag{3.20}$$

3.3.2.3 CFL condition

This method is an explicit method. For a stable computation, the CFL condition described as the Eq. (3.21) [54] must be satisfied:

$$c\Delta t \leq \Delta x \tag{3.21}$$

The pipelines are separated into several computation meshes according to the length. The length of one grid is 1.0m which can satisfy the CFL condition.

3.3.3 Cylinder model

Fig.3.8 shows the cylinder chambers, the model of which is designed based on the motion equation and the state equation of ideal gas.

The equation of motion is given as:

$$m\ddot{x}_d = A_L P_L - A_R P_R + B\dot{x}_d \tag{3.22}$$

The state change of pressurized chambers is treated as an isothermal condition. The total differentiation of the state equation of ideal gas around the equilibrium point is given as:

$$V_{oL}\frac{dP_L}{dt} = R\theta G_L - A_L P_{oL}\dot{x}_d \tag{3.23}$$

$$V_{oR}\frac{dP_R}{dt} = R\theta G_R + A_R P_{oR}\dot{x}_d \tag{3.24}$$

The model of the cylinder chambers is shown in the Fig.3.9.

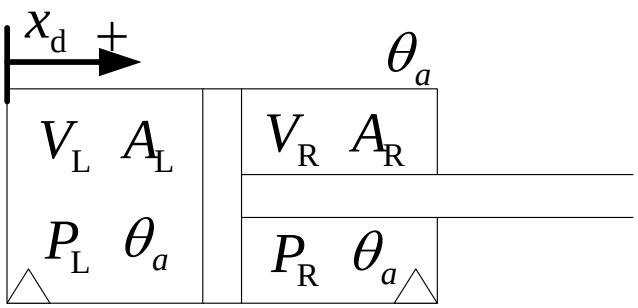

Fig.3.8 The cylinder chamber

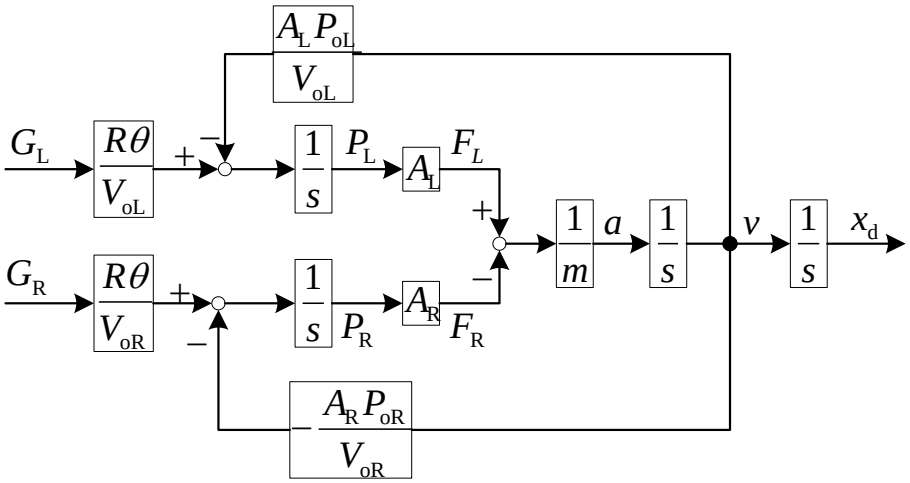

Fig.3.9 The cylinder model

3.4 Experimental methods

3.4.1 Block diagrams

Fig.3.10 and Fig. 3.11 are block diagrams when the used pressure signals measured by sensors located in different positions. When pressure signals measured by pressure sensors at the control ports of the servo valve which are symbolized as P_{1_IN} and P_{2_IN} are used, the block diagram is shown as Fig. 3.10. Fig. 3.11 shows the block diagram when pressure signals are measured by sensors at the cylinder chambers. The pressure values are symbolized as P_{1_OUT} and P_{2_OUT}. The block diagram of the proposed method is presented in Fig. 3.12. The pressure sensors are used at the control ports of the servo valve. The pressure values calculated by the distributed model of pipelines in real time are utilized.

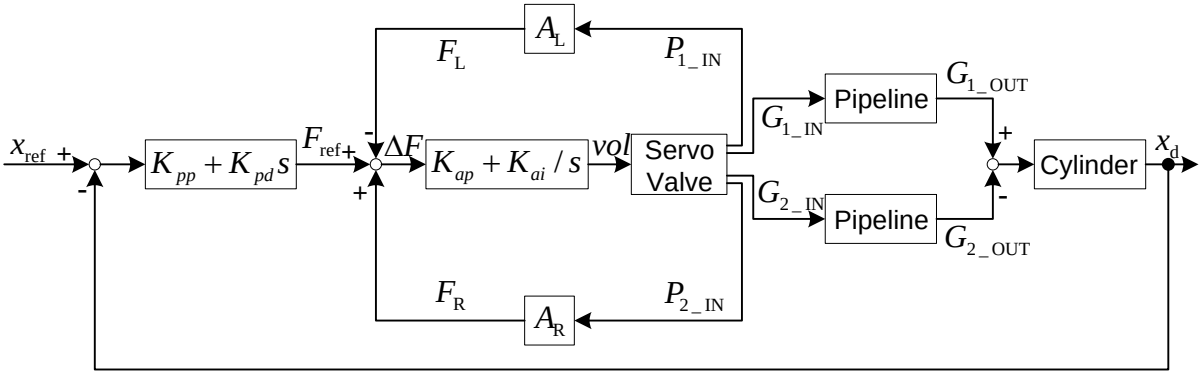

Fig.3.10 Block diagram
(pressure signals measured by sensors at the control ports of the servo valve)

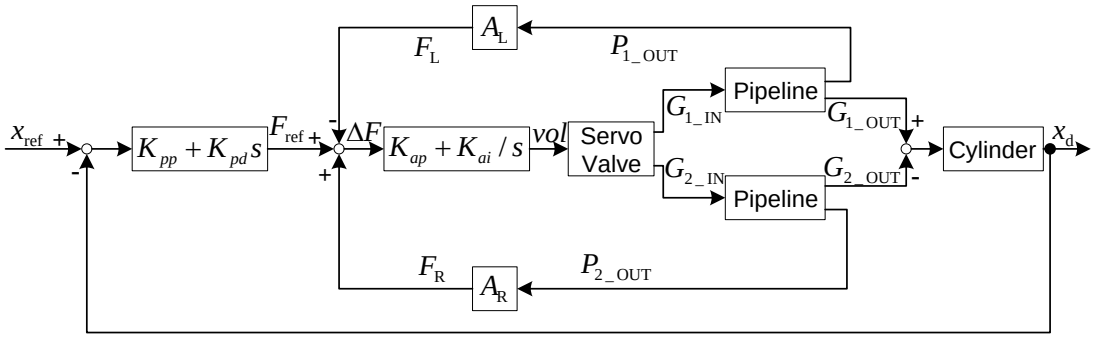

Fig.3.11 Block diagram
(pressure signals measured by sensors at the cylinder chambers)

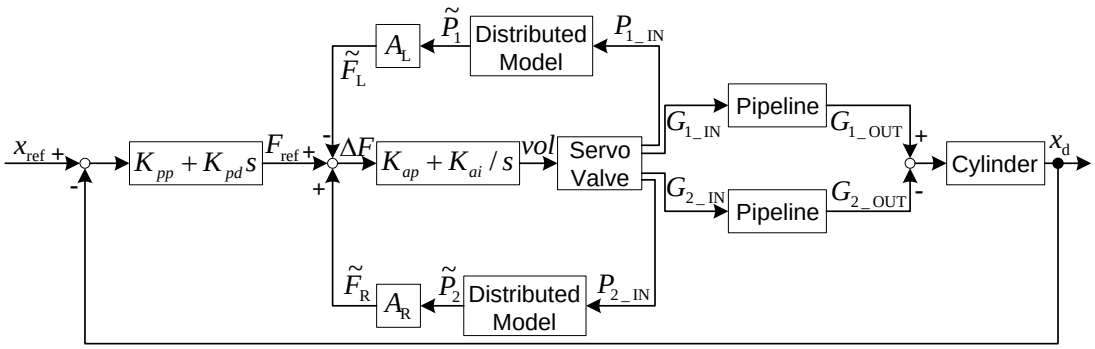

Fig.3.12 Block diagram
(pressure signals estimated by distributed model in real time)

3.4.2 Boundary conditions of the pipelines model

The inlet boundary condition of the distributed model used in experiments is different from the one used in simulation. Since the pressure at the control ports of the servo valve is measured, this value is used as the inlet boundary. The initial pressure values of every grid of the pipeline are equal to the atmospheric pressure and the gradient of flow velocity is equal to 0. At the first moment, the velocity of the first grid is calculated by the motion equation as shown in Eq. (3.2) using the pressure difference between the initial pressure and the measured pressure in the first grid.

While the outlet boundary condition of the distributed model both used in simulation and experiments is same, which is calculated from the state equation and energy equation in cylinder chambers.

The pipelines are separated into several computation meshes according to the length. The length of one grid in experiments is 1.0m which can satisfy the CFL condition as shown in Eq. (3.21).

3.5 Experimental and simulation results

3.5.1 Experimental results comparison

Here an example set of experiment results are presented. The pipelines shown in the example have lengths of 10.0m and diameters of 7.65mm. The system is doing free movement. When the pressure signals measured at the control ports of the servo valve are used, the results are shown in Fig.3.13. The maximum position error is 56.6mm. When the pressure signals measured in the cylinder chambers are used, the results are shown in Fig.3.14. The maximum position error here is 13.0mm. Compared with the position response, the position accuracy has been improved by 43.6mm, when pressure signals are measured at the cylinder chamber. A reduction in position error can also be seen in experiments with different pipelines and input signals. Based on these results, it is found that long connected pipelines cause bad effect on the system.

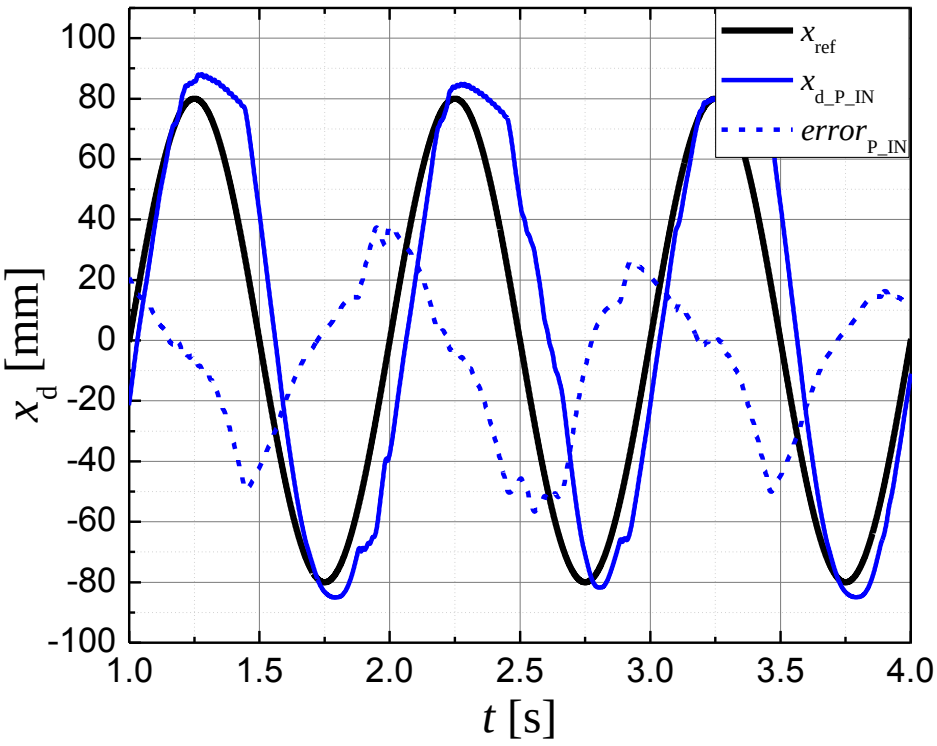

Fig.3.13 Experiment results
(pressure signals measured by sensors at the control ports of the servo valve, *D*=7.65mm, *L*=10.0m)

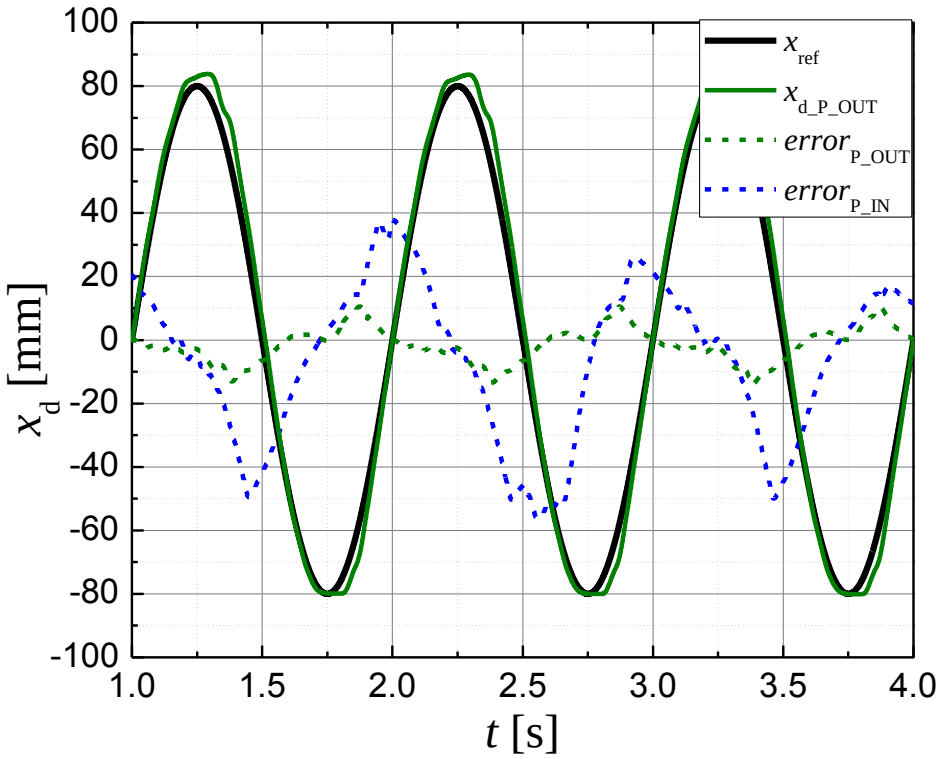

Fig.3.14 Experiment results
(pressure signals measured by sensors at the cylinder chambers, *D*=7.65mm, *L*=10.0m)

3.5.2 Simulation results

Simulation results are shown in Figs.3.15-3.17. In Fig.3.15, the black line is the reference of position, while the blue one is the experimental result using the pressure signals measured by pressure sensors at the cylinder chambers; the simulation result is plotted as the red dash line. The pressure results near the servo valves are shown in Fig.3.16. The black solid and green dot lines are the pressure values measured by pressure sensors in the experiment, while the red dash and blue dash dot lines are the ones calculated by the simulated model. Fig.3.17 shows the pressure results in the cylinder chambers. The P_{1_OUT} – experiment and P_{2_OUT} – experiment are the pressure values measured by pressure sensors, while P_{1_OUT} – simulation and P_{2_OUT} – simulation are the ones calculated by the simulated model. From the results, it is found that in the simulation, the distributed model of pipelines estimates the pressure values well. The repeatability of this simulation model has also been confirmed not only when pipelines

with different parameters are used, but also when different frequency signals are inputted.

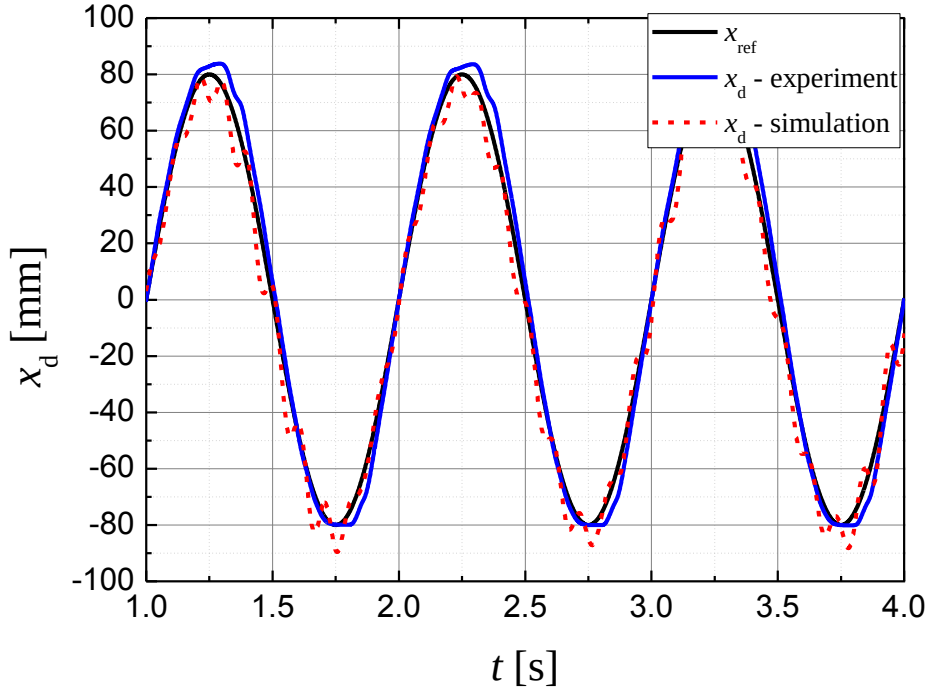

Fig.3.15 Simulation and experimental results (*D*=7.65mm, *L*=10.0m)

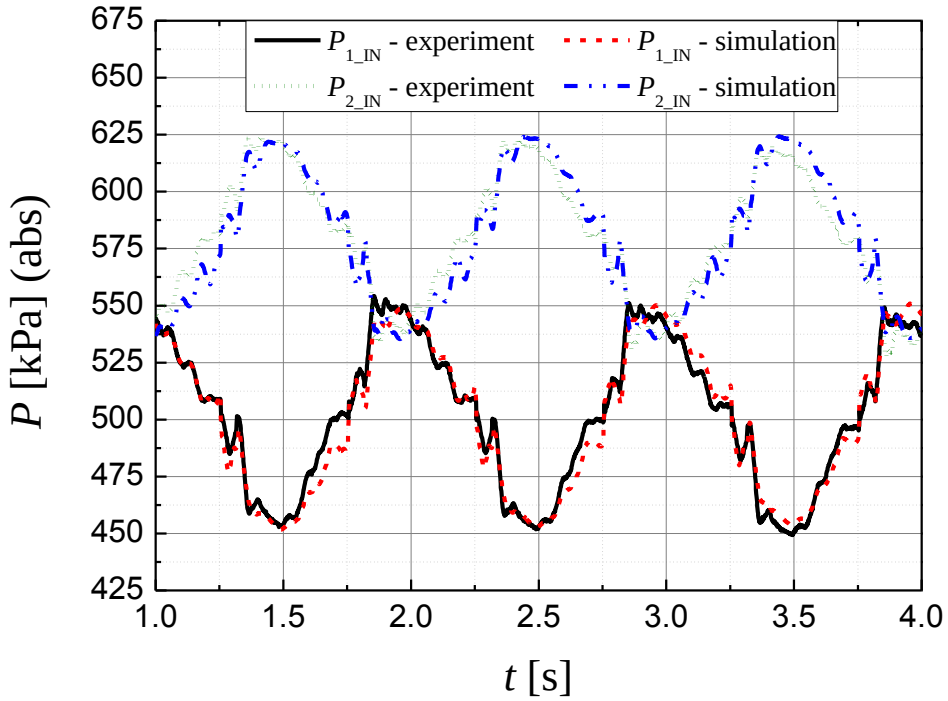

Fig.3.16 Pressure results at the control port of the servo valve (*D*=7.65mm, *L*=10.0m)

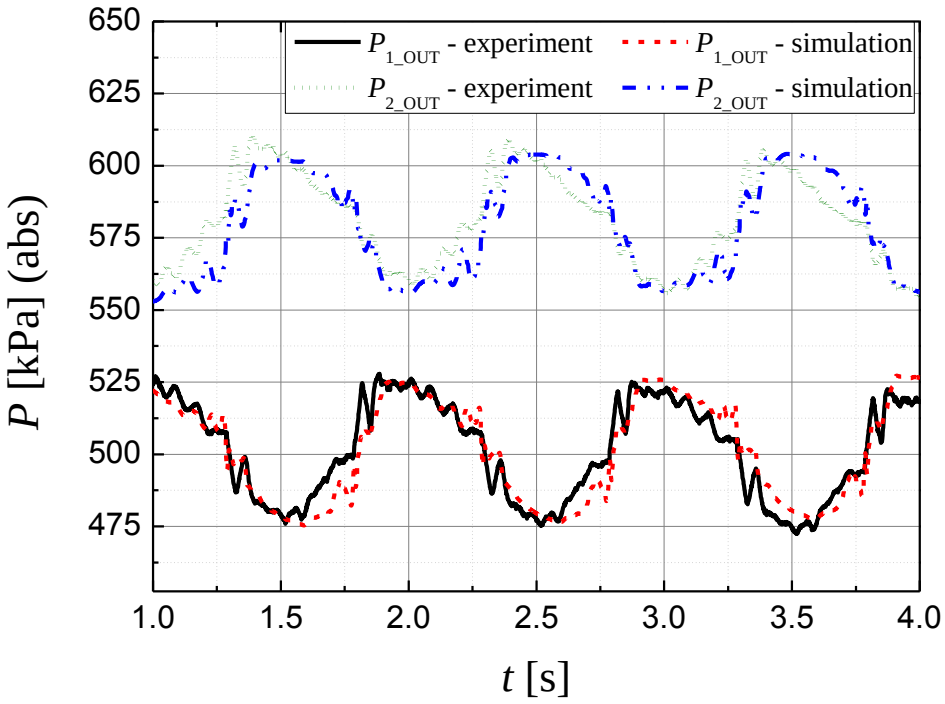

Fig.3.17 Pressure results in the cylinder chambers (*D*=7.65mm, *L*=10.0m)

3.5.3 Effectiveness of the distributed model

Before the distributed model of pipelines applied in the real control system, the effectiveness of this model has been confirmed by experiments. The pressure results are plotted in Fig.3.18 and Fig.3.19. P_{1_IN} and P_{2_IN} are the pressure values measured by pressure sensors at the control ports of the servo valve, while P_{1_OUT} and P_{2_OUT} are the ones measured by pressure sensors at cylinder chambers. The pressure values calculated by the distributed model of pipelines in real time are plotted as P_{1_DM} and P_{2_DM}. It is found from Fig.3.18 that the distributed model estimates the pressure values in the cylinder chambers in real time well when the system is doing free movement. According to Fig.3.19, the distributed model can also estimate the pressure values in the cylinder chambers in real time well when there is a payload in the system. The accurate estimate has been also found when different parameters pipelines and different input signals are used.

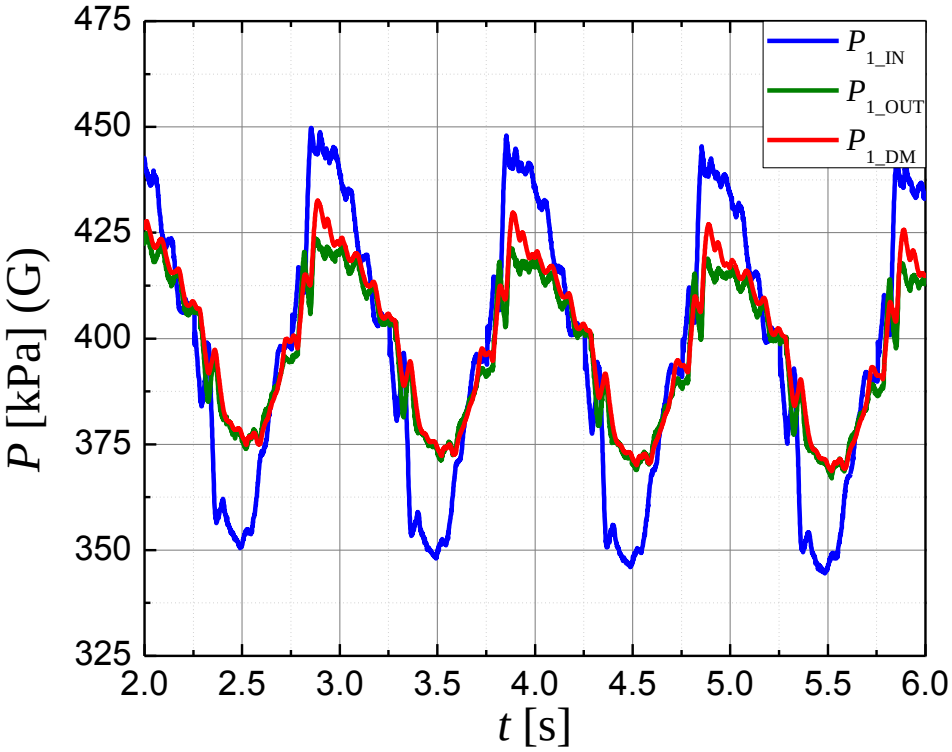

(a) Pipeline 1

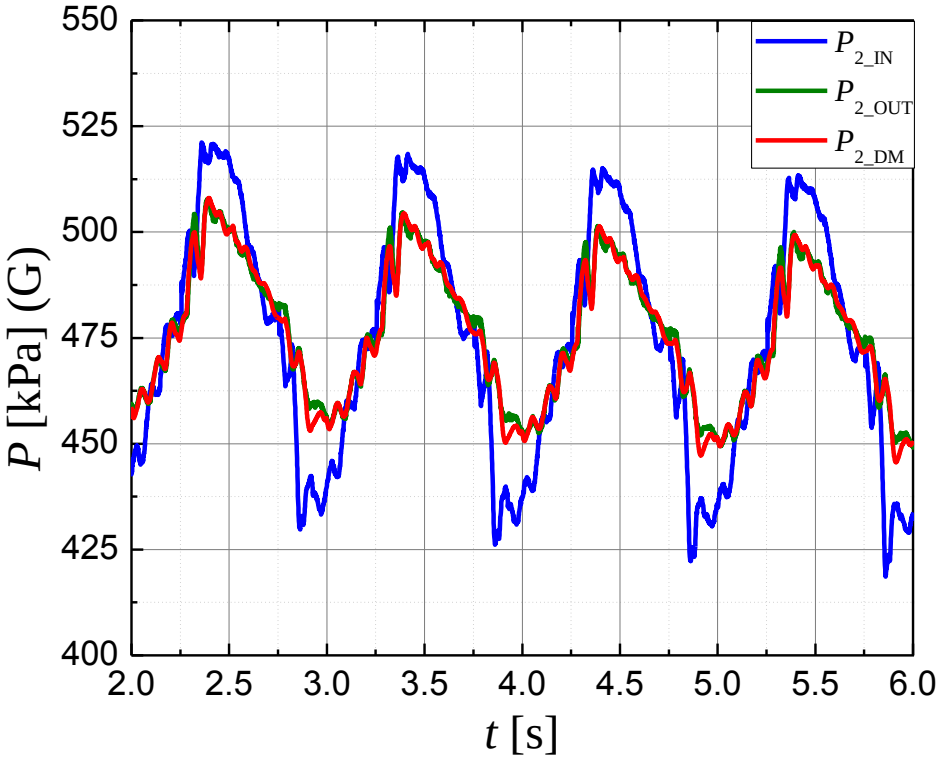

(b) Pipeline 2

Fig.3.18 Experimental results of pressure
(when the system is doing free movement, *D*=7.65mm, *L*=10.0m)

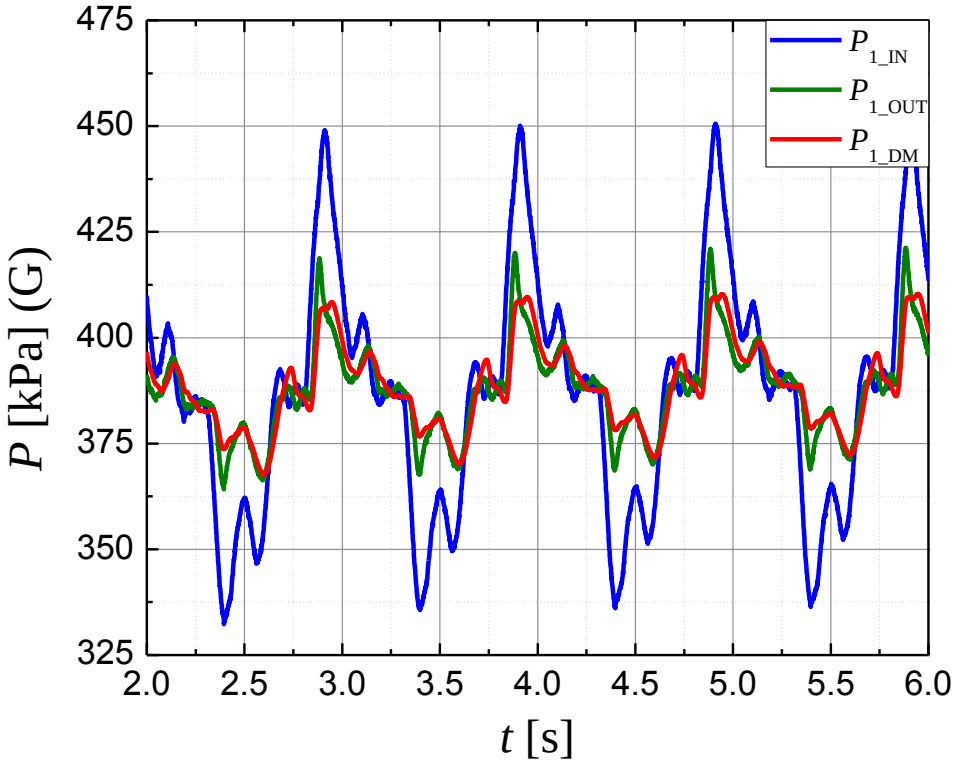

(a) Pipeline 1

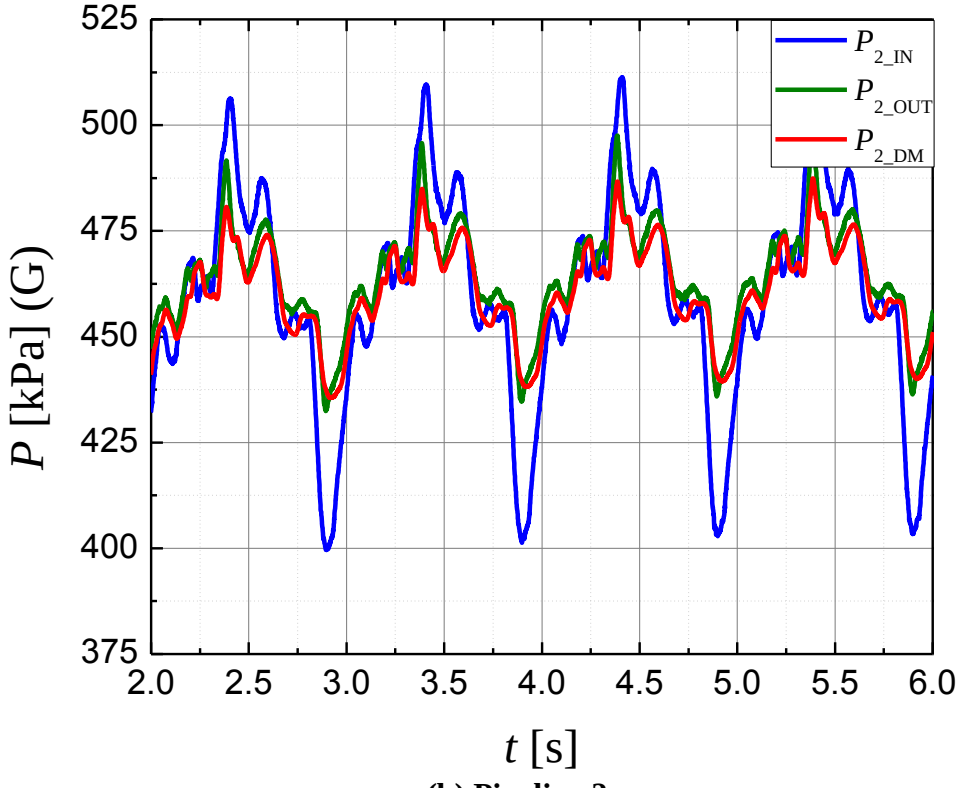

(b) Pipeline 2

Fig.3.19 Experimental results of pressure (with payload, *D*=7.65mm, *L*=10.0m)

3.5.4 Experimental results using the distributed model in real time

Based on the effectiveness of the distributed model, the estimated pressure values are used as control signals in real time. The position response is presented in Fig.3.20 and Fig.3.21. In these two figures, the position errors are shown as $error_{P\_DM}$, when the estimated pressure signals are used. When the pressure signals measured by sensors at the cylinder chambers are utilized, the position errors are shown as $error_{P\_OUT}$. From the results, it is found that the position accuracy is almost the same as that of using the measured pressure signals at the cylinder chambers, when the system is doing free movement which has also been confirmed by experiments with different pipelines and input signals. When there is a payload in the system, the position accuracy is higher than that of using the measured pressure signals in cylinder chambers, since the noise of the estimated signal is low. By using this distributed model in the control system, the influence of long connected pipelines can be ignored.

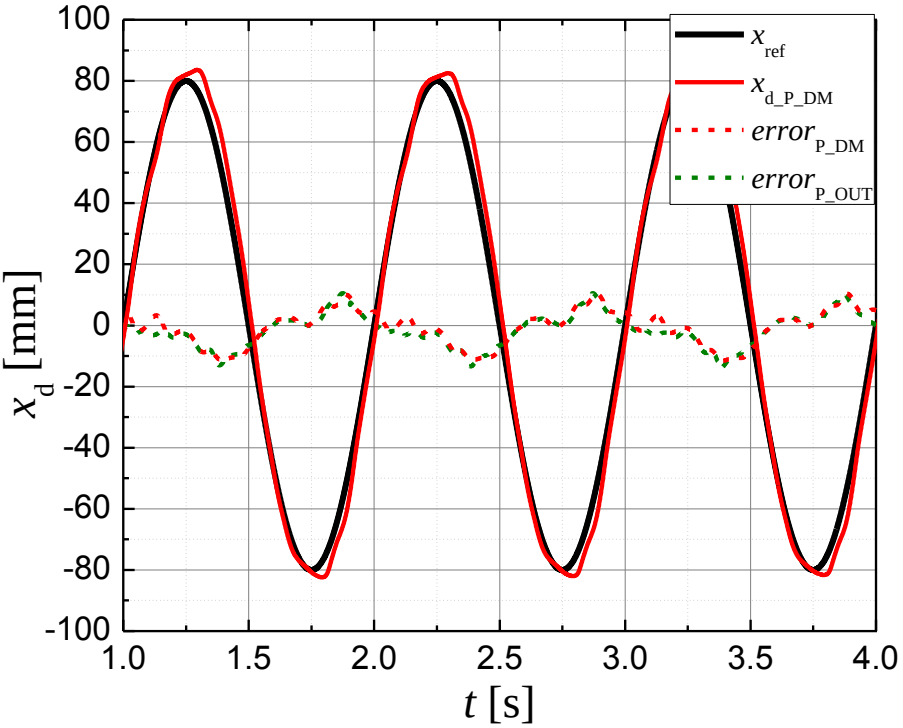

Fig.3.20 Experimental results
(pressure signals estimated by the distributed model, the system is dong free movement, *D*=7.65mm, *L*=10.0m)

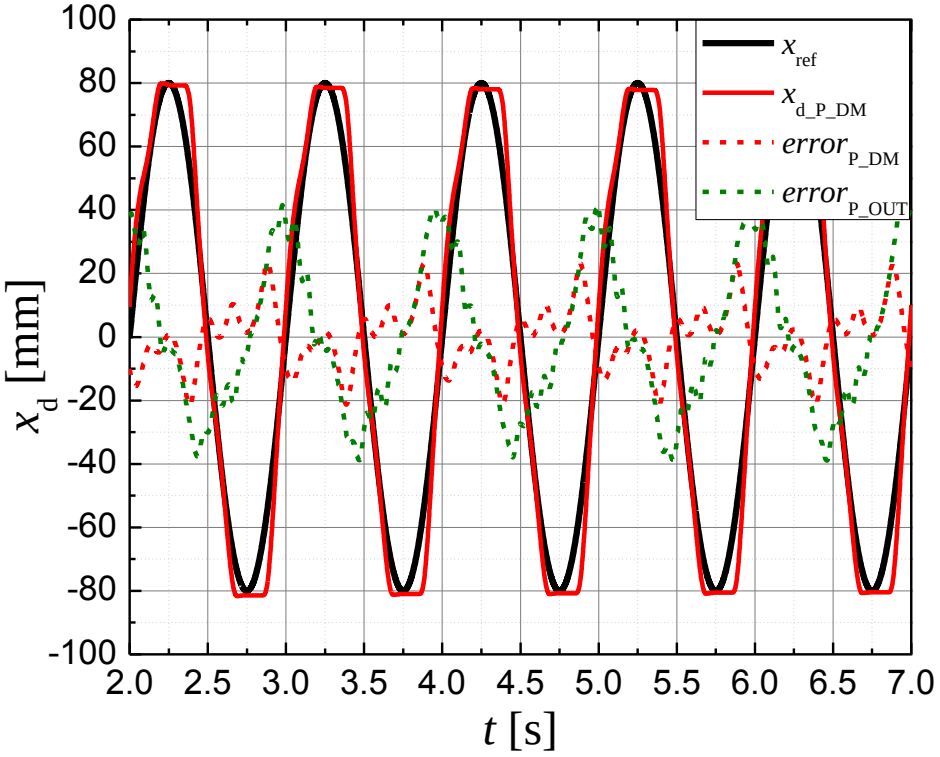

Fig.3.21 Experimental results
(pressure signals estimated by the distributed model, with payload, *D*=7.65mm, *L*=10.0m)

3.6 Conclusions

In this chapter, the control design of a pneumatic system using long connected pipelines is proposed to remove pressure sensors at cylinder chambers. The distributed model estimates the pressure losses and time delay through long connected pipelines in real time. To confirm the effectiveness of the proposed control method, a simulation model of the whole system is designed. The pipelines with different parameters are used. Compared simulation and experimental results, it has been found that the simulation model represents the real system well. Based on the estimated and measured pressure values in cylinder chambers, it is found that with this distributed model, the pressure in the cylinder chambers is estimated precisely by the measured values at the control ports of the servo valve in the real time. The experimental results demonstrate that the position accuracy is almost the same as that of using the measured pressure signals in the cylinder chambers. With this distributed model in the control system, the influence of long connected pipelines can be ignored and the cylinder sider is free of pressure sensors. With the commercial non-electromagnetic position sensors, electromagnetics can be avoided at the cylinder side.

Chapter 4 Index to judge the necessity of the distributed pipeline model

With the distributed model, the pressure in the cylinder chambers is estimated precisely by the measured values at the control ports of the servo valve in the real time. However, the distributed model is complex and in some situations, the effect of connected pipelines can be ignored. The index to judge the necessity of the distributed pipeline model in the pneumatic servo system is needed.

4.1 Acceptable pressure loss

Fig.4.1 shows the photo of the pressure sensor used in the experimental. The resolution of this kind of pressure sensors are ±10kPa (25±10℃).According to the resolution of the pressure sensor, the value of the acceptable pressure loss along pipeline which will not cause obvious influence on the position response of the system is assumed as ±10kPa according to the resolution of pressure sensors. Some experiments have been done to confirm this acceptable pressure loss.

Fig.4.1 Photo of pressure sensor

4.2 Pressure loss

The index is designed based on the pressure loss along the pipeline. The pressure loss along pipelines is influenced by the pipeline diameter, pipeline length, supply pressure, pressurized area of cylinder chamber, moving speed of the slider and type of servo valve. The expression of pressure loss is shown as Eq. (4.1).

$$\Delta P = \frac{\lambda}{2D} u^2 \rho L \tag{4.1}$$

$$\lambda = \frac{64}{R_e} \qquad R_e \leq 2300 \tag{4.2}$$

$$\lambda = 0.3164 {R_e}^{-0.25} \qquad R_e > 2300 \tag{4.3}$$

In order to calculate the pressure loss along pipelines, the velocity and density of air in the pipeline is needed. To calculate this two unknown parameters, the total differentiation of the state equation of ideal gas linearized around the equilibrium point in the cylinder chamber is need.

$$V_{0\mathrm{L}} \frac{dP_{\mathrm{L}}}{dt} = R\theta G_{\mathrm{L}} - A_{\mathrm{L}} P_{0\mathrm{L}} \dot{x}_d \tag{4.4}$$

$$V_{0\mathrm{R}} \frac{dP_{\mathrm{R}}}{dt} = R\theta G_{\mathrm{R}} + A_{\mathrm{R}} P_{0\mathrm{R}} \dot{x}_d \tag{4.5}$$

At the first moment, there is no air charging into the cylinder chamber and the pressure change in the cylinder chamber is equal to 0. The pressure in cylinder chambers is equal to the equilibrium values. Based on this condition, the mass flow in pipeline can be calculated as Eqs. (4.6) and (4.7). The density of air at the first moment is shown in Eqs. (4.8) and (4.9).

$$G_{\mathrm{L}} = \frac{A_{\mathrm{L}} P_{0\mathrm{L}}}{R\theta} \dot{x}_d \tag{4.6}$$

$$G_{\mathrm{R}} = \frac{A_{\mathrm{R}} P_{0\mathrm{R}}}{R\theta} \dot{x}_d \tag{4.7}$$

$$\rho_{\mathrm{L}} = \frac{P_{0\mathrm{L}}}{R\theta} \tag{4.8}$$

$$\rho_{\mathrm{R}} = \frac{P_{0\mathrm{R}}}{R\theta} \tag{4.9}$$

The velocity of air in the pipelines is expressed as the following formulas.

$$u_{\mathrm{L}} = \frac{4A_{\mathrm{L}}}{\pi D^2}\dot{x}_d \tag{4.10}$$

$$u_{\mathrm{R}} = -\frac{4A_{\mathrm{R}}}{\pi D^2}\dot{x}_d \tag{4.11}$$

After the velocity and density of the air in the pipeline at the first moment is calculated, the maximum pressure loss along pipelines can be expressed as the following formulas.

$$|\Delta P_1|_{\max} = 32\frac{\mu}{D}L\frac{4A_{\mathrm{L}}}{\pi D^2}|\dot{x}_d|_{\max} \qquad R_e \le 2300 \tag{4.12}$$

$$|\Delta P_1|_{\max} = 0.1582\frac{\mu}{D^2}{R_e}^{0.75}L\frac{4A_{\mathrm{L}}}{\pi D^2}|\dot{x}_d|_{\max} \qquad R_e > 2300 \tag{4.13}$$

$$|\Delta P_2|_{\max} = 32\frac{\mu}{D}L\frac{4A_{\mathrm{R}}}{\pi D^2}|\dot{x}_d|_{\max} \qquad R_e \le 2300 \tag{4.14}$$

$$|\Delta P_2|_{\max} = 0.1582\frac{\mu}{D^2}{R_e}^{0.75}L\frac{4A_{\mathrm{R}}}{\pi D^2}|\dot{x}_d|_{\max} \qquad R_e > 2300 \tag{4.15}$$

The index to use the distributed model is calculated as Eq.4.16. The upper part is the pressure loss along pipeline while the lower part is the resolution of pressure sensors. The values of parameters are shown in Table 4.1.

$$\frac{|\Delta P|_{max}}{P_{re}} \tag{4.16}$$

Table 4.1 Parameters values

A_L	pressurized area of cylinder chamber	1257×10^{-6}	[m^2]
A_R	pressurized area of cylinder chamber	1056×10^{-6}	[m^2]
D	pipelines diameter	4.15 6.10 7.65	[$\times10^{-3}$m]
f	frequency		[Hz]
L	pipelines length	2.0 5.0 10.0	[m]
P_{0L}	equilibrium pressure	470×10^3	[Pa] (abs)
P_{0R}	equilibrium pressure	530×10^3	[Pa] (abs)
P_{re}	resolution of the pressure sensor	10×10^3	[Pa]
P_s	supply pressure	700×10^3	[Pa] (abs)
$\lvert\dot{x}_d\rvert_{max}$	maximum of the slider moving speed	$0.16f\pi$	[m/s]
θ	temperature of air	293	[K]

4.3 Experimental results

To confirm the effectiveness of the index, experiments with different pipelines have been done. In these experiments, the input curve is the sine curve, the amplitude of which is equal to 80mm and the frequency of which is equal to 1Hz. According to experimental resulats, the maximum position difference, less than 7.5% of the amplitude of the position signal is defined as the acceptable position difference and the influence of connected pipelines can be ignored. While the maximum position difference is larger than 7.5% of the amplitude of the position signal, the distributed model should be used in the control system.

When the length of pipelines used in this experiment is 5.0m and the diameter is 7.65mm, experimental results are shown in Fig.4.2. The pressure values measured at the control port of the servo valve are plotted as the blue lines while the ones measured at the cylinder chambers are plotted as the green lines. The red lines are the difference between the input and output of pipelines. The pressure loss along pipelines is less than ±10kPa. The pressure loss along pipelines can be ignored according to the resolution of pressure sensors. The position response is shown in Fig.4.3. The blue line is the position response when the pressure measured at the control port of the servo valve is used and the green line is the result when pressure measured at the cylinder chambers is used. The position difference is plotted in red. It is found from these results that the maximum position difference is 7.4%, which is less than 7.5% of the amplitude of the position signal. In this case the influence of connected pipelines can be ignored. The design index in this situation is equal to 0.80.

When the 10.0m-long pipelines are used, the diameter of which is 7.65mm, the experimental results are shown in Fig.4.4. The blue lines are the pressure values measured at the control port of the servo valve and the green lines are the ones measured at the cylinder chambers. The red lines are the difference between the input and output of pipelines. The pressure loss along pipelines in this case is larger than ±10kPa. When the pressure measured at the control port of the servo valve is used, the

position response is plotted as the blue line in Fig.4.5 and the green line is the result when pressure measured at the cylinder chambers is used. The position difference is plotted in red. It is found from these results that the maximum position difference is larger than 7.5% of the amplitude of the position signal and the position accuracy of the system is high when the pressure values measured at the cylinder chambers are used. The influence of connected pipelines cannot be ignored and the distributed model of pipelines is needed in this situation. The design index in this situation is equal to 1.61.

When the length of pipelines used in this experiment is 2.0m and the diameter is 6.10mm, experimental results are shown in Fig.4.6. The pressure values measured at the control port of the servo valve are plotted as the blue lines while the ones measured at the cylinder chambers are plotted as the green lines. The red lines are the difference between the input and output of pipelines. The pressure loss along pipelines in this case is larger than ±10kPa. The position response is shown in Fig.4.7. The blue line is the position response when the pressure measured at the control port of the servo valve is used and the green line is the result when pressure measured at the cylinder chambers is used. The position difference is plotted in red. It is found from these results that the maximum position difference is larger than 7.5% of the amplitude of the position signal and the position accuracy of the system is high when the pressure values measured at the cylinder chambers are used. The influence of connected pipelines cannot be ignored and the distributed model of pipelines is needed in this situation. The design index in this situation is equal to 1.02.

The results with different pipelines are shown in Table 4.2. In these experiments, the input curve is the sine curve, the amplitude of which is equal to 80mm and the frequency of which is equal to 1Hz. When the 10.0m-long pipelines are used, the diameter of which is 6.10mm, the experimental results are shown in Table 4.3. In these experiments, the amplitude of the input sine curve is equal to 80mm. According to these two tables, it is found that when the index is smaller than 1.0, the maximum position difference is less than 7.5% of the amplitude of the position signal and the influence of connected pipelines can be ignored. When this index is equal to or large than 1.0, the

maximum position difference is larger than 7.5% of the amplitude of the position signal, the position results will be influenced by connected pipelines and the distributed model of pipelines is needed.

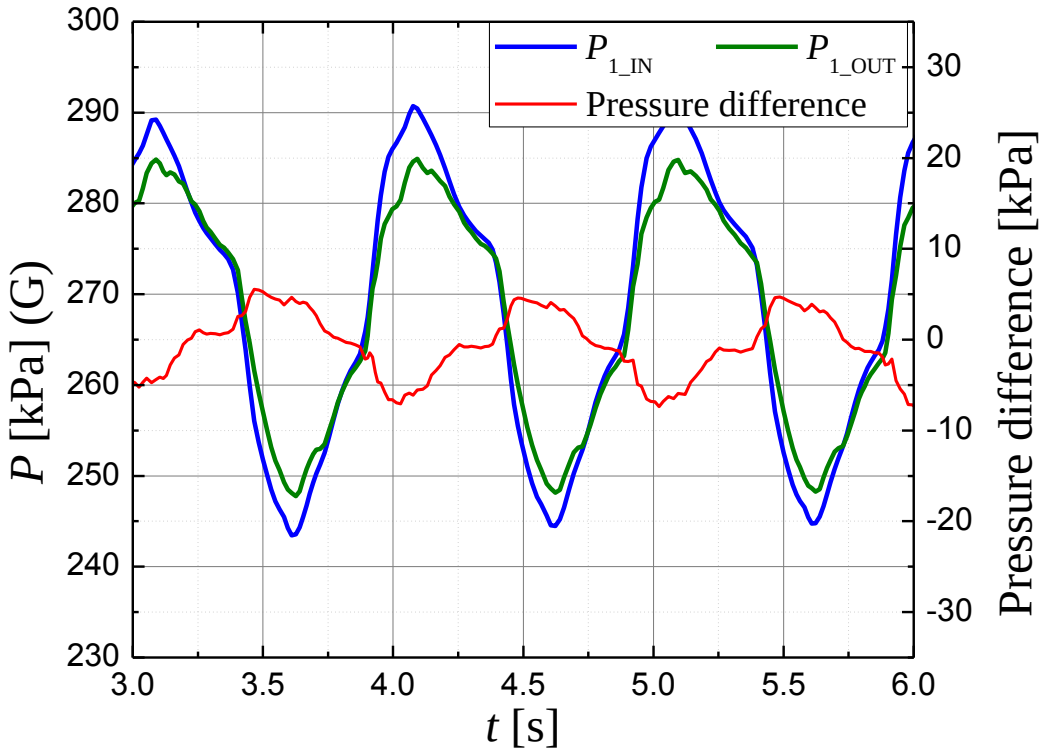

(a) Pipeline 1

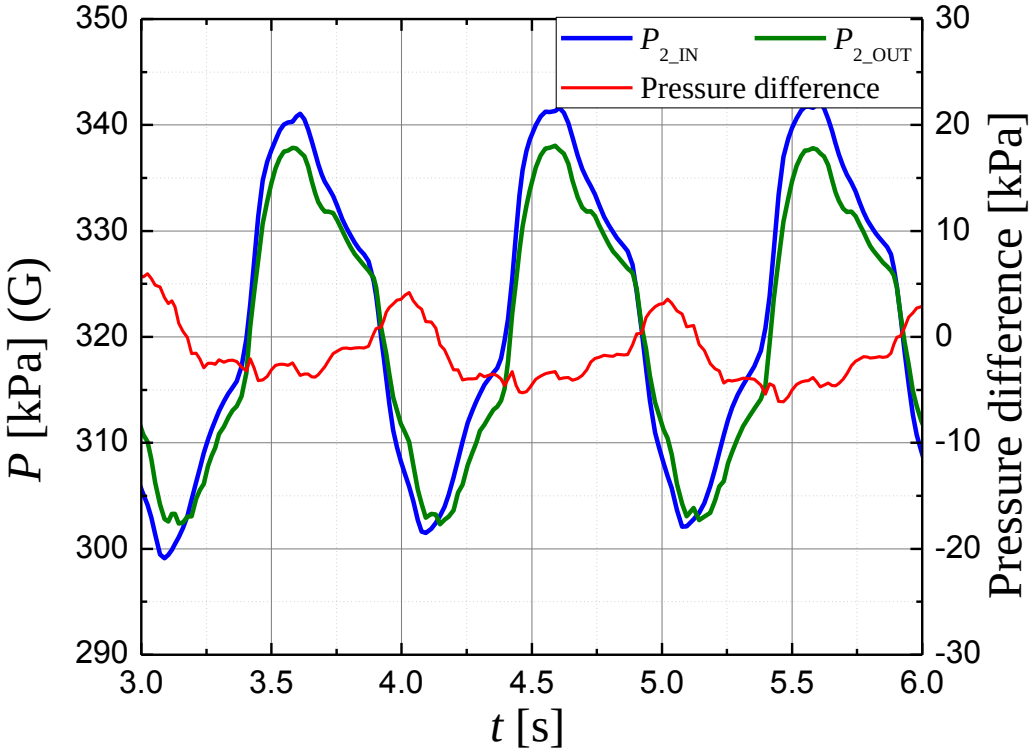

(b) Pipeline 2

Fig.4.2 Experimental results of pressure (*D*=7.65mm, *L*=5.0m, *f*=1.0Hz)

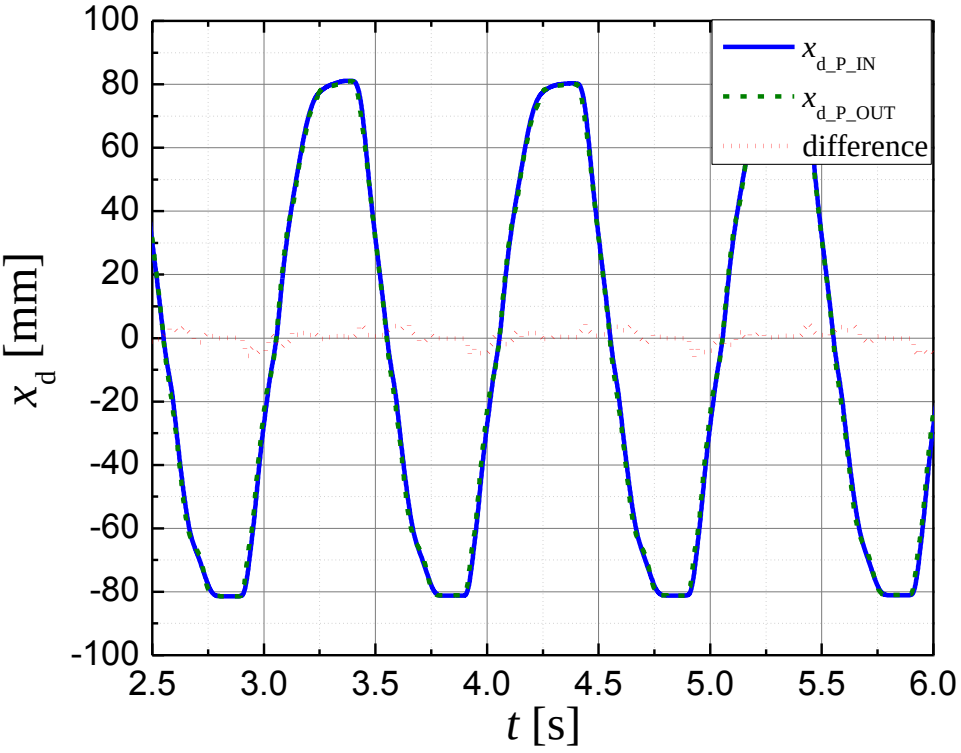

Fig.4.3 Experimental results (*D*=7.65mm, *L*=5.0m, *f*=1.0Hz)

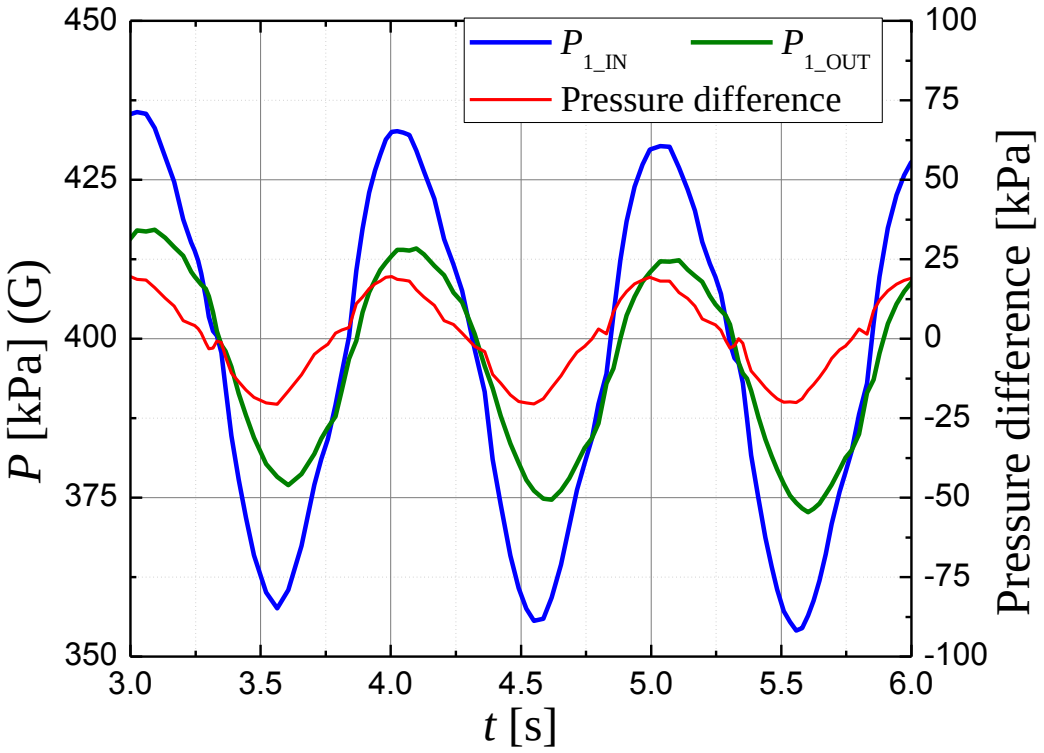

(a) Pipeline 1

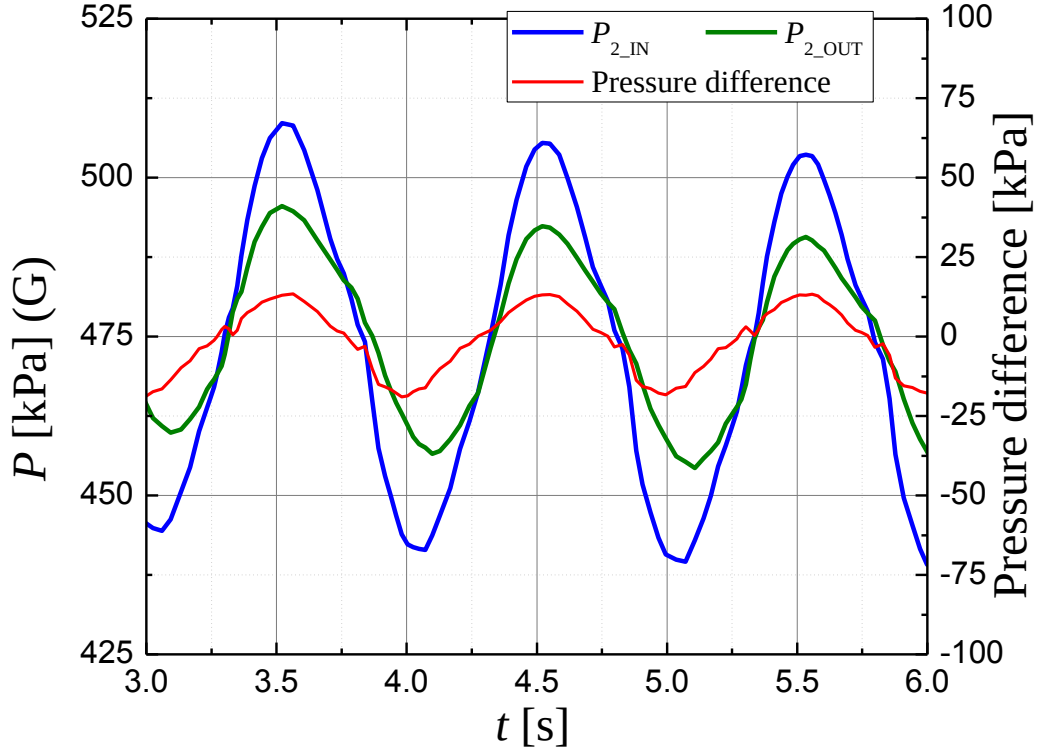

(b) Pipeline 2

Fig.4.4 Experimental results of pressure (*D*=7.65mm, *L*=10.0m, *f*=1.0Hz)

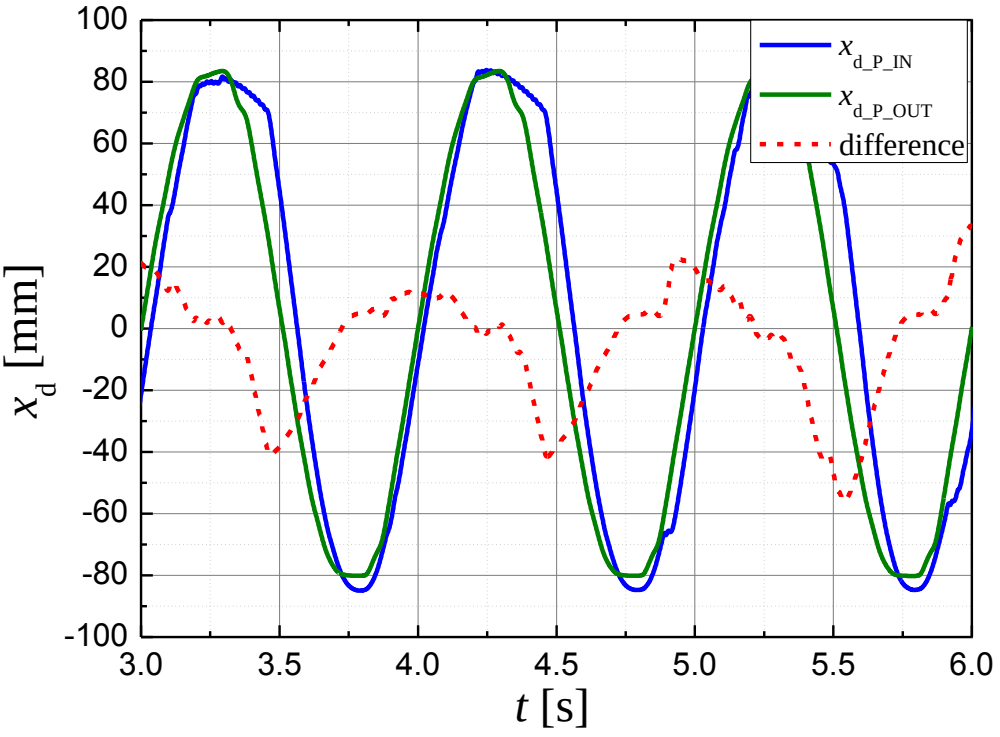

Fig.4.5 Experimental results (*D*=7.65mm, *L*=10.0m, *f*=1.0Hz)

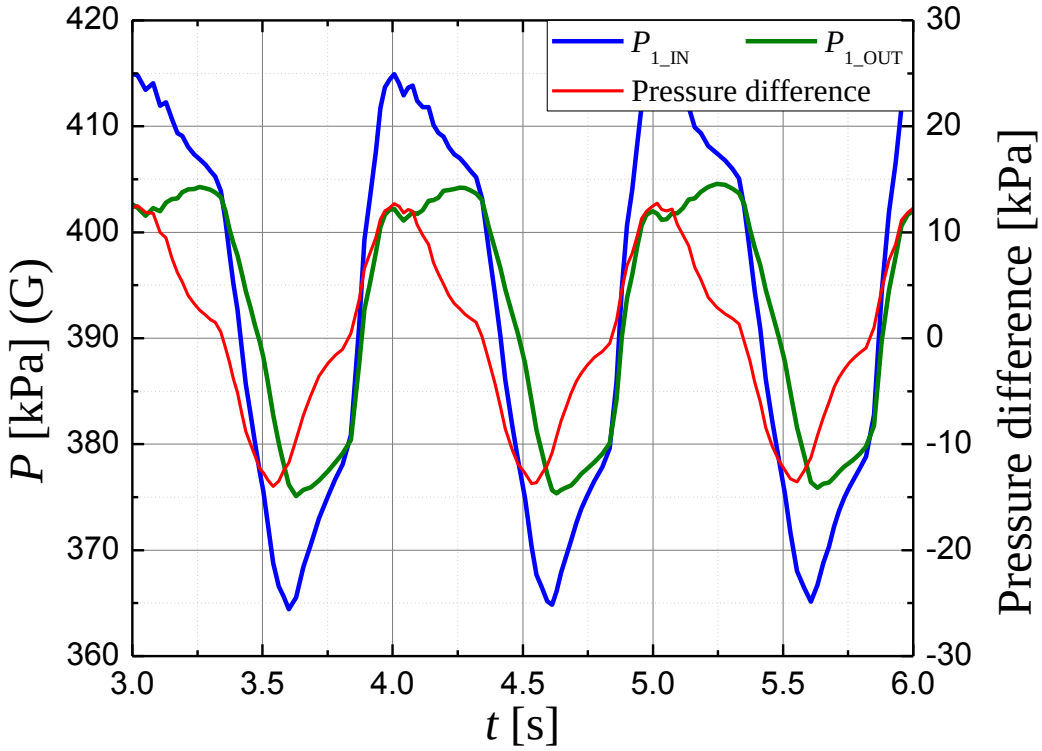

(a) Pipeline 1

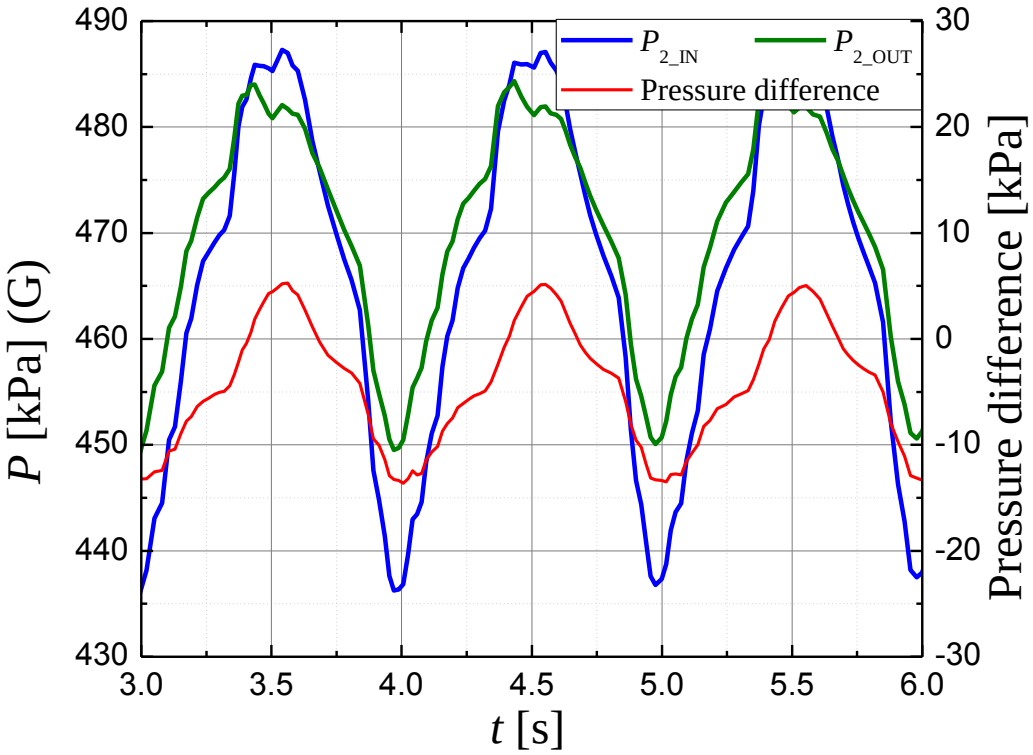

(b) Pipeline 2

Fig.4.6 Experimental results of pressure (*D*=6.10mm, *L*=2.0m, *f*=1.0Hz)

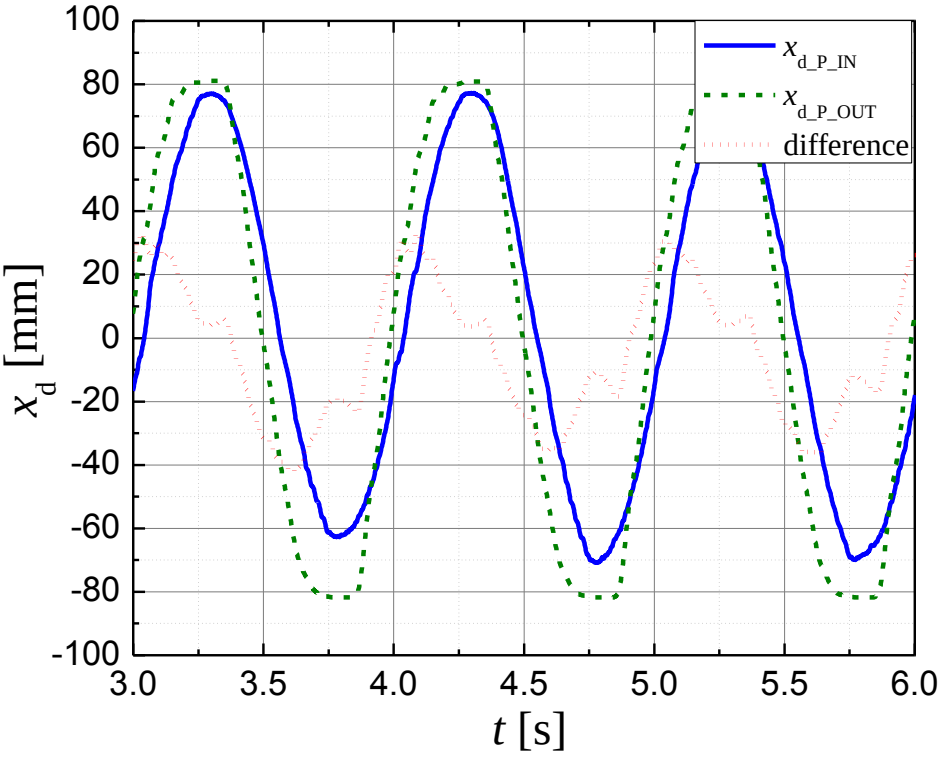

Fig.4.7 Experimental results (*D*=6.10mm, *L*=2.0m, *f*=1.0Hz)

Table 4.2 Influence of pipeline parameters

$x_{ref}=80sin(2f\pi t)$mm f=1.0Hz			
D [mm]	L [m]	Connected pipeline model	$\frac{\lvert\Delta P\rvert_{max}}{P_{re}}$
4.15	2.0	distributed model	5.88
	5.0	distributed model	14.69
	10.0	distributed model	29.39
6.10	2.0	distributed model	1.02
	5.0	distributed model	2.36
	10.0	distributed model	4.72
7.65	2.0	--	0.32
	5.0	--	0.80
	10.0	distributed model	1.61

Table 4.3 Influence of moving speed

x_{ref}=80sin(2$f\pi t$)mm	D=6.10mm	L=10.0m
f [Hz]	Connected pipeline model	$\frac{\lvert\Delta P\rvert_{max}}{P_{re}}$
0.2	--	0.28
0.5	distributed model	1.40
1.0	distributed model	4.72
1.5	distributed model	9.59
2.0	distributed model	15.86
2.5	distributed model	23.44
3.0	distributed model	32.25
3.5	distributed model	42.24

4.4 Conclusions

In this chapter, an index to use the distributed model of pipelines has been introduced. The index is designed based on the judgment of pressure loss along the pipeline. After the type of servo valve is determined, the pressure losses along pipelines are influenced by pipeline diameter, pipeline length, supply pressure, moving speed of the slider and pressurized area of cylinder chamber. The index is the maximum pressure loss along pipelines and the resolution of the pressure sensor. Based on experimental results, when the index is smaller than 1.0, the maximum position difference is less than 7.5% of the amplitude of the position signal and the influence of connected pipelines can be ignored. When this index is equal to or large than 1.0, the maximum position difference is larger than 7.5% of the amplitude of the position signal, the position results will be influenced by the connected pipelines and the distributed model of pipelines is needed.

Chapter 5 Conclusions and future work

5.1 Summary

Due to design and space considerations, in many applications long pipelines are needed to connect the servo valve with the pneumatic cylinder and the pneumatic actuator are non-electromagnetic. To reduce the total magnetic leak of the pneumatic actuator, pressure sensors are removed from the cylinder chamber side. For this reason, the design method is developed to reduce the bad influence of connected pipelines on the position control of the system when pressure sensors are removed from the cylinder chambers. In this thesis, the integrated control method is developed to control the pneumatic servo table system with air bearing (Chapter2). The distributed model of pipelines is design to compensate the influence of long connected pipelines in the pneumatic servo system (Chapter3) and an index to use the distributed model is developed (Chapter4).

The content of this research is summarized as follows:

Chapter 1 “Introduction”

This chapter first introduced the pneumatic servo table system with air bearing, which is mainly composed by a pneumatic actuator, high-performance pneumatic servo valves, a linear scale and pipelines. The pneumatic actuator includes a slider which is 1DOF moving part and a fixed guide. The slider is mounted externally pressurized air bearing which acts through holes in the surface of the guide. Use of this air bearing can avoid contact between the slider and the guide and also allows smooth acceleration and movement without stick-slip effect.

Secondly, the system to compensate the influence of long connected pipelines is introduced, which is mainly composed by a pressure regulator, a five-port servo valve, four pressure sensors, long connected pipelines, a metal pneumatic cylinder, an encoder and an AD/DA converter. The five-port servo valve is used to control the mass flow at

the inlets of pipelines. Pressure values at the inlets of the pipelines and cylinder chambers are obtained by the AD converter and pressure sensors. In this experiment, to confirm the influence of pressure sensors' locations on the position accuracy and the effectiveness of the distributed model of pipelines, four pressure sensors are utilized. In every case, two pipelines with the same length and diameter are used to connect the two cylinder chambers with the control ports of the servo valve. The supply pressure is 700kPa (absolute) and the full stroke of the cylinder is 300mm. Sampling time of the AD / DA converter is 1 ms.

Thirdly, the purpose of this research is proposed.

The suitable linear model of each main element used in the pneumatic servo table system with air bearing is develop, including the linear model of pneumatic actuator, connected pipeline and high-performance pneumatic servo valve. A linear model for whole pneumatic servo table system with air bearing is developed and different orders models are compared to find a suitable and easy to realized linear model. A feed forward is needed to decrease the trajectory errors of the pneumatic servo table system with air bearing.

The distributed model of connected pipelines can estimate the pressure in the cylinder chambers precisely by the measured values at the control ports of the servo valve in the real time, with which pressure sensors can be released from the cylinder chamber to reduce total magnetic leak around cylinder side in the pneumatic servo system with long connected pipelines. Then the estimated pressure values are used as control signal in the real control system which can compensate the influence of long connected pipelines without using pressure sensors around the cylinder chamber side. Since the distributed model is complex, an index is designed to determine when the distributed model is needed in the control system.

Chapter 2 "Precise position control of the pneumatic servo table considering the dynamics of pipelines"

The integrated control method of the pneumatic servo table system with air bearing, considering the dynamics of the pipeline and the servo valve is proposed in this chapter.

The pneumatic servo table system used in the study and main components, like pneumatic actuator, servo valve and pipelines are introduced. Mathematical models of the main components used in the system are designed. A linear model which takes into consideration the dynamics of pneumatic actuator, connected pipelines and servo valve is designed to simulate the system. At first, we considered only the pneumatic actuator when the control model was designed, since the servo valve response is much faster than that of the pneumatic actuator. The servo table system was approximated as a 3^{rd} order linear model. A PPD^2 controller involving position, velocity and acceleration feedback is used in the control system. Comparing experimental and simulation results, we found that there is a large discrepancy between simulation and experimental results. Based on this, we designed a 7^{th} order linear model whose simulation results matched experimental results well. Based on this result, it is found that the servo valve and connected pipelines greatly impacted on system accuracy. Minimizing errors requires feed forward, but the 7^{th} order linear model is complex. A low-dimensional model is necessary for practical use. The analysis showed that in the pole loci of the 7^{th} order model, two poles are much farther from the imaginary axis than are the other five poles. Therefore, the model can be reduced to one of the 5^{th} order. By comparing the simulation and experiment results, we confirmed that the 5^{th} order model could also match up well with the system.

The 5^{th} order control model's maximum trajectory error with feedback control is 3.036×10^{3}μm when stoke is 100mm, which is still too large for precision positioning, however, and 5^{th} order feed forward is required to minimize it. We therefore plan to design an input curve which is derived five times to obtain 5^{th} order feed forward in the real system. Based on the linear model obtained before, 3^{rd} and 5^{th} order feed forward

controls have been designed. We have found from the experimental results that the feed forward used in the system can significantly reduce trajectory errors. By comparing the experimental results using different orders of feed forwards, we have found that the 5^{th} order feed forward can decrease the maximum trajectory error into 0.3μm when stoke is 100mm.

Chapter 3 "Distributed model of connected pipelines"

In this chapter, the control design of a pneumatic system using long connected pipelines is proposed to release pressure sensors at cylinder chambers. The distributed model estimates the pressure losses and time delay through long connected pipelines in real time. To confirm the effectiveness of the proposed control method, a simulation model of the whole system is designed. The pipelines with different parameters are used. Compared simulation and experimental results, it has been found that the simulation model represents the real system well. Based on the estimated and measured pressure values in cylinder chambers, it is found that with this distributed model, the pressure in the cylinder chambers is estimated precisely by the measured values at the control ports of the servo valve in the real time. The experimental results demonstrate that the position accuracy is almost the same as that of using the measured pressure signals in the cylinder chambers. With this distributed model in the control system, the influence of long connected pipelines can be ignored and the cylinder sider is free of pressure sensors. With the commercial non-electromagnetic position sensors, electromagnetics can be avoided at the cylinder side.

Chapter 4 "Index to judge the necessity of the distributed pipeline model"

In this chapter, the index to judge the necessity of the distributed pipeline model is proposed for the pneumatic servo system. The distributed model is complex and in some situations, the effect of connected pipelines can be ignored. The index is designed

based on judgment of the pressure loss along pipelines for practical use. The pressure loss along pipelines is influenced by pipeline diameter, pipeline length, supply pressure, moving speed of the slider and pressurized area of cylinder chamber. The index is designed from the maximum pressure loss along pipelines divided by the resolution of the pressure sensors (±10kPa). Based on experimental results, when the index is smaller than 1.0, the maximum position difference is less than 7.5% of the amplitude of the position signal and the influence of connected pipelines can be ignored. When this index is equal to or large than 1.0, the maximum position difference is larger than 7.5% of the amplitude of the position signal, the position results will be influenced by the connected pipelines and the distributed model of pipelines is needed.

5.2 Future work

The steady state errors of the pneumatic servo table system are caused by the leakage of the joints used in the system and the difference between the movements in both two chambers. A control method which can compensate the leakage of the joints is needed to reduce the steady state errors.

The pneumatic servo system with long connected pipelines

- The feed forward is needed to improve the position accuracy of the system.
- Since the resolution of the pressure sensors is low, the pressure loss along pipelines is needed to be measured by high accuracy differential pressure sensors.
- The control design to remove the position sensor from cylinder chamber is needed to keep the cylinder side from electromagnetics.

References

[1] Otsuka J, Hayama S, Ohashi Y. Present and future technologies of precision and ultra-precision positioning. The Japan Society for Precision Engineering, 2001, 67(2): 173-178.

[2] Sato H, Yamamoto H. High Precision Positioning Device. United States Patent, 1980, 4, 234.

[3] Oiwa T, Katsuki M. Survey of Questionnaire on Ultra-precision Positioning. The Japan Society for Precision Engineering, 2003, 69(8): 1077-1082.

[4] Pahk H J, Lee D S, Park J H. Ultra precision positioning system for servo motor–piezo actuator using the dual servo loop and digital filter implementation. International Journal of Machine Tools and Manufacture, 2001, 41(1): 51-63.

[5] Endo S, Kobayashi H, Kempf CJ, Kobayashi S, Tomizuka M, Hori Y. Robust digital tracking controller design for high-speed positioning systems. Control Engineering Practice, 1996, 4(4): 527-536.

[6] Horiuchi O. Speed Up of Precision/Ultra-precision Positioning –Ball Screw vs. Linear Motor. The Japan Society for Precision Engineering, 2001, 67(2): 179-183.

[7] Moriyama S, Harada T, Takanashi A. Precision X-Y Stage with a Piezo-driven Fine-table. The Japan Society for Precision Engineering, 1983, 50(4): 80-85.

[8] Liu Y, Higuchi T. Precision Positioning Device Utilizing Combined Piezo-VCM Actuator. The Japan Society for Precision Engineering, 2001, 67(1): 70-75.

[9] Ma W, Ikeo S. Position Control of Hydraulic Cylinder Using Constant Pressure system. Journal of the Japan Fluid Power System Society, 2003, 34(5):99-105.

[10] Wu C, Kitagawa A. A Study of a Hydraulic Cylinder with Built-in Compound Control Function of Displacement and Thrust. Journal of the Japan Fluid Power System Society, 2004, 35(4): 70-76.

[11] Sato K. Fundamentals of Precision Positioning Control. The Japan Society for Precision Engineering, 2006, 72(11):1341-1344.

[12] Richer E, Hurmuzlu Y. A high performance pneumatic force actuator system: Part I-Nonlinear mathematical model. ASME Journal of Dynamic Systems Measurement and Control, 2000, 122(3): 416-425.

[13] Liu S, Bobrow J E. An analysis of a pneumatic servo system and its application to a computer-controlled robot. Journal of dynamic systems, measurement, and control, 1988, 110(3): 228-235.

[14] Kimura T, Hara S, Fujita T, Kagawa T. Feedback linearization for pneumatic actuator systems with static friction. Control engineering practice, 1997, 5(10): 1385-1394.

[15] Kosaki T, Sano M. An Observer-Based Friction Compensation Technique for Positioning Control of a Pneumatic Servo System. Journal of System Design and Dynamics, 2009, 3(1): 37-46.

[16] Shearer J.E. Study of Pneumatic Process in the Continuous Control of Motion with Compressed Air-I, II. Transactions of ASME, Feb., 1956, 233-249.

[17] Burrows C.R, Webb C.R. Use of the root Loci in Design of Pneumatic Servo-Motors. Control, Aug., 1966, 423-427.

[18] Bobrow J E, Jabbari F. Adaptive pneumatic force actuation and position control. American Control Conference, 1989. IEEE, 1989, 1508-1513.

[19] McDonell B W, Bobrow J E. Adaptive tracking control of an air powered robot actuator. Journal of dynamic systems, measurement, and control, 1993, 115(3): 427-433.

[20] Paul A K, Mishra J E, Radke M G. Reduced order sliding mode control for pneumatic actuator. Control Systems Technology, IEEE Transactions on, 1994, 2(3): 271-276.

[21] Tang J, Walker G. Variable structure control of a pneumatic actuator. Journal of dynamic systems, measurement, and control, 1995, 117(1): 88-92.

[22] Ben-Dov D, Salcudean S E. A force-controlled pneumatic actuator. Robotics and Automation, IEEE Transactions on, 1995, 11(6): 906-911.

[23] Richard E, Scavarda S. Comparison between Linear and Nonlinear Control of an Electro-pneumatic Servo-drive. Journal of Dynamic Systems, Measurement and Control, 1996, 118:245-118.

[24] Schulte H, Hahn H. Fuzzy state feedback gain scheduling control of servo-pneumatic actuators. Control Engineering Practice, 2004, 12(5): 639-650.

[25] Gao X, Feng Z J. Design study of an adaptive Fuzzy-PD controller for pneumatic servo system. Control Engineering Practice, 2005, 13(1): 55-65.

[26] Miyajima T, Fujita T, Sakaki K, Kawashima K, Kagawa T. Development of a digital control system for high-performance pneumatic servo valve. Precision engineering, 2007, 31(2): 156-161.

[27] Jang J. Pressure Control of a Volume-Terminated Pneumatic Control System with a Long Transmission Line. Journal of the Japan Fluid Power System Society, 2003, 34(6): 423-427.

[28] Bideaux E, Scavarda S. Pneumatic Pipe modeling: Theory and experimental approach (part II). Fluid Power Systems and Technology-2000. New York: American Soc. Mech. Engineers, 2000, 77-81.

[29] Kitagawa A. Treatment of pipelines' dynamics – Introduction of the fundament of pipelines' dynamics and various models. Pneumatic and Hydraulic Pressure Technology, 1996, 35(11): 1-5.

[30] Eom KS, Suh IH, Chung WK, 0h SR. Disturbance observer based force control of robot manipulator without force sensor. Proceedings of the 1998 IEEE,

International Conference on Robotics & Automation Leuven, Belgium, 1998, 3012-3017.

[31] Ohishi K, Miyazaki M, Fujita M, Ogino Y. H^{∞} Observer Based Force Control without Force Sensor. Proceedings of IEEE Int. Con. on Industrial Electronics, Control and Instrumentation, 1991, 1049-1054.

[32] Hougen JO, Martin OR, Walsh RA. Dynamics of Pneumatic Transmission Lines. Energy Conservation and Management, 1963, 35(1): 61-77.

[33] Whitmore SA, Lindsey WT, Curry RE, Gilyard GB. Experimental characterization of the effects of pneumatic tubing on unsteady pressure measurements. NASA Technical Memorandum 1990, 4171: 1-26.

[34] Elmadbouly EE, Abdulsadek NM. Modelling, simulation and sensitivity analysis of a straight pneumatic pipeline. Energy Conservation and Management, 1994, 35(1): 61-77.

[35] Matko D, Geiger G, Gregoritza W. Pipeline simulation techniques. Mathematics and Computers in Simulation, 2000, 52(3): 211-230.

[36] Tadano K, Kawashima K. Development of a master-slave system with force-sensing abilities using pneumatic actuators. Advanced Robotics, 2010, 24: 1763-1783.

[37] Brown, FT. The transient response of fluid lines. Trans. ASME, J. Basic Engineering, 1962, 84(4): 547-553.

[38] Zielke, Werner. Frequency dependent friction in transient pipe flow. Trans. ASME 1966, Ser. D90-1: 109-115.

[39] Kitagawa A, Kagawa T, Takenaka T. High speed and accurate computing method for transient response of pneumatic transmission line using characteristics method. Transactions of the society of instrument and control engineering, 1984, 20(7): 648-653.

[40] Kagawa T, Lee I, Kitagawa A, Takenaka T. High speed and accurate computing method of frequency-dependent friction in laminar pipe flow for characteristics method. Transactions of the Japan Society of Mechanical Engineers, 1983, 49(447): 2638-2643.

[41] Krivts I L. Optimization of performance characteristics of electropneumatic (two-stage) servo valve. Journal of dynamic systems, measurement, and control, 2004, 126(2): 416-420.

[42] Andersen B.W. The Analysis and Design of Pneumatic Systems. John Wiley & Sons, Inc., 1967.

[43] Backe W. The Application of Servo Pneumatic Drives for Flexible Mechanical Handling Techniques. Robotics, 1986, 2(1): 45-56.

[44] Pu J, Weston R.H. A New Generation of Pneumatic Servo for Industrial Robot. Robotics, 1988, 7:17-23.

[45] Kagawa T. Basic Characteristics of Pneumatic Components (I). Journal of the Japan Hydraulics and Pneumatics Society, 1987, 18(6):455-459.

[46] ISO 6358: Pneumatic Fluid Power - Components using compressible fluids - Determination of flow rate characteristics, 1989.

[47] Kawashima K, Arai T, Tadano K, Fujita T, Kagawa T. Development of coarse/fine dual stage using pneumatically driven bellows actuator and cylinder with air bearings. Precision Engineering, 2010, 34(3): 526-533.

[48] Izumi Y, Arai T, Kawashima K, Kagawa T. Considering of Tube influence in Pneumatic Servo Table System. The Proceedings on Autumn Conference of Japan Fluid Power System Society, 2007, 194-196.

[49] Hanafusa H. Design of electrohydraulic servo mechanism for articulated robot control. Japan Hydraulics and Pneumatics Society, 1982, 13(7): 429-436.

[50] Martins FG. Tuning PID Controllers using the ITAE Criterion. International Journal of Engineering Education, 2005, 21(5):867-873.

[51] Kagawa T, Hoshino T, Oyama O, Shimizu M. A study of unsteady flow in pneumatic pipe-chamber system. Transactions of the society of instrument and control engineering, 1992, 28(6): 655-663.

[52] Kagawa T, Tokashiki LR, Fujita T. Influence of Air Temperature Change on Equilibrium Velocity of Pneumatic Cylinders. Transactions of the ASME: Journal of Dynamic Systems, Measurement and Control, 2002, 124(2):336-341.

[53] Kagawa T, Shimizu M. Non-dimensional Pressure Responses of Pneumatic RC Circuits Considering Heat Transfer. Journal of the Japan Hydraulics and Pneumatics Society, 1988, 19(4):306-311.

[54] Gottlieb D, Tadmor E. The CFL condition for spectral approximations to hyperbolic initial-boundary value problems. Mathematics of Computation, 1991, 56(194): 565-588.

Acknowledgements

I here express the special gratitude to my academic supervisor, Professor Kenji KAWASHIMA, for the encouragement and valuable advices along the past 4 years of study at Tokyo Institute of Technology. The support he provided me in the studies and life in Japan was fundamental for this work.

I also express special gratitude to Professor Toshiharu KAGAWA, Associate Professor Kotaro TADONO for their valuable advices and orientations in the study and the life during these four years.

I would like to gratefully acknowledge

Professor Toshiharu KAGAWA

Professor Shinichi YOKOTA

Associate Professor Kazuhiro YOSHIDA

Associate Professor Hayato YOSHIOKA

for the attention and the valuable advices on the elaboration of this work.

Thanks to Mr. Yu Okamoto, for his friendship, and helpful discussions in the course of this study. Thanks are due to Dr. Daisuke Haraguchi, Dr. Mitsuhiro Nakao, Mr. Joonmyeong Choi, Ms. Natuko TanadaMr. Daisuke Sakamoto, Mr. In Kim, Mr. Hangjie Jiang, Ms Lai Lai OO, Mr. Shengzhi Chen, for their friendship and enthusiasm in the course of this study.

Thanks are due to the Japanese Government that provided me the scholarship along the doctor course at Tokyo Institute of Technology.

Finally, I wish to dedicate this work to my parents, for their lifelong support.

Jun Li

August 1st, 2013